UNIVERSITY OF BELGRADE

FACULTY OF PHYSICS

INSTITUTE OF METEOROLOGY

Đorđe N. Romanić

DYNAMIC CHARACTERISTICS OF THE KOSHAVA WIND

Doctoral Dissertation

Belgrade, 2016

УНИВЕРЗИТЕТ У БЕОГРАДУ

ФИЗИЧКИ ФАКУЛТЕТ

ИНСТИТУТ ЗА МЕТЕОРОЛОГИЈУ

Ђорђе Н. Романић

ДИНАМИЧКЕ КАРАКТЕРИСТИКЕ КОШАВЕ

докторска дисертација

Београд, 2016

Подаци о ментору и члановима комисије

Ментор:

Проф. др. Млађен Ђурић, редовни професор

Институт за метеорологију, Физички факултет, Београд

Чланови комисије:

Проф. др. Млађен Ђурић

Редовни професор, Физички факултет, Београд

Проф. др. Дејан Јанц

Вандредни професор, Физички факултет, Београд

Проф. др. Мирјана Румл

Вандредни професор, Пољопривредни факултет, Београд

Acknowledgment

Dynamic characteristics of the Koshava wind

Abstract

Koshava is a local wind usually observed in the cold part of the year over the large part of Serbia, parts of Romania, parts of Hungary, and east Croatia. Koshava blows from southeast quadrant. The Eurasian high and Mediterranean cyclones, together with the orography of the eastern Balkan, are the main drivers of the Koshava wind. In this study, a comprehensive analysis of long-term trends of the Koshava wind in the period between 1949 and 2010 is carried out. The trend analyses are performed on wind data sets from five synoptic weather stations, all situated in the region where the Koshava wind is fully developed. In order to obtain more accurate trends, Koshava speeds are divided into two categories: (1) all wind speeds and, (2) wind speeds above 5 m s^{-1}. Two homogeneity tests are used to inspect the quality of wind speed and wind direction time series. The Mann-Kendall test and the Sen's slope estimator are used to analyze trends of the Koshava speeds and the annual number of days with the Koshava wind. Statistically significant negative trends of the Koshava speeds and wind activity are observed at almost all weather stations and are generally more pronounced for wind speeds above 5 m s^{-1}. The negative trends of the Koshava wind are mostly related to the changes in the synoptic circulation, temperature and weakening of the Eurasian high and West-Mediterranean cyclones. It is shown that observed declining of the Koshava wind does not have a significant impact on reducing the wind energy potential in the region.

The main characteristics of the Koshava wind are its high wind speed, southeasterly direction, persistence, and gustiness. This thesis furthermore analyzes the synoptic (Mediterranean cyclones and Eurasian anticyclones) as well as the mesoscale contributors to the Koshava wind. Time and spatial features of the pressure systems have been analyzed using an automatic cyclone and anticyclone tracking scheme. The results show that the Mediterranean cyclones and Eurasian anticyclones that generate Koshava are approximately 1000 km away from the KR. It is demonstrated that the strong anticyclones are the main trigger for the Koshava wind. Less than 3 % of the Koshava winds occurred without the occurrence of either an anticyclone or a cyclone. The Synoptic Koshava Index (SKI), developed in this study and defined as the difference between the area-averaged mean sea level pressures in the anticyclone and cyclone regions, has been shown to be a good indicator of the Koshava occurrence. Koshava has also been investigated from the perspective of the gap flow and fohen windstorm. The across-mountain pressure difference is the most important mesoscale contributor to the Koshava characteristics. The across-mountain potential temperature difference, together with the across-mountain pressure difference, can be successfully used to predict Koshava's occurrence. A simple linear probabilistic model for forecasting the Koshava mean hourly wind speed has been constructed. The results demonstrate that the occurrence of the Koshava wind can be predicted with the significantly higher accuracy than the Koshava mean hourly speed. The correlation between Koshava and winds at higher levels is small.

An extreme Koshava episode (EKE) from January 30 to February 4, 2014 has been studied in order to investigate the vertical structure of the Koshava wind, dynamics of extreme Koshava winds and capabilities of numerical models to

simulate EKEs. EKE was characterized by wind gusts above 45 m s^{-1}, deep snowdrifts and blizzard conditions. Strong Eurasian anticyclone (central pressure of 1055 hPa) in combination with large temperature difference between the anticyclone region and the Mediterranean (about 50°C) caused the EKE. It is demonstrated that the anticyclone had the probability of occurrence of 0.1 %. Koshava layer was either statically stable or adiabatic. The event is numerically modelled using two mesoscale models: WRF-NMM and NMMB. Wind directions were forecasted more accurately than the mean speed and gusts. It is concluded that more research is needed in the field of numerical modelling of stable atmospheric layers and wind gusts. This thesis also introduces a novel methodology for snowdrift forecasts based on a relationship between the horizontal gradients of wind speed and snowdrift locations. The method is tested in the case of the EKE and the results are in a good agreement with the observations.

Keywords: Koshava wind, local winds, Mediterranean cyclones, Eurasian anticyclones, gap flow, Synoptic Koshava Index, trend analysis, homogeneity testing, WRF, snowdrifts.

Scientific field: Earth science

Field of academic expertise: Meteorology

UDC number: 551.5 (043)

Динамичке карактеристике Кошаве

Резиме

Кошава је локални ветар који се најчешће јавља у хладној половини године изнад већих делова Србије, делова Румуније, делова Мађарске и изнад источне Хрватске. Кошава дува из југоисточног квадранта. Евроазијски антициклон и медитерански циклони у комбинацији са орографијом источног Балкана су главни узрочници Кошаве. Ова студија представља детаљну анализу дугорочних трендова Кошаве за педиод од 1949. до 2010. године. Анализе трендова су урађене користећи податке са пет синоптичких метеоролошких станица које се налазе у кошавском региону. У циљу добијања што прецизнијих трендова, брзине Кошаве су подељене у две категорије: (1) све брзине и (2) брзине изнад 5 m s^{-1}. Два теста за анализу хомогености података коришћена су за испитивање квалитета података о брзини и смеру ветра. Ман-Кендал (Mann-Kendall) тест о постојању тренда и Сенов метод за оцену нагиба тренда коришћени су за анализе трендова брзине Кошаве и годишњег броја дана са Кошавом. Статистички значајни негативни трендови брзине Кошаве и њене активности забележени су на свим анализираним станицама и генерално су израженији за брзине ветра изнад 5 m s^{-1}. Израчунати негативни трендови Кошаве условљени су променама у синоптичкој циркулацији, трендовима температуре у региону и слабљењем Евроазијског антициклона и западномедитеранских циклона. Показано је да слабљење Кошаве нема значајног економског утицаја на ветроенергетски потенцијал у региону.

Кошава се карактерише јаким брзинам ветра, југоисточним смером, постојаношћу и јаким ударима. Ова докторска дисертација такође анализира синоптичке (медитерански циклони и евроазијски антициклнои) као и мезоразмерне факторе који доводе до Кошаве. Временске и просторне карактеристике синоптичких система притиска анализиране су користећи шему за аутоматско детектовање и праћење циклона и антициклона. Резултати показују да су медитерански циклони и евроазијски антициклони који доводе до Кошаве удаљени око 1000 km од кошавског региона. Демонстрирано је да су изражени антициклони главни узрочници Кошаве. Мање од 3 % од свих забележених Кошава јавило се без присуства циклона или антициклона. Показано је да Синоптички Кошава индекс (СКИ), конструисан у овој студији и дефинисан као разлика између просторно осредњених притисака сведених на ниво мора у региону антициклона и региону циклона, представља добар индикатор појаве Кошаве. Кошава је такође анализирана као каналисани и фенски ветар. Прекопланинска разлика притисака је најзначајнији мезоразмерни кошавски фактор. Показано је да се прекопланинска разлика потенцијалних температурам у комбинацији са прекопланинском разликом притисака може успешно користити за детектовање Кошаве. Једноставни модел линеарне регресије конструисан је за прогнозу средње сатне брзине Кошаве. Резултати ове студије показују да се појавност Кошаве може прогнозирати много прецизније од средње сатне брзине Кошаве. Корелација између Кошаве и ветрова на већим висинама је слаба.

Екстремна кошавска епизода (ЕКЕ) која се јавила између 30. јануара и 4. фебруара 2014. године анализирана је како би се испитала вертикална структура Кошаве, динамика екстремних бризина Кошаве и способност

нумеричких модела да симулирају ЕКЕ. ЕКЕ из 2014 се карактерисала ударима ветра преко 45 m s⁻¹, дубоким снежним наносима, вејавицом и мећавом. Врло изражени евроазијски антициклон (централни притисак од 1055 hPa) у комбинацији са јаким температурним разликама између антициклоналног региона и Медитерана (око 50°С) проузроковали су ЕКЕ. Показано је да је вероватноћа појаве овако дубоког антициклона мања од 0,1 %. Кошавски слој је био стабилан или адијабатски стратификован. Ова ситуација нумерички је моделована користећи два мезоразмерна модела: WRF-NMM и NMMB. Смерови ветра су прогнозирани много тачније од брзина и удара ветра. Закључено је да потребно више истраживања у областима нумеричког моделовања стабилних атмосферских услова и удара ветра. Ова докторска дисертација такође представља нову методологију за прогнозу снежних наноса која се заснива на повезаности хоризонталних градијената брзине ветра и локација снежних наноса. Предложени метод је тестиран на примеру ЕКЕ и резултати се добро слажу са осматрањима.

This thesis is dedicated to my parents,

Nikola and Dušanka Romanić,

for their endless love, support and encouragement.

Ову докторску дисертацију посвећујем својим родитељима

Николи и Душанки Романић,

за њихову бескрајну љубав, подршку и охрабрење.

Table of contents

List of figures

List of tables

Abbreviations

a.g.	above ground
a.s.l.	above sea level
A0; A10; A1	Strong closed; weak closed; strong open highs/anticyclones
BG	Belgrade weather station Karađorđev Park
C0; C10; C1	Strong closed; weak closed; strong open lows/cyclones
CAR	Caransebes weather station
DTS	Drobeta-Turnu Severin weather station
EA	Eurasian anticyclone
EKE	Extreme Koshava episode
IFS	Integrated Forecast System
K5	Koshava winds above 5 m s^{-1}
KR	Koshava region
LOM	Lom weather station
MC	Mediterranean cyclone
MSLP	Mean sea level pressure
NCAR	National Center for Atmospheric Research
NCEP	National Centers for Environmental Prediction
NEG	Negotin weather station
NMM	Nonhydrostatic Mesoscale Model
NMMB	NMM on Arakawa-B grid
NS	Novi Sad weather station Rimski Šančevi
PBL	Planetary boundary layer
PDF	Probability density function
QNSE	Quasi-Normal Scale Elimination scheme
SKR	Source Koshava region
SP	Smederevska Palanka weather station
UTC	Coordinated Universal Time
VG	Veliko Gradište weather station
VR	Vršac weather station
W&NW	Westerly and northwesterly (winds)
WRF	Weather Research and Forecasting

This page intentionally left blank

CHAPTER 1

1. Introduction

1.1 General introduction

Air is almost always moving. The horizontal movement of air is called wind and it represents one of the most important dynamical features of the atmosphere. Wind is characterized by its direction and intensity. Wind direction is defined as the direction the wind is blowing from. It is graphically represented on the wind rose in the units of degrees (°). Wind speed is defined as the rate of the movement of air flow in distance per unit of time. Herein, the wind speed will be expressed in the units of meters per second (m s^{-1}). The International System units are used throughout this text.

Wind arises due to difference in air pressure between two places. The greater the difference in air pressure, the stronger the winds. There are four primary forces that drive wind: (1) pressure gradient force, (2) the Coriolis force, (3) the centrifugal force, and (4) friction force. The detailed physical and mathematical descriptions of these four forces can be found in Ćurić (2002). The geostrophic balance implies an exact equilibrium between the Coriolis force and the horizontal component of the pressure gradient force. The gradient balance, on the other hand, accounts for the curvature of the isobars and thus represents the balance between the above-mentioned two forces and the centrifugal force. The geostrophic/gradient winds are good approximations of the actual winds in the free atmosphere – the portion of the atmosphere above the planetary boundary

layer (PBL). The PBL is defined as a layer in the atmosphere directly influenced by the Earth's surface. The depth of the PBL depends on many factors, but in mid latitudes is approximately 1 km from the ground. Because the surface effects are decrease moving away from the surface, the wind profile inside the PBL follows the Ekman spiral (Ćurić, 2002).

Depending on the size of the region over which they occur, winds can be divided into global and local. Global winds represent movements of large air masses around Earth. These winds are an integral part of the general circulation of the atmosphere. The major global wind systems in the North Hemisphere, also known as the wind belts, are trade winds, westerlies, and polar easterlies. Trade winds occupy most of the tropics and in the Northern Hemisphere have northeastern direction. The westerlies blow in the belt located between 30° and 60° latitudes. Most regions of Europe, North America and Asia are located in the westerlies belt. The polar easterlies are irregular easterly winds that occur in the latitudes above 60°. For the detailed description of the general circulation of the atmosphere, the reader is referred to Satoh (2004).

Local winds blow over smaller regions and last shorter compared to the global winds. Furthermore, they are characterized by more frequent changes of their speed and direction. Local winds depend significantly on physical and geographical features of the region above which they occur. Typical examples of local winds are: sea and land breezes (Puygrenier *et al.*, 2005; Hara *et al.*, 2009; Drobinski and Dubos, 2009; Crosman and Horel, 2010; Qian *et al.*, 2011), local winds between urban and rural areas (Haeger-Eugensson and Holmer, 1999; Niino *et al.*, 2006), local winds caused by orography (Sturman, 1987; Vergeiner

and Dreiseitl, 1987; McNider and Pielke, 1984) and katabatic winds (Oard, 1993; Giaiotti *et al.*, 2007; Gaffin, 2007).

The focus of this thesis is to investigate in detail certain dynamical and climatological characteristics of one local wind which blows over the Southeastern Europe and the Balkan Peninsula – the Koshava wind. The Balkan Peninsula is surrounded by water on three sides (Figure 1.1). The Adriatic Sea is located to the west and southwest, the large Mediterranean Sea to the south and the Black Sea to the east. The peninsula is covered by several large mountain ranges (Balkan Mountains, Rhodope Mountains and Dinaric Alps) which are stretching from northwest to southeast.

1.2 Koshava (Košava) wind

Koshava is a vigorous local wind that blows from the southeast quadrant over north, central and eastern regions of Serbia. Though the wind is the most pronounced in the aforesaid regions of Serbia, it can sometimes be detected in south Hungary, east Croatia, and parts of Romania and Bulgaria found near the Danube River. The main drivers of the wind are two pressure systems – a high pressure system located over Eastern Europe and/or Western Asia, and a low pressure system positioned over the Mediterranean Sea (Figure 1.1 and Figure 1.2). The high pressure system is usually associated with the Eurasian anticyclone (EA), while the low pressure system is made-up of Mediterranean cyclones (MCs) with west to east trajectories. The EA is usually the extension of the Siberian High to Europe and Middle East (Shahgedanova, 2002). As shown in Figure 1.1a, these synoptic pressure systems must have sufficient strength to create strong and persistent pressure gradients that spread over the Western Balkan region. Under these meteorological conditions, the isobars over the

Western Balkans have a meridional (north - south) orientation. This results in the movement of air masses from Moldavia and Ukraine towards the Adriatic and Mediterranean seas. These air masses, however, soon encounter long and tall mountain massifs - the Southern Carpathians (Transylvanian Alps) to the north and the Balkan Mountains to the south. Due to these natural obstacles, the cold air is forced to flow into the Danube Valley towards the Iron Gates (Figure 1.1b). The convergence of air at the Iron Gates creates a strong, persistent and gusty wind, known as Koshava. Influenced by the local orography of eastern Serbia, Koshava exits the Iron Gates in two major branches (Figure 1.1c). The north branch of the Koshava wind continues to follow the Danube River, subsequently reaching the northern part of Serbia (otherwise known as the Pannonian Plane). Meanwhile, the mountains in eastern Serbia influence the south branch of Koshava directing the wind towards the west and southwest, to the Morava River Valley, from where it continues to follow the river. The wind is the strongest along the Danube River and in the region around Vršac (VR).

The EA and MCs can have profound influences on the weather and climate quite a distance from their source regions (e.g. Rex, 1950; Makorgiannis *et al.*, 1981; Radinović, 1987; Ding and Krishnamurti, 1987; Lingis and Michaelides, 2009;. Nissen *et al.*, 2010). The complexity of the Koshava wind, however, lies in the fact that it is caused and influenced by the EA and MCs simultaneously. More specifically, this characteristic of Koshava causes difficulties in its classification. Figure 1.3 shows that while Koshava operates on meso spatial scales, it works on meso to synoptic temporal scales. Due to the orography of the Balkan region, Koshava is a local wind. However, due to the synoptic time scales of the EA and MCs, Koshava typically lasts longer than the most local winds in the region.
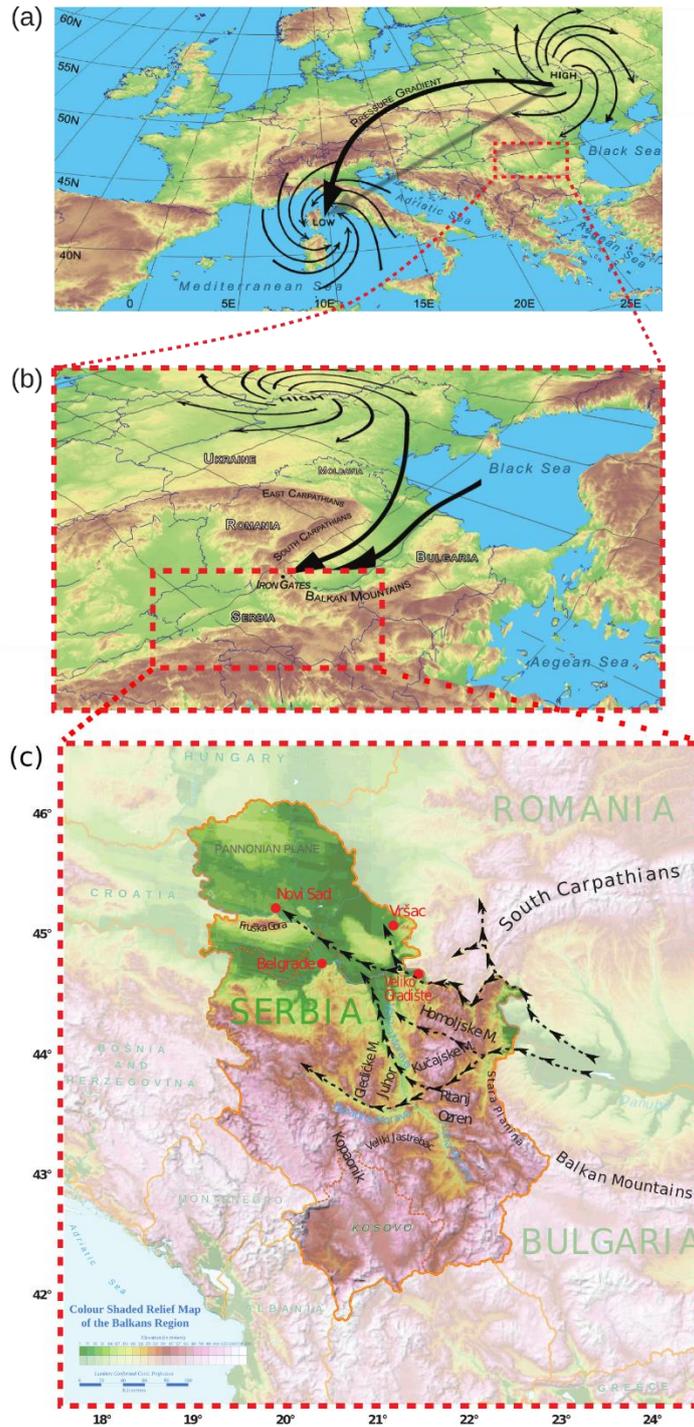
Figure 1.1. Sketch of a synoptic situation favorable for development of the Koshava wind (a, b). In c) the black dashed lines schematically represent typical Koshava paths.

These results are in accordance with the finding by Trigo *et al.* (1999) that MCs usually last for 2 days. These studies suggest that, since the EA is a long lasting pressure system, the weakening and deterioration of the MCs are the main causes of the weakening and consequential disappearance of the Koshava wind.
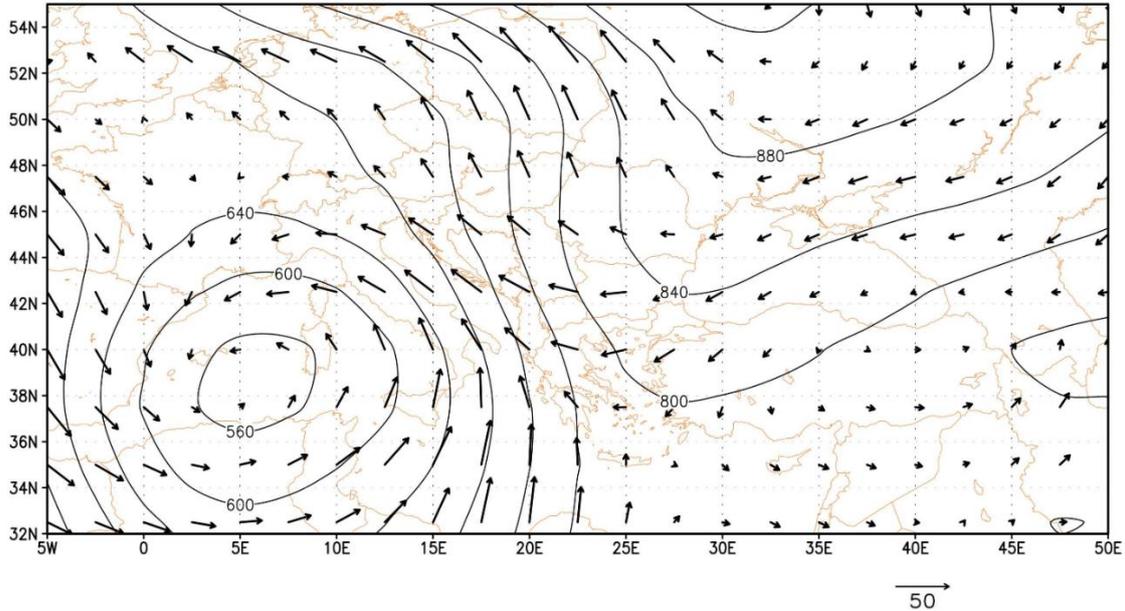
Figure 1.2. Synoptic situation (at 925 hPa pressurelevel) favorable for development of the Koshava wind. The map is for 18 January, 1972 (00 Coordinated Universal Time (UTC)). Data source is the National Centers for Environmental Prediction/National Center for Atmospheric Research (NCEP/NCAR) reanalysis 1 dataset (Kalnay *et al.*, 1996).

Koshava can reach very high wind speeds. For instance, in the period from January 26 to February 4, 2014, Koshava's gusts reached 47 m s^{-1} and 29 m s^{-1} in VR and Belgrade (BG), respectively. These high wind speeds created snowdrifts that were up to 3.5 m high. This natural disaster impacted everyday life across the country; schools and roads were closed, there was severe damage to infrastructure, and emergency situations were raised in several cities. This wind

speed would not be the fastest ever recorded for the Koshava wind, however, as a gust speed of 48 m s⁻¹ was recorded for the wind on January 11, 1987, in VR.
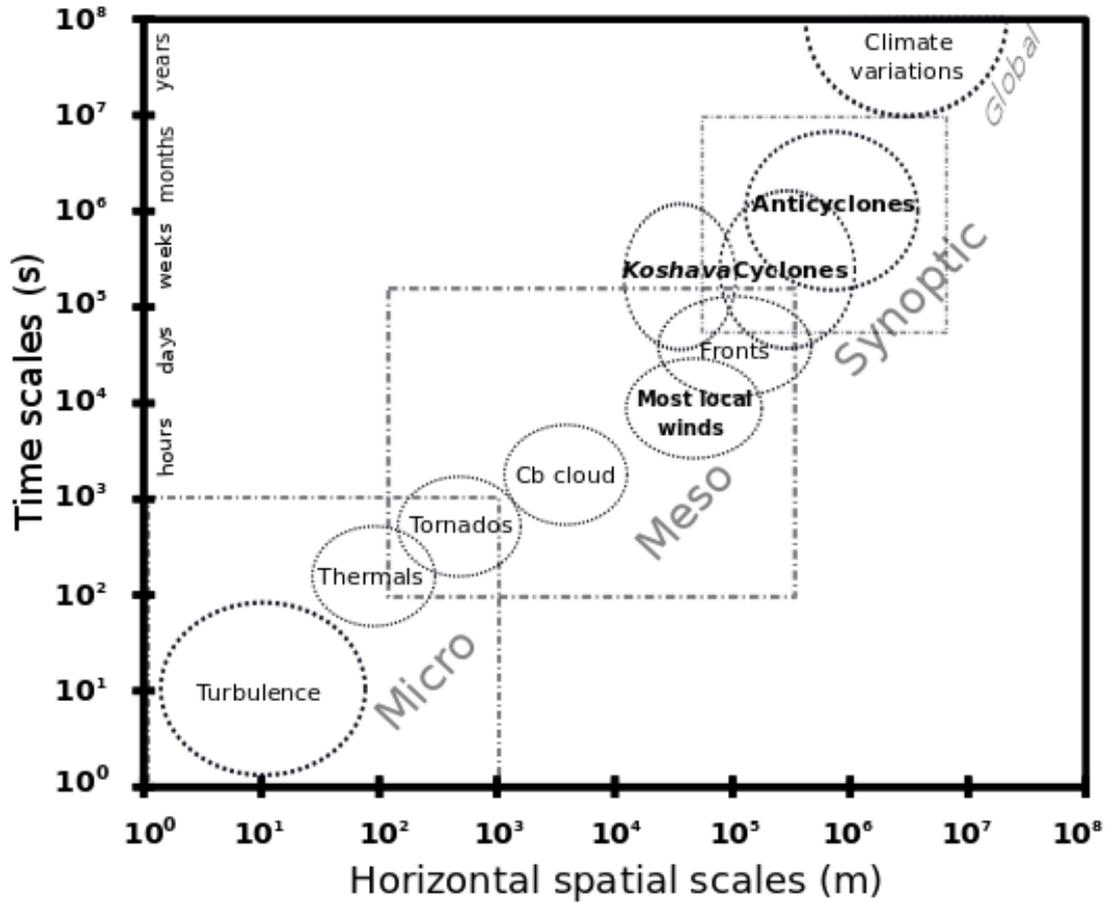
Figure 1.3. Time and horizontal spatial scales of the Koshava wind. Modified after Steyn *et al.* (1981) and Laing and Jenni-Louise (2011).

Koshava is the most dominant wind in most regions of Serbia. As such, the wind has a profound influence on weather and climate of the whole Balkan area. Moreover, Koshava is the main wind energy resource in Serbia (Gburčik *et al.*, 2006; Đurišić *et al.*, 2007). Koshava's high speeds and gustiness also play an important role in the control of air pollution in cities and in wind loadings on structures. Koshava is most frequent during the winter months, while the lowest

occurrence is detected in the summer season. The detailed literature review on Koshava is provided in Chapter 2.

1.3 Motivations and objectives

As mentioned in the previous section, Koshava is very important climatological factor in the Balkan region. Although being the most dominant local wind in Serbia and nearby territories, Koshava has not been extensively researched. The comprehensive overview of literature on the Koshava wind is presented in Chapter 2. Motivations for this research are numerous. The first and foremost motivation for this scientific investigation of Koshava is the need for better understanding of the dynamical and climatological characteristics of the Koshava wind. Despite of satisfactory dense network of weather stations in the KR with long history of meteorological measurements, there are only few scientific peer-reviewed studies on the Koshava wind. Bora wind, for example, has been extensively researched in the scientific literature (Grisogono and Belušić, 2009). Koshava, although not being less meteorologically significant than the Bora wind, has not received the same attention in the scientific community. This research is aimed to fill that gap in literature and put the Koshava wind on the same level with the other local winds in the region.

Most of the Koshava studies are based on meteorological data acquired from a single weather station in the KR. Although, the results are still very valuable indeed, it is questionable to which extent they are valid for the rest of the KR. Therefore, another motivation for this research is to analyze Koshava using data from weather stations which are located throughout the KR. Results obtained utilizing this approach are more reliable and versatile.

An additional motivation is to conduct a research that will produce results that can be directly applicable to industry and energy sectors. Namely, the results and findings will be discussed from two perspectives: (1) their theoretical importance for science, meteorology and climatology of Balkan region and Serbia in particular, and (2) their practical importance and applicability in industry.

The research objectives of this thesis are to investigate the following topics in details:

- Homogeneity analysis of wind data. The test for homogeneity will be performed on wind speed and wind direction time series in order to ensure that the measured wind data are accurate representation of the wind climate of the region. In a homogeneous data record, the only variabilities are due to climate. The homogeneity testing will point out to which extent the presented results on the Koshava wind are climatologically reliable. The sources of inhomogeneities in wind data shell be investigated and discussed.

- Long-term trends of the Koshava wind. The trend analysis will be focused on investigating the existence of trends of the following Koshava characteristics: (1) speed, (2) occurrence, and (3) length of the Koshava periods. Although containing important climatological information, the trend analysis of the Koshava wind has so far not been performed. Koshava's trends could have a direct impact on the wind energy sector in Serbia. Additionally, such an analysis is important for the better understanding of the climatology of Serbia and the whole Balkan region. Lastly, the trend analysis can provide valuable information concerning a

potential influence of both global and regional climate changes on the Koshava wind.

- Synoptic pressure systems that generate Koshava. It is a well known fact that Koshava is driven by an anticyclone usually located northeast of the Koshava region (KR) and a cyclone positioned over the Mediterranean Sea. However, it has not been investigated if Koshava can occur in the absence of these pressure systems or in a situation when only one of these two pressure systems is present. Characteristics of pressure systems which are creating Koshava will be investigated in details. The following questions, for example, will be addressed. What are the main characteristics of the anticyclones and cyclones that result in Koshava? What distinguishes anticyclones and cyclones that generate Koshava from pressure systems that do not result in Koshava? What features of these pressure systems are the most influential contributors to the Koshava wind? What are the typical positions and dynamics of these pressure systems in relation to the KR?

- Synoptic Koshava Index. Since Koshava is triggered by an anticyclone (an EA) and a cyclone (an MC), it should be possible to theoretically define an index that would depict the pressure differences between these two pressure systems and hence indicate the occurrence of the Koshava wind. The idea of this dynamical concept is important because the resulting index would directly connect synoptic and local weather phenomena, i.e. synoptic pressure systems and local wind.

- Mesoscale contributors to Koshava. Koshava will be investigated from a perspective of a gap flow wind phenomena. It has been known that

orography of the Balkan region (South Carpathian and Balkan Mountains in particular) is a key factor in Koshava's formation. The scientific literature on the gap flow winds shows that the across-mountain mean sea level pressure (MSLP) and across-mountain potential temperature differences are the most important factors that influence dynamical characteristics of orographic winds. These mesoscale contributors will be tested for the case of the Koshava wind and the results will be discussed. This analysis will quantify the influence of orography on the Koshava wind.

- Diagnostic model for Koshava's occurrence and speed. A linear regression (stochastic) model for diagnostics of the occurrence and speed of the Koshava wind will be constructed taking into account both synoptic and mesoscale Koshava contributors. The accuracy and reliability of the model will be tested and discussed.

- Koshava as a wind storm. Koshava is the strongest local wind in Serbia. The extreme nature of the Koshava wind will be investigated on an example of an extreme Koshava episode (EKE) which occurred at the end of January and the beginning of February of 2014. During this EKE Koshava's gusts reached 47 m s^{-1} in VR. The following questions shall be addressed. What caused such high wind speeds? What were the characteristics of synoptic and mesoscale Koshava's contributors before and during this extreme wind episode? The vertical structure of the Koshava layer will also be investigated.

- Numerical modelling of Koshava. EKE shall be numerically simulated employing two mesoscale numerical weather prediction models: Weather

research and Forecasting – Nonhydrostatic Mesoscale Model (WRF-NMM) and WRF-NMM on Arakawa-B grid (NMMB). In order to investigate the accuracy of forecasts, the results will be compared to the observations. This analysis is particularly important since the EKE was characterized by stable atmospheric stratification and numerical simulations of stable layers are challenging and scarce in literature.

- Koshava and snowdrifts. The above mentioned EKE will be used to develop and test a novel methodology for detection of snowdrifts in flat regions. The methodology is based on a postulate that there is a relationship between the location of snowdrifts, on one side, and horizontal wind gradients on the other side. Koshava predominantly blows during the cold part of the year and therefore the relation between Koshava and snowdrifts in the KR is important research topic with direct practical implication for the transportation and industry.

1.4 Expected contributions

Fulfillment of the objectives defined in the previous section will have numerous contributions to meteorology and climatology of Southeast Europe, Balkan region, and Serbia in particular. Some of these contributions as well as their practical importance are presented below.

Investigation of possible existence and strength of Koshava trends is of profound importance for climatology of the whole region. Namely, Koshava is one of the most important local winds in Serbia and large parts of Romania, Bulgaria, Hungary and Croatia. This study would be the first systematic long-term trend analysis of one local wind in the region of Southeast Europe and as such it

provides a valuable contribution to the field of climatology of local winds on both regional and global levels. Wind trend analysis in Southeast Europe and Balkan region has not being addressed in literature (McVicar *et al.*, 2012).

Climate change is a hot topic in climatology and media these days. For that reason, it is important to find causes of Koshava trends and their relation to global and regional climate changes. Determination of the trends of Koshava's occurrence and speed has practical application in wind energy sector and air quality. The connection to the wind energy sector is straightforward. Namely, positive trends of wind speed, occurrence and duration are favorable for wind farm developers. These trends are consequentially reflected as the upward trends of electricity production over the lifetime of a wind farm. Negative Koshava trends, on the other hand, might lead to decrease of electricity production and hence economic and financial losses for wind farm developers and owners. Negative (positive) Koshava trends decrease (increase) windiness of the region. Koshava trends would have negative (positive) effects on air quality in cities. Lastly, wind speed trends can result in trends of other meteorological quantities, such as evaporation (McVicar *et al.*, 2012). This relationship would further impact the agricultural sector.

Presenting outcomes of the homogeneity analysis of wind data series in the KR is particularly important for wind farm developers. Feasibility of the whole wind farm project depends on the quality and reliability of wind data. Wind measurements from tall meteorological masts installed on wind farm sites are typically few years long. For that reason, the onsite wind measurements are correlated with the meteorological measurements from weather stations to ensure the long-term reliability of onsite data. If the wind data from weather

stations contain large inhomogeneities, the correlated onsite wind measurements will be inhomogeneous and the estimated electricity production will be inaccurate. As the final consequence, the financial stability of the wind farm project is in jeopardy. Weather stations with largest inhomogeneities will be listed and the causes of inhomogeneities will be determined. The Sector of Meteorological Measurements at the Republic Hydrometeorological Service of Serbia could also use this information to improve the quality of their wind measurements. Finally, the homogeneity analysis presented in this thesis could be used by other researchers to estimate the uncertainties of their wind studies.

The first thorough analysis of synoptic pressure systems which trigger Koshava advances the current state of knowledge of the Koshava wind. Both dynamical and climatological characteristics of the EAs and MCs associated with Koshava could be beneficial in the weather forecasting sector. Forecasters might use these information to distinguish the EAs and MCs that generate Koshava from their counterparts which do not result in Koshava. The results of this investigation are highly reliable since the analysis will be based on a 43-year long data record. The EAs and MCs are among the most significant synoptic pressure systems in the Northern Hemisphere. Therefore, this study is important for the climatology on the global scales. There are no many scientific studies on these two pressure systems (the EAs in particular) which are based on such a long record of data. The analysis of Koshava contributors on mesoscales will result in the development of a simple statistical model for determination of Koshava's speed and occurrence. This multiple linear regression model can be directly used for Koshava's forecasting.

The Synoptic Koshava Index (SKI) is a novel approach in meteorology which aims to demonstrate how a synoptic scales phenomena can directly influence and dictate a meteorological phenomena on the local scales. The SKI is defined as the area-averaged and normalized MSLP between high-pressure (EAs) and low-pressure (MCs) regions. It will be demonstrated that the SKI is a good indicator of Koshava's occurrence. Therefore, the index could have direct application in weather forecasting and wind energy sector.

High winds inflict damage to structures, disrupt transportation, cause pedestrian discomfort and unfortunately can result in fatalities. The results of investigation of an extreme Koshava event can help in mitigating some of these negative effects of high wind speeds. For that reason, dynamics of the EKE of 2014 will be investigated in details. The event will also be reconstructed utilizing two numerical weather prediction models. This numerical analysis will test the capabilities of current weather prediction models in simulating high-intensity winds, wind gusts and stable boundary layers.

Methods for determination of deep snowdrifts in flat regions are scarce. The proposed methodology for identification of deep snowdrifts in flat terrains is based on the relationship between the horizontal gradients of wind speed and the snowdrift locations. The developed method could be easily implemented into the weather forecasting procedure. The accurate forecasts of snowdrift locations would be of great significance for the transportation sector and industry. The methodology is tested in the case of the EKE and the results are in good agreement with observations.

This doctoral thesis contains some unique findings about Koshava. The results of the research presented herein are published as three separate journal articles in

the leading meteorological journals. The research centered around Koshava trends, homogeneity of wind data series and their impact on wind energy sector in Serbia is published in the International Journal of Climatology (Romanić *et al.*, 2015a). The research on synoptic and mesoscale contributors to the Koshava wind has also been published in the same journal (Romanić *et al.*, 2015b). The results concerning the investigation of the EKE from 2014 are published in the Atmospheric Science Letters (Romanić *et al.*, 2015c). Some of the results are also presented at several conferences and published in their proceedings. These publications further contribute to already high reputation of the Serbian school of meteorology in the world.

1.5 Organization of the thesis

This thesis is written in the "monograph" format as specified by the Faculty of Physics at the University of Belgrade.

Chapter 1 provides a general introduction to the Koshava wind and the motivations behind this study. The expected outcomes and contributions of this research are also presented in this chapter. The next chapter contains the comprehensive literature review on local winds in the Balkan region with particular emphasis on the Koshava wind. Chapter 2 therefore documents the present state of knowledge on the Koshava wind. Mathematical tools and methodologies used to conduct this research are described in Chapter 3. The same chapter describes the input data used for all analysis presented in this thesis. The results concerning Koshava trends and homogeneity of wind data are given in Chapter 4. Applicability of these results in wind energy sector is also discussed. The research on synoptic and mesoscale contributors to the Koshava wind is given in Chapter 5. The SKI as well as the linear regression model for

Koshava's speed are also presented in Chapter 5. Chapter 6 addresses the EKE from 2014 and discusses the meteorological factors that led to it. A new methodology for identification of locations favorable for deep snowdrifts in flat areas is also presented in Chapter 6. The methodology was tested in the case of the above mentioned EKE of 2014. At the end, conclusions and recommendations for future research are provided in Chapter 7.

CHAPTER 2

2. Literature review

2.1 Local winds above Balkan Peninsula

Mediterranean Basin is the region with the largest number of different local winds. Its unique climate complemented with the mountain ranges that define the basin are favorable for development of many local winds. The list of named local winds in the Mediterranean is very long, probably numbering hundreds of winds. Most popular local winds in the Mediterranean Basin are portrayed in Figure 2.1. It is interesting to note that due to diversity of cultures and languages in Mediterranean, the same wind sometimes has different names in different regions over which it blows. For instance, the summer wind that blows from northwest over Greece, Aegean Sea and Turkey is called Etesian in Greece and Meltemi in Turkey. Descriptions of local winds presented in Figure 2.1 can be found in Heidorn (2007) and on the website of the Royal Meteorological Society (Royal Meteorological Society, 2015)

Figure 2.1 indicates that the southerly winds in Mediterranean are generally hot, bringing warm weather (red arrows). Zonal winds in the western Mediterranean are also associated with the increase of temperature (yellow arrows), but the increase is not as pronounced as in the case of the southerly winds. Northern

winds, on the other hand, bring cold weather (blue arrows). Local winds that are usually not followed by a significant change in weather conditions are indicated with the gray arrows.
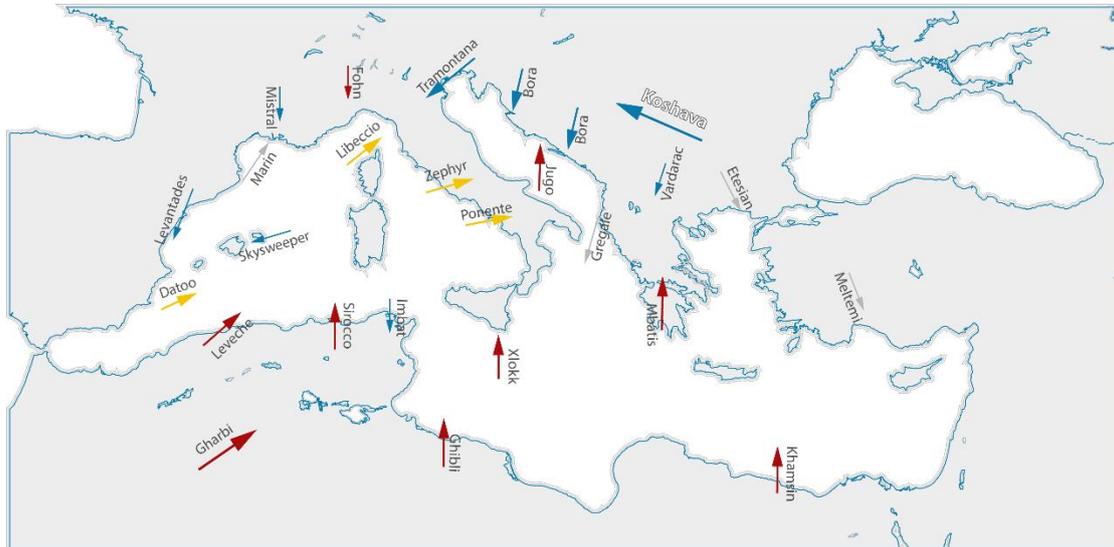
Figure 2.1. Local winds in the Mediterranean region.

The Balkan Peninsula is located in the southeastern part of Europe. Formally, the Balkan Peninsula is defined as the region south of the Sava and Danube Rivers. To simplify terminology, the Balkan Peninsula in this thesis will be defined as the region south of the Serbia-Hungary border (south of approximately 46°N latitude). The simplification comes from the fact that most of the local winds which will be described in this section, as well as the Koshava wind, can now be defined as the winds occurring over the Balkan Peninsula instead of constantly saying that these winds blow over Balkan region, Southeast Europe and southeast parts of the central Europe. The territorial difference between the formal definition and the new (modified) definition of Balkan Peninsula is minor.

Due to its specific geographical position, the Balkan region possesses several climate zones (Peel *et al.*, 2007). South parts of the Balkan Peninsula close to the Mediterranean Sea are characterized by temperate climate with dry and hot summers (Csa climate zone based on the Köppen-Geiger climate classification). Central regions of Balkan (central and south Serbia, parts of Croatia and Bosnia and Herzegovina, and western regions of Bulgaria and Romania close to the Danube River) also have temperate climate with dry, but more mild summers (Csb) compared to the Csa climate zone. North and northeast parts of the Balkan region are characterized by cold climate and the negative temperatures in the coldest month (Dfb). Summers are warm and the region is typically without dry season. Mountain peaks above 2000 m above ground (a.g.) are the regions characterized by the ET climate (polar tundra climate). Diversity of climate zones, numerous water surfaces surrounding the peninsula, as well as the mountains that intersect the Balkan region are the result in a large number of local winds that form and blow above the Balkan Peninsula. Local winds typical for the Balkan region are: Bora, Etesian, Jugo, Vardar, and Koshava. The last one – Koshava wind - represents the main focus of research of this theses. Prior to presenting the literature review on Koshava, a brief description of other local winds in Balkans is provided.

Bora is a cold and gusty wind that blows from north and northeast over the costal regions of Croatia (Figure 2.1). The wind is most frequent in cold part of the year. Bora is probably the most researched local wind in the region (Prtenjak *et al.*, 2010). Horvat *et al.* (2007) reported that the costal slopes of Velebit Mountain represent the region with the highest occurrence of Bora. The mean Bora speed in this region is 11 m s^{-1} with the highest frequency of occurrence in December and the lowest in June (Makjanić, 1978). There are three types of the Bora wind

20

depending on the synoptic factors that lead to its formation: cyclonic, cyclonic-anticyclonic and anticyclonic Bora (Pandžić and Likso, 2005; Grisogono and Belušić, 2009). It is common that Bora in its early stage is cyclonic, anticyclonic in its dissipation stage, and the cyclonic-anticyclonic type in between (Pandžić and Likso, 2005). Sometimes Bora can also be associated with the passage of atmospheric front (Grisogono and Belušić, 2009). This type of Bora is similar to the cyclonic type and it is generally stronger than the anticyclonic Bora (Prtenjak *et al.*, 2010). Bora wind is a typical example of a downslope wind with characteristics of a gap flow (Mayr *et al.*, 2007; Grisogono and Belušić, 2009). Another local wind that occurs in the same region as Bora is Levant. However, Levant is more easterly orientated compared to Bora (Peros *et al.*, 2009) and is mostly observed in the period February-March (Tomasevic *et al.*, 2014).

Etesian (or Meltemi) is a northern wind typical for the eastern Mediterranean region in the warm part of the year. Although it sometimes possesses downslope characteristics typical for the Bora wind (Koletsis *et al.*, 2009), Etesian is a foehn (föhn) wind (Ziv *et al.*, 2004). This dry wind prevents the formation of clouds and results in clear sky. In addition to being an important climatological factor in the eastern Mediterranean (Tyrlis and Lelieveld, 2013), Etesian has a significant environmental impact as it regulates air quality in the costal region of south Balkan (Kalabokas *et al.*, 2008).

Jugo is a warm and humid southerly and southeasterly wind that occurs in the Adriatic region, especially in Dalmatia. The wind originates in the Sahara dessert region from which it crosses the Mediterranean Sea (where it is called Sirocco) and finally arrives in the area of the Adriatic Sea (where it is called Jugo). Jugo is caused by the MCs that are formed in the Gulf of Genoa and afterwards have

easterly trajectories (Tutiš, 2002). After Bora, Jugo is the most common wind in the Adriatic region (Jeromel *et al.*, 2009). Numerical modeling of Jugo is performed by Malačič *et al.* (2012).

Vardar (Vardarac) is a cold northwesterly wind that blows over northern Greece and Macedonia. It is a downslope wind that is additionally enhanced by the channeling effect of the Morava-Vardar basin ("Wind of the World," 2015). The wind is most frequent in the winter when there is the pressure gradient directed from east Europe towards the Aegean Sea.

There are several reasons for the above description of the major local winds in the Balkan region. Firstly, prior to analyzing meteorological characteristics of any local wind in a region, it is beneficial to be knowledgeable of the characteristics of other local winds in that same geographical region. Secondly, different local winds can sometimes possess a number of similar characteristics. A good example of this principle are Bora and Koshava winds. These two local winds have many different features, but nevertheless both Bora and Koshava can be classified as the downslope and gap winds, both are gusty and highly turbulent and both winds have similar synoptic scale drivers. One more example of the above-stated principle could be a certain similarity between Jugo and Koshava. These two local winds have different climatology, but both winds are driven by the same low pressure systems – the MCs. Lastly, it is important to perform a comprehensive literature review on other local winds in the region in order to be able to identify potential gaps in the body of literature on the Koshava wind.

2.2 Dynamics of downslope and gap flow winds

Downslope winds are not the same as katabatic winds. Katabatic winds are flows driven by cooling of surface air over mountain sides whereas downslope winds are deeper and refer to a larger air mass that is forced to go over mountain (Durran, 2003). Downslope winds, for example, include Bora (see previous section), chinook, and Koshava. Since mountains between Wallachia Valley and KR have many gaps (e.g. Danube River basin) and passes (see Figure 1.1, Figure 5.1 and Section 5.4), Koshava possesses the characteristics of a gap flow wind. Gap winds are low level jets of air with high speeds compared to the flow that enters the gap due to the Venturi effect. The dynamics of the gap flows, however, is not entirely determined by the Venturi effect because in the real atmosphere there is no a rigid lid and therefore the strongest winds typically occur at the exit of the gap, not inside the gap. Three-dimensionality of the flow in real atmospheric conditions can also lessened the Venturi effect. Some of the widely known gap flow sites in Europe are Brenner Pass with the Wipp Valley and Innsbruck (Austria, Seibert, 1990; Mayr *et al.*, 2007) and Vratnik Pass at Senj (Croatian Bora wind, e.g. Grisogono and Belušić, 2009).

The mechanisms leading to downslope and gap flows are deeply investigated in literature (e.g. Scorer, 1952; Overland, 1984; Seibert, 1990; Zängl, 2002a; Mayr *et al.*, 2007; Drechsel and Mayr, 2008). It has been found that the main drivers for these winds are the mesoscale pressure gradient over the mountain range (ΔP), across-mountain potential temperature difference ($\Delta \theta$), the descent of isentropes downstream from the crest ($\Delta \theta'$), and wind speed at higher levels.

These factors are portrayed in Figure 2.2 and applied for an idealized and simplistic analysis of the Koshava wind.
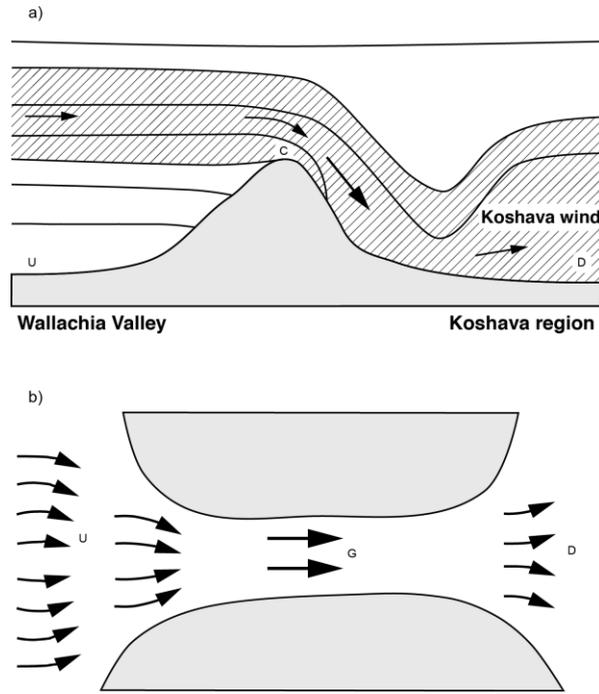
Figure 2.2. Schematic representation of (a) downslope (after Plavcan *et al.* 2013) and (b) gap flow winds. Symbols U and D denote upstream and down stream locations, respectively, from crest (C) or gap (G). The solid lines in (a) are isentropes. The black arrows are wind vectors.

With respect to Figure 2.2, the MSLP and potential temperature differences (i.e. ΔP and $\Delta\theta$ or $\Delta\theta'$, respectively) can than be defined as (Drechsel and Mayr, 2008):

$$\Delta P = P_U - P_D, \tag{2.1}$$

$$\Delta\theta = \theta_U - \theta_D, \tag{2.2}$$

$$\Delta\theta' = \theta_{C,G} - \theta_D, \tag{2.3}$$

with the subscripts U, D, C and G indicate upstream, downstream, crest and gap locations. Therefore, during downslope and gap flow winds (such as the Koshava wind), typically $\Delta P > 0$ whereas $\Delta\theta < 0$ and $\Delta\theta' < 0$ (e.g. Gaberšek and Durran, 2004; Mayr *et al.*, 2007; Drechsel and Mayr, 2008).

2.3 Climatological studies on the Koshava wind

The first scientific studies related to the Koshava wind were conducted by Vujević (Vujević, 1933; Vujević, 1948) and Sergijevski (Sergijevski, 1940). Based on a 45-year long set of data (1897-1932), Vujević (1933) analyzed the frequency of occurrence of all winds above BG. He concluded that Koshava was active in 26.8 % of the time during the winter and spring seasons and 28.7 % of the time in the fall season. In the summer, however, Koshava was present in only 13 % of the time. He also reported that Koshava in the winter, spring and fall months is more frequent than calms. In his second study, Vujević (1948) again inspected the frequency of occurrence of winds and calms in BG, but this time analyzing only data for January and July in the period 1921-1940. His findings showed that Koshava in BG has ESE (14.6 % of the time and mean speed of 6 m s^{-1}) and SE (13.9 % of the time and mean speed of 4.5 m s^{-1}) directions in January. Koshava's occurrence in July was below 10 % of the time and its mean speed was 2.2 m s^{-1}. Sergijevski (1940) analyzed winds above BG for the periods 1906-1907, 1925-1930 and 1937-1939 (11 years of data in total). That study, however, is not available anymore.

Milosavljević (1950a) in his PhD thesis described physical characteristics of winds above BG. He processed data for the period 1920-1945 (26 years) and reported that Koshava (ESE and SE wind directions) in BG was mostly active in November (35.7 %) and December (32.2 %). January and March followed with 28.9 % and 27.5 % of the time, respectively. Koshava in February and April was active in 26.5 % and 21.8 % of the time, respectively. The small differences between the results by Milosavljević (1950a) and Vujević's findings (Vujević 1948; Vujević, 1933) are due to the fact that their data cover different time periods. Milosavljević

(1950a), furthermore, found out that Koshava was strongest when it was coming in from ESE direction with the mean annual wind speed of 4.2 m s^{-1} whereas Koshava from the SE direction was for 1 m s^{-1} weaker. The highest Koshava speed occurred in March (5.8 m s^{-1}) and January (5.4 m s^{-1}). The mean maximum Koshava speed followed the same monthly pattern as the Koshava's mean speed. Namely, the strongest mean maximum Koshava speed occurred from the ESE direction in March (12 m s^{-1}) and January (11.9 m s^{-1}), November (11.8 m s^{-1}) and December (10.6 m s^{-1}). The mean maximum Koshava speeds from SE direction were slightly weaker. The absolute maximum Koshava speed in BG in the period 1920-1945 was 27 m s^{-1} and it occurred in November (from SE direction) and December (from ESE direction). Milosavljević (1950a) documented that the ESE Koshava winds are on an annual basis for 0.9 °C colder than the SE Koshava winds. Koshava in March usually lasted between 2 and 4 days, but there were situations when Koshava was active for 22 days. He also reported that Koshava caused temperature rise in months from October to April. Lastly, Milosavljević (1950a) analyzed influence of the Koshava wind on absolute and relative humidly and cloud cover. He found out that absolute humidity is generally increasing, relative humidity decreasing and that there is no well defined relationship between Koshava and cloud cover. It can be seen that in all these studies Koshava was analyzed based only on wind data from the BG station. The rest of the KR had not been taken into consideration.

A number of research on Koshava was published in the period from the 1970s to the 1990s (Stanojević, 1959; Milosavljević, 1972; Milosavljević, 1975; Čadež, 1976; Milosavljević, 1976; Ćurić, 1978; Ćurić, 1980; Radosavljević and Vojnović-Kljaić, 1985; Vukmirović, 1985a). Čadež (1976) proposed an interesting classification of

Koshava wind in 1976. He defined Koshava days as wet or dry depending on the prevailing influence of MCs or EA, respectively.

Several journal articles on Koshava's climatological characteristics were published after 1995 (Unkašević *et al.*, 1998; Unkašević *et al.*, 1999; Unkašević *et al.*, 2007) Based on 5 years of instantaneous maximum wind speed data (1971-1975) from two weather stations in BG, Unkašević *et al.* (1998) determined the best statistical distributions for the instantaneous and mean (hourly and seasonal) wind data. They also showed that there is a linear correlation between the maximum hourly and the hourly mean wind speeds. Moreover, they found out that there is a negative correlation between gustiness factor, on one side, and the hourly mean Koshava speed, on the other side. The paper by Unkašević and her colleagues from 1999 (Unkašević *et al.*, 1999) is very similar to their study published in 1998 (Unkašević *et al.*, 1998). Besides confirming previously obtained results, they presented some dynamical features of Koshava in the lower troposphere above BG (see Section 2.4). Analyzing 31 consecutive day with Koshava wind in 1972, Unkašević with her colleagues concluded that the mode of the mean hourly Koshava speeds was in the interval from 6.25 to 6.75 m s^{-1}. The maximum hourly wind speeds were mostly between 14 and 15 m s^{-1}. Their spectral analysis of Koshava showed a 5-day peak in the spectrum which corresponds to synoptic time scales.

Unkašević and Tošić (2006) prepared a monograph on Koshava in which they summarized some of the literature on the Koshava wind and presented in details results of several Koshava studies (i.e. Petrović, 1977; Vukmirović, 1997; Unkašević *et al.*, 1998; Unkašević *et al.*, 1999; Lazić and Tošić, 2000; Unkašević *et al.*, 2007). Only climatological parts of the monograph are discussed in this

section. Unkašević and Tošić (2006) analyzed wind data for the period 1888-1991 (103 years) and showed that after calms (18.3 % of the time), Koshava from the SE direction is the most frequent wind above BG (14.5 %). The strongest Koshava winds were occurring in March. These winds were coming in from the ESE direction with the mean speed of 5.9 m s⁻¹. Although analyzing much longer time series of data compared to Vujević (1948) and Milosavljević (1950a), climatological findings in all these studies are in good agreement. Vukmirović (1997) showed that Koshava is an efficient ventilator that cleans the atmosphere in BG of pollutants.

2.4 Dynamical and numerical studies on the Koshava wind

Koshava possesses characteristics of a downslope wind with the particular features of a gap flow (Flamant *et al.*, 2002; Mayr *et al.*, 2007). Although having the gap flow characteristics, Koshava has not been deeply investigated in this context. Küttner (1940) defined Koshava as being a katabatic windstorm stronger than foehn, but weaker than Bora.

Analyzing the pressure gradients in the KR, Radosavljević and Vojnović-Kljaić (1985) used multiple linear regression to obtain diagnostic equations for the mean hourly ($\bar{V}_K$) and maximum hourly ($\hat{V}_K$) velocities for the Koshava wind, i.e.:

$$\bar{V}_K = 3.445 + 0.179X_1 - 0.006X_2 + 0.627X_3, \tag{2.4}$$

$$\hat{V}_K = 7.434 + 0.387X_1 + 0.018X_2 + 1.501X_3. \tag{2.5}$$

Here, X_1 is the surface pressure gradient over 500 km (in hPa per 1000 km), X_2 is the curvature radius of prevailing pressure center (in km⁻³) and X_3 is Laplacian of the surface pressure (in hPa per (500 km)²). The model is fairly accurate as the mean absolute deviation of the mean hourly Koshava speed was 1 m s⁻¹. It was

operationally used in the Republic Hydrometeorological Service of Serbia. Their study, however, is restricted to the period October 1982-March 1983 and they analyzed Koshava based only on data from the BG station.

Analyzing several case studies and defining Koshava as a low-level jet, Vukmirović (1985b) demonstrated that the level of the maximum Koshava speed is between 200-300 m a.g. in the south parts of the KR (close to Morava River), and between 500-600 m a.g. in the northern part of the KR. Furthermore, he concluded that the vertical temperature lapse rate in the Koshava surface layer is superadiabatic, followed by the adiabatic lapse rate. The maximum Koshava speeds occurred at the top of the adiabatic layer. The atmosphere above the level of maximum Koshava wind speed is stable with one or two inversion layers. The inversions were due to the passage of elevated warm fronts or due to the advection of warm air in the front of the MCs (Vukmirović, 1985b). Unkašević *et al.* (1999) reported that the maximum Koshava speeds above BG during the 31 consecutive Koshava day in 1972 occurred in the layer between 200 and 300 m a.g. Since the Koshava was decreasing moving upwards from that layer, they also concluded that Koshava behaves as a low-level jet (Vukmirović and Merkle, 1991). Furthermore the study reported that Koshava was followed with surface or elevated inversions.

Petrović (1977) analyzed the characteristics of an EKE that occurred in the period October 16-18, 1976. Wind gusts during this frontal type of Koshava (Vukmirović, 1985b) were above 30 m s^{-1}. Koshava was strongest when there was a pronounced positive pressure difference between east and west KRs. An increase of pressure in the west parts of the KR coincided with weakening of Koshava. The strongest Koshava speeds were observed in VR and Veliko

Gradište (VG). Koshava started with surface temperature inversion (October 16, 1976, 01 h). The inversion was lifted during the EKE (Vojnović-Kljaić and Popović, 1978). Synoptic situation during a non-frontal Koshava event in the period December 5-6, 1996 is described by Unkašević and Tošić (2006). The strongest gusts in VR were reaching 28 m s^{-1}.

Lazić and Tošić (2000) performed a numerical modeling of Bora and Koshava winds with the aim to determine the sensibility of forecasted trajectories on the frequency of input data. They showed that Koshava was less sensitive to the frequency of input wind data than Bora. When the frequency of input data was 15 min, 30 min or 1 h, the mean relative error of forecasted Koshava trajectories was below 5 %. They demonstrated that trajectories calculated from the analysis wind data (each 12 h) are inaccurate. The horizontal resolution in their simulations was 28 km with only 16 vertical layers.

Todorović and Paskota (2002) analyzed the relationship between Koshava speed in BG and pressure difference between BG and Negotin weather stations (as described by Eq. (2.1)) for eight Koshava situations in 1994. Their linear regression model of mean hourly ($\bar{V}_K$) and maximum hourly ($\hat{V}_K$) Koshava speeds is:

$$\bar{V}_K = 2.7905 + 0.4604\Delta P, \qquad\qquad (2.6)$$

$$\hat{V}_K = 5.8269 + 1.0957\Delta P. \qquad\qquad (2.7)$$

Model's coefficients of determination (R^2) are 0.414 and 0.513 for $\bar{V}_K$ and $\hat{V}_K$, respectively. Their sample, however, is too small in order to draw statistically reliable conclusions about the quality of the model.

2.5 Literature review summary

The overall conclusions of the literature review can be summarized as follows:

- There are at least ten local winds above Balkan Peninsula and Koshava is among the most pronounced and most vigorous.

- The mesoscale factors that drive downslope and gap flow winds are identified in literature, but not applied for the Koshava wind case.

- Most of the climatological studies on Koshava wind is based on wind data from weather stations in BG. A comprehensive climatological Koshava study that will cover the whole KR has not been performed. Koshava trends have not been addressed.

- Wind data in climatological studies were not inspected for inhomogeneities.

- Many studies concluded that Koshava is a mutual product of the EAs and MCs. However, dynamical and statistical quantification of that relationships has not been documented.

- Radosavljević and Vojnović-Kljaić (1985) constructed a statistical model for prediction of Koshava speed. However, their model is based on only 6 months of data and moreover it was developed based only on wind data from BG station.

- Most of dynamical studies on Koshava was concentrated on analyzing vertical structure of Koshava in the lower troposphere above BG.

- Koshava as a gap flow windstorm has not been investigated from dynamical point of view.

- There has been only one numerical study on Koshava.

- Experimental wind tunnel tests of the Koshava wind have not been performed so far.

CHAPTER 3

3. Methodology

This chapter introduces the research methodology used in this study. The subsequent sections provide procedures, methods and techniques used for data analysis and development of theories.

3.1 Homogeneity tests

Inspecting the homogeneity of data sets used in climatological studies has become an important element of climatological studies (e.g. Alexandersson, 1986; Brohan *et al.*, 2006; Wan *et al.*, 2010). By definition, a series can be considered as homogeneous "if its variations are caused only by variations in weather and climate" (Conrad and Pollak, 1962). Usual reasons for inhomogeneities of data include instrumental inaccuracy, changes in the surroundings of the weather station and station relocation, as well as changes in measurement techniques and procedures. Most data series are not found to be homogeneous (Auer *et al.*, 2005), but accounting for daily or sub-daily inhomogeneity in data sets is a challenging task, and as of yet, the World Meteorological Organization has not published any standards or recommendations on how researchers should approach such a task (Costa and Soares, 2009). Instead of adjusting the data series, anomalies have to be detected, reported, and only then can their influence on the climate series be evaluated.

The wind data series are tested for homogeneity using the ReDistribution Method, not only in its basic form (Petrović, 2006), but also in its modified form (Petrović, 2011). The method is based on comparing two distributions of values from two consecutive series of equal window data span. Half the sum of all differences between each category ($\sum_{i=1}^{n}|d_i|/2$) is the number of redistributed frequencies. The ReDistribution Index (RDI) is then:

$$\text{RDI} = \frac{1}{2N}\sum_{i=1}^{n}|d_i| \qquad (3.1)$$

where n is the number of categories and N is the total number of values in distribution.

Theoretically, the RDI might have values from zero (for identical distributions) to one (where the second set of values are completely redistributed, and do not overlap the first range of values). Since distributions of values over the fixed window data span vary from one point to another, the RDI values are calculated as series of values from the record number that equals to double window data span to the end of series. Peaks of the RDI series indicate the largest differences between the two distributions and thus potential inhomogeneity. Each dataset under consideration consists of two parallel series, wind direction and wind speed. Thus, the ReDistribution Method is used on each series, giving the complete picture of homogeneity of the collected data.

The criteria for selecting RDI peaks depends upon the significance of redistributions. The basic form of the ReDistribution Method shows in practice (Petrović, 2003) that significant RDI peaks are at least 0.15, meaning that 15 % of data are redistributed due to inhomogeneity. The modified form of this method

34

uses only selected subsets of the series, focusing on specific causes of inhomogeneities. Thus, the data series are also examined for distributions of direction frequencies using a subset of significant wind speed range. Such an analysis might reveal potential inhomogeneities of wind direction series for strong winds. The basic form of the ReDistribution Method reveals more general inhomogeneities in the dataset. Wind series, though, are specific for their coupled series of direction and speed. Therefore, any survey of data homogeneity must also deal with both series in order to detect the nature of any detected inhomogeneities. If both series have RDI peak values at approximately the same point in time, the anomaly is likely caused by a relocation of the measurement site, a change in the instruments used, or a change in observers. On the other hand, if the RDI peaks only in one of the two series, it might indicate other causes (i.e. possible inhomogeneity in the direction only, it might indicate change of obstacles around the measurement site, or a wind vane misalignment, while wind speed inhomogeneities usually come from changes in calibration or sensitivity of an instrument).

The settings of the ReDistribution Method values were chosen to show inhomogeneities on a large temporal scale in order to avoid high noise of the RDI series. The moving window span was chosen to be 4 years, represent a fair range of climate variation (Petrović and Curley, 2008). Therefore, time of RDI peaks return problems with homogeneity occurred four years earlier. The number of categories of wind direction included in this study was 16, which was in accordance with distinguishable wind directions in the series. The number of speed categories included in this study was 8, which was in accordance with the optimal performances of this method (Petrović and Curley, 2008). The wind

speed categories were given in steps of 2 m s^{-1}, merging all wind speeds greater than 14 m s^{-1} into one category for extremely strong winds.

In order to detect inhomogeneities for strong winds, the modified form of the ReDistribution Method was applied to data where wind speed was at least 5 m s^{-1}. Such wind speeds result from synoptic scale systems, and many local influences such as instrument siting and sensitivity can be disregarded. Thus, all detected potential anomalies would be thought to come from serious changes in the calibration of instruments and the wind vane misalignment. The settings for the modified form of the ReDistribution Method included the moving window span of 2000 records that are usually taken within four years, which is approximately the same period used for the moving window span in the basic form of the method. Note that the modified form of the method does not follow the temporal scale, but rather strictly follows the number of records for the moving window. The inhomogeneities found in the modified form of the method are clearly indicated. The homogeneity testing was performed in MS Excel software.

The results of the homogeneity analysis are presented in Chapter 4.

3.2 Trend analysis

The Mann-Kendall test for trend (Mann, 1945; Kendall, 1970) and Sen's slope estimates (Sen, 1968) have been used to detect and estimate trends in the time series of the wind data. Both methods have been used in many climatological studies (e.g. Hisdal *et al.*, 2001; Domonkos *et al.*, 2003; Jaagus, 2006) and wind trend analysis (e.g. Bakker and Hurk, 2012; Tyrlis and Lelieveld, 2013; Bakker *et al.*, 2013; Dadaser-Celik and Cengiz, 2013).

Mann-Kandall test is based on the assumption that the data values, x_i, of a time series can be accurately described with the model

$$x_i = f(t_i) + \varepsilon_i. \tag{3.2}$$

Here, $f(t)$ is a continuous monotonic function of time t and ε_i is the residual. The two-tailed Mann-Kendall test tests the null hypothesis (H_0) of trend absence in the time series, against the alternative of the trend (H_1). In this case, the result of the test is returned in $H_1 = 1, 2, 3$ or 4 indicating a rejection of the null hypothesis at the a significance level, where $a = 0.1, 0.05, 0.01$ and 0.001, respectively. $H_1 = 0$ indicates a failure to reject the null hypothesis at $a = 0.1$ significance level. For example, at the significance level of 0.05 there is a 5 % chance that the values x_i are randomly distributed and existence of a monotonic trend is very probable.

The Mann-Kendall test statistics, S, can be represented by

$$S = \sum_{i=1}^{n-1} \sum_{j=i+1}^{n} sgn(x_j - x_i), \tag{3.3}$$

where x_j and x_i denote the annual values in years j and k, respectively, n is the total number of years and sgn is the sign function. For $n > 10$ statistics is Gaussian with the mean value of zero and variance (σ) given by the following equation:

$$\sigma = \frac{1}{18} \left(n(n-1)(2n+5) - \sum_{k=1}^{M} t_k(t_k - 1)(2t_k + 5) \right). \tag{3.4}$$

Here t_p is the number of data values in the kth group and M is the total number of tied groups. Finally, using values of S and σ, the test statistic Z is equal to

$$Z = \begin{cases} \dfrac{S-1}{\sqrt{\sigma}}, & S > 0, \\ \quad 0, & S = 0, \\ \dfrac{S+1}{\sqrt{\sigma}}, & S < 0. \end{cases} \qquad (3.5)$$

Sen's test is a nonparametric method to estimate the magnitude of a trend's slope. It is applicable if the data in the time series are equally spaced. Sen's slope (Q) is the median of individual slopes (Q') computed for each time period, i.e.:

$$Q' = \frac{x_j - x_k}{j - k}, \qquad (3.6)$$

where x_j and x_k are data values at time j and k, respectively and $j > k$. Sen's slope estimate is then equal to:

$$Q = \begin{cases} Q'_{\left[\frac{N+1}{2}\right]}, & \text{if } N \text{ is odd,} \\ \dfrac{1}{2}\left(Q'_{\left[\frac{N}{2}\right]} + Q'_{\left[\frac{N+2}{2}\right]}\right), & \text{if } N \text{ is even,} \end{cases} \qquad (3.7)$$

where N is the number of calculated slopes. The whole trend analysis was conducted in MS Excel 2013.

For the trend analysis. Koshava wind speeds were grouped into two categories: (1) all wind speeds and (2) wind speeds above 5 m s^{-1} (named K5 winds). Since the lower wind speeds are particularly influenced by measurement inaccuracies and inhomogeneities (see Section 3.1), trends of the K5 winds have been analyzed separately. High wind speeds are especially important in wind energy sector, since the cut-in wind speed for many wind turbines is approximately 5 m s^{-1}. Trend analyzes were conducted for the mean annual wind speeds, the annual number of days when Koshava was blowing, and the annual number of the Koshava periods. The trend analysis results are presented in Chapter 4.

3.3 A cyclone and anticyclone detection and tracking scheme

The University of Melbourne automatic cyclone tracking scheme is used for the detection and tracking of Koshava cyclones and anticyclones from the NCEP/NCAR reanalysis 1 MSLP data (Kalnay *et al.*, 1996). The details of the scheme's algorithm are given in Murray and Simmonds (1991a), Murray and Simmonds (1991b), Simmonds *et al.* (1999) and Lim and Simmonds (2007). Therefore, this section provides an overview of the main features of the scheme. The scheme's algorithm is composed out of two main steps.

First, using the bicubic spline interpolation, the MSLP data are transformed from a latitude-longitude grid to a polar stereographic array. The second step consists of the actual search for lows and highs. The geographical region over which the search for cyclones is conducted includes the area from 2°E to 35°E (longitude), and from 30°N to 48°N (latitude). The area in which the search for anticyclones is performed is delineated by the coordinates of 20°E to 65°E (longitude), and 40°N to 60°N (latitude). The scheme settings for the detection of highs were different than the settings used for the detection of lows. The input parameters for the scheme are described below.

The scheme settings for cyclone detection were very similar to those used by Flocas *et al.* (2010) and Pinto *et al.* (2005) in their study of cyclonic tracks over the Mediterranean region. The configuration for the anticyclone case is similar to the setup used by Pezza and Ambrizzi (2003). The stereographic grid has 121×121 points for the cyclone case and 161 × 161 points for anticyclones. In order to minimize the influence of any noise that may be present in the reanalysis data, the diffusive smoothing of pressure and topography over a radius of 2° for

cyclones and 4° for anticyclones (lows above 1500 m have been excluded from the search) is employed. The strength of a cyclone (or anticyclone) is associated with a maximum (or minimum) of the Laplacian of its central pressure, $\nabla^2 P_C$ (Petterssen, 1956). A cyclone (anticyclone) is detected at any point at which $\nabla^2 P_C = \frac{\partial^2 P}{\partial x^2} + \frac{\partial^2 P}{\partial y^2}$ is larger (smaller) than it is at any of 4 (8) surrounding grid points. Since most of the MCs are weak systems in their early stage of development (Trigo *et al.*, 1999), no strength criteria has been set for the minimum value of $\nabla^2 P_C$. The lows and highs that have been searched for are: strong closed cyclones/anticyclones (C0/A0), weak closed cyclones/anticyclones (C10/A10), and strong open depressions/ridges (C1/A1). A pressure system was considered "strong" based on the "concavity criterion", i.e. $\nabla^2 P_C > 0.6$ hPa over 2 (° latitude)^2 for cyclones, and $\nabla^2 P_C < 0.2$ hPa over 2 (° latitude)^2 for anticyclones. The cyclone/anticyclone effective radius (*R*) and depth (*D*) was then calculated as (Lim and Simmonds, 2007):

$$R = \sqrt{\frac{\sum_{i=1}^{N} r_i}{N}}, D = \frac{R^2 \nabla^2 P_C}{4}. \tag{3.8}$$

Here, r_i is the distance from the pressure system center to the points where $\nabla^2 P_C = 0$, and N is the number of radii (the radial increment of 0.5° latitude and 12 radial directions was used). The depth of a pressure system is a good measure of its kinetic energy (Simmonds and Keay, 2000). The scheme also provides the coordinates of the pressure system centers. Using this information, the distances between the cyclone/anticyclone centers and the weather stations in the KR are calculated on the WGS-84 ellipsoidal Earth using Vincenty's method (Vincenty, 1975). The code for calculation of distances between pressure systems and weather stations was written in Matlab® 2014 software, whereas the cyclone and

anticyclone identification and tracking model was created (and provided) in Fortran 77 programing language.

The trajectories of cyclones were also determined. See Murray and Simmonds (1991a) and Simmonds *et al.* (1999) for details about the tracking algorithm used. Tracks are estimated by calculating the probability that a particular system at time t is the same system that was observed at the time $t - 6$ hours. The prediction velocity u_{pred} at time t is given by (Kouroutzoglou *et al.*, 2011):

$$u_{pred} = (1 - w_{steer})u_M + w_{steer}(f_{steer}u_S), \qquad (3.9)$$

where u_M is the velocity of the system during the previous reanalysis interval (i.e. $t - 6$ hours), $f_{steer}u_S$ is the scaled steering velocity u_S (the scaling factor f_{steer} of 2 has been used (Simmonds *et al.*, 1999)), and $w_{steer} = 0.6$ is the weighting factor for u_S.

Due to the time resolution of the NCEP/NCAR reanalysis 1 data, the tracking scheme provides outputs at 6-h intervals. Although the wind speed measurements are available at each hour, matching the Koshava wind speeds with the scheme outputs could only be performed for 00, 06, 12 and 18 hour measurement terms. The results regarding the Koshava cyclones and anticyclones obtained using the above identification and tracking scheme are given in Chapter 5.

3.4 Bayesian information criterion and distribution overlap

The Bayesian information criterion (BIC) is a statistical method for detection of the best suitable distribution to fit observational data. The BIC is defined as (Schwarz, 1978):

$$\text{BIC} = -2 \ln \hat{L} + k \ln n \qquad (3.10)$$

where n is the number of observations, k is the number of parameters in the model ($n \gg k$) and $\hat{L}$ represents the likelihood of an observation for a candidate model. The candidate model with the lowest BIC value is preferred.

The overlaps between two distributions are calculated using Weitzman's method (Weitzman, 1970). The employed equation to calculate the overlap (OVL) is

$$\text{OVL} = \int_{-\infty}^{+\infty} \min\big(f(x), g(x)\big)dx, \qquad (3.11)$$

where *f(x)* and *g(x)* are the probability density functions of two distributions (PDFs) for which the overlap wants to be calculated. The method is essentially computing the overlap area of two PDFs. Hence $0 \leq \text{OVL} \leq 1$.

These two statistical methods are used to determine the best fits for ΔP and $\Delta \theta$ sets, and to calculate overlaps between distributions describing Koshava and "no-Koshava" cases. The parameters of statistical distributions are denoted as follows: μ - the location parameter, σ - the scale parameter, ν - the shape parameter. The codes are written in Matlab® 2014 software. The results are presented in Chapter 5.

3.5 Statistical methods for derivation of the Koshava stochastic equations

Deterministic equations for mean hourly Koshava speeds ($\bar{V}_{Ki}$) are derived using the multiple linear regression model, *viz.*

$$\bar{V}_{Ki} = \beta_0 + \sum_{k=1}^{K} \beta_k f_k (X_{i1}, X_{i1}, \dots, X_{ip}) + \epsilon_i, \quad i = 1, 2, \dots, n. \qquad (3.12)$$

In this equation, β_k is the kth coefficient whereas β_0 is the constant term in the model, X_{ij} ($j = 1, 2, \dots, p$) is the ith observation of the jth predictor and ϵ_i are the error terms. It is important to mention that the scalar functions f_k might be any nonlinear functions or polynomials because the linearity of the model refers to the linearity between the response variable $\bar{V}_K$ and coefficients β_k. The coefficients are estimated utilizing the method of least squares which minimizes the mean squared difference between the prediction vector $\beta f(X)$ and the true response vector $\bar{V}_K$.

The cyclone and anticyclone properties (Section 3.3) that were considered for the derivation of the Koshava stochastic equations include: (1) central pressure, P_c, (2) Laplacian of pressure, $\nabla^2 P_c$, (3) depth, D, (4) radius, R, (5) altitude, H, (6) steering velocity, S, and (7-8) distances from the pressure and vorticity centers to the weather stations in the KR, d_v and d_c respectively. In addition, the pressure gradients above the KR are also taken into consideration. The mesoscale Koshava contributors (both presented in Chapter 5) such as the across-mountain MSLP and potential temperature differences, and winds at higher levels are also considered. If all of the above variables are accounted for, the stochastic equations constructed to diagnose Koshava's speed would then include 20 predictors (8 for cyclones, 8 for anticyclones, the pressure gradient in the KR, and 3 mesoscale contributors) and 1 response variable (Koshava mean hourly speed). Any model with 20 (or possibly more) terms would have been cumbersome to analyze and difficult to use. Therefore, the number of predictors had to be reduced.

Identification of the most important predictors was carried out using the stepwise regression method (Efroymson, 1960). The starting model is the constant model. The predictors are added one at a time and at each step the p-value of an F-statistic was calculated to test the model with and without the given predictor. An F-statistic follows an F-distribution and therefore can be used to compare statistical models. Namely, the F-statistic is computed as (e.g. Draper and Smith, 1998):

$$F = \frac{(SS_1 - SS_2)/(df_1 - df_2)}{SS_2/df_2}, \tag{3.13}$$

where SS_1 is the residual sum of squares of the starting model, SS_2 is the residual sum of squares of the model after adding an additional predictor, and df_1 and df_2 are the degrees of freedom of each model equation. Recall that the residual sum of squares of each model can be calculated from Eq. (3.12) as: $SS = \sum_{i=1}^{n} \epsilon_i^2 = \sum_{i=1}^{n} \left(\bar{V}_{Ki} - \beta_0 - \sum_{k=1}^{K} \beta_k f_k (X_{i1}, X_{i1}, \dots, X_{ip}) \right)^2$ There are $n - k$ degrees of freedom, where n is the number of predictors' observation and k is the number of estimated parameters in the model (see Eq. (3.12)). Thus, the predecessor model has to be the simpler one.

Now, the F-statistics and the degrees of freedom can be further used to determine the p-value. Namely, the p-value of an F-statistics represents the tail area beyond the observed F-value on the F-distribution. If the calculated p-value is smaller than the entrance tolerance of 0.05, the predictor is added to the model. If, on the other hand, the term is already in the model and its calculated p-value of the F-statistic is larger than the exit tolerance of 0.1, the predictor is removed from the model. In this way, the statistical significance of a given predictor was measured. The full explanation of the stepwise model algorithm can be found in Draper and

Smith's book on applied statistics (Draper and Smith, 1998). The stepwise method basically tests the null hypothesis that the predictor would be insignificant if added to the model. If it turns out that the predictor is statistically significant (based on the calculated p value), the null hypothesis is rejected and the predictor is added to the model. The whole multiple linear regression analysis including the stepwise method procedure were performed in Matlab® 2014 software. The resulting deterministic equations for the Koshava mean hourly speed are provided in Chapter 5.

3.6 Numerical modeling of EKE

This study uses the WRF model for the numerical simulation of the EKE. The employed solver is the Nonhydrostatic Mesoscale Model (NMM; version 3.6.1), which solves the compressible, nonhydrostatic Navier-Stokes equations on Arakawa-E grid. The vertical coordinate is a hybrid sigma-pressure coordinate. Two different configurations of the NMM model were tested (Table 3.1). In addition, two more numerical simulations were performed using a modified version of the NMM model on Arakawa-B grid, called NMMB. In total, four simulations with different models' configurations are performed – two using NMM and two using NMMB. The forecasts (mean hourly wind speed, wind gust and wind direction) were compared against measurements from four weather stations situated in the KR (BG, NS, VR and VG). The results are also benchmarked against the European Center for Medium range Weather Forecast's Integrated Forecast System (IFS) analysis.

Models' configurations are summarized in Table 3.1. The NMM, NMMB_1 and NMMB_2 configurations are operationally employed at the Republic Hydrometeorological Service of Serbia.

Table 3.1. Overview physical packages, initial and boundary conditions, and computational domain characteristics used in numerical modelling of the EKE.

	NMM	NMMB_1	NMMB_2	NMM_QNSE
Microphysics	Ferrier (Ferrier *et al.*, 2002)			
Longwave radiation	GFDL (Schwarzkopf and Fels, 1991)			RRTMG (Iacono *et al.*, 2008)
Shortwave radiation	GFDL (Lacis and Hansen, 1974)			RRTMG (Iacono *et al.*, 2008)
Surface layer	Janjic similarity scheme			QNSE (Sukoriansky *et al.*, 2005)
Land surface	Noah-MP (Ek *et al.*, 2003)	LISS		Noah-MP (Niu *et al.*, 2011)
PBL	MYJ			QNSE (Sukoriansky *et al.*, 2005)
Cumulus convection	BMJ (Janjić, 1994)	-		
Initial and boundary conditions	IFS	Nested in parent NMMB	Global NMMB	IFS
Horizontal resolution (km)	~2.2	~3	~9	~2.2
Domain centre	LON 17.5°E LAT 44.5°N	LON 18.8°E LAT 44.2°N	LON 8.0°E LAT 48.5°N	LON 17.5°E LAT 44.5°N
Grid points	400×450×45	326×287×64	394×356×64	400×450×45
Time step (s)	5	6.67	20	5
Nest ratio	-	3:1	-	-

Due stably stratified planetary boundary layer (PBL), the NMM_QNSE configuration uses the Quasi-Normal Scale Elimination scheme (QNSE; Sukoriansky *et al.*, 2005) for PBL parametrization. The NMM and NMMB

simulations have similar physics, but the forecasts are based on different initial and boundary conditions. Namely, the quality of forcing data can have a pronounced influence on the accuracy of forecasts (Talbot *et al.*, 2012).

Numerical modelling of surface and near-surface variables under stable atmospheric conditions is more challenging compared to unstable stratification (Shin and Hong, 2011). This difficulty partially arises because turbulent eddies in stable atmosphere are much smaller compared to unstable (convective) conditions (Beare *et al.*, 2006). For that reason, the NMM_QNSE simulation relies on the QNSE PBL scheme. This scheme is particularly designed for stable stratifications. Namely, QNSE is a turbulent kinetic energy prediction scheme based on a quasi-Gaussian spectral closure model with the surface layer parameters derived from large eddy simulations of stably stratified atmosphere (Sukoriansky *et al.*, 2005).

For motions with characteristic horizontal scales below 100 km (γ scale), such as the Koshava wind and the EKE in particular, deviations from the pure hydrostatic balance can be significant (Xu *et al.*, 1995). For this reasons, the non-hydrostatic models have been selected for the numerical simulation of the EKE.

CHAPTER 4

4. Homogeneity testing and Koshava trends

This chapter is the first result chapter in this thesis. It contains a comprehensive overview of the Koshava climatology from the year 1949 to the year 2010. As mentioned in Chapters 1 and 2, the Koshava wind dictates many aspects of weather and climate in the region, influences the air quality in cities, influences city planning projects, and is a valuable wind energy resource. Therefore, a study of Koshava's behavior over the 62-year-long period will prove valuable, either directly or indirectly, to all of the previously mentioned fields.

The chapter also contains the results of the first detailed homogeneity analysis of the wind speed and direction series from five weather stations located in the KR.

4.1 Introduction

Much research has been conducted focusing on analysis of wind speed trends (e.g. Pirazzoli and Tomasin, 2003; Pryor and Barthelmie, 2003; Smits *et al.*, 2005; Brázdil *et al.*, 2009; Vautard *et al.*, 2010; Guo *et al.*, 2011; Baule and Shulski, 2013; Dadaser-Celik and Cengiz, 2013) as well as wind speed variability (Palutikof *et al.*, 1987; Saji and Goswami, 1996; Klink, 1999; Klink, 2002). Using data from 822 weather stations, Vautard *et al.* (2010) showed that surface wind speeds in the northern mid-latitudes demonstrated between a 5 to 15 % drop in the period from 1979 to 2008. In a more recent study, Dadaser-Celik and Cengiz (2013) analyzed

the surface wind speed over Turkey and again found a negative trend from 1975 to 2006 on 72 % of the 206 analyzed weather stations. Brázdil *et al.* (2009) also noticed that wind speed were significantly showering in the period from 1961 to 2005 in the Czech Republic. On the other hand, while Pirazzoli and Tomasin (2003) did observe a decrease in wind speeds from 1951 to the 1970s, they found there was an increase in the surface wind activity in the following years. Using wind speed measurements, Smits *et al.* (2005) observed a general decrease in the speed of moderate and strong winds over the Netherlands. Overall, the literature review suggests that surface wind speeds have been decreasing over a large region in Europe. The Balkan region, however, has not been studied so far. This region, situated in the southeast part of the Europe, has a unique wind climate that is characterized by many local winds such as Bora, Foehn, Koshava, Ostro, Sirocco, Tramontane and Vardarac (see Section 2.1). Among these local winds, Koshava is one of the most dominant throughout the year, though this wind is particularly wide-spread during the winter and spring seasons and the highest wind speeds occur in autumn and winter (Unkašević *et al.*, 1999). Koshava's long-term trends have, to date, not yet been investigated.

As pointed out by Vautard *et al.* (2010), surface wind measurements are influenced by three major factors. The first factor affecting surface winds is large-scale synoptic weather systems (Bakker *et al.*, 2013). Though long-term trends in wind speed observations do not always reflect trends in large-scale phenomena (Alexandersson *et al.*, 1998; Bakker and Hurk, 2012) but rather may reflect urbanization and surface roughness changes (Smits *et al.*, 2005; Wever, 2012). Lastly, changes in the measurement techniques, instrumentation and location of weather stations would also affect surface wind measurements. Usually, each of

these factors influence observed trends, and it is often difficult to estimate the contribution that each of them makes to the observed trends.

Because the EAs (mostly Siberian high) and MCs are synoptic pressure systems that form the Koshava wind, any observed trends in these two weather systems should be reflected on climatology and trends of the Koshava wind. Panagiotopoulos *et al.* (2002) noticed that the Siberian high had a downward trend of -2.5 hPa decade-1 from 1978 to 2001. They have also concluded that this decline has had effects on circulation and temperature patterns well outside of the Siberian high region. The analysis of the frequency of the cyclonic tracks over the Mediterranean Sea has also shown a statistically negative trend on an annual basis (Maheras *et al.*, 2001; Flocas *et al.*, 2010). Maheras *et al.* (2001) showed that the occurrence of the cyclones in the West-Mediterranean had decreased from 1958 to 1996. Nissen *et al.* (2010) and later Nissen *et al.* (2013) have analyzed the frequency and the trend of the cyclones and windstorms in the Mediterranean region, and have demonstrated that there has been a significant decrease in the number of wind events and number of cyclones in this region. Koshava's long-term trends have, to date, not yet been investigated, as demonstrated in Section 0. Moreover, wind trends are mostly investigated on the large scales and hardly on local scale.

4.2 Data

Koshava trends are analyzed based on a 62-year data record (January 1, 1949 – December 31, 2010) from five synoptic weather stations (Table 4.1 and Figure 1.1). Measurements were conducted at the main climatological terms, i.e. 7:00, 14:00 and 21:00 hours (local time). The weather station in BG is located in the city center and is a typical example of an urban station, while the stations in Novi Sad (NS)

and Smederevska Palanka (SP) are typical suburban stations and the stations in VG and VR represent the rural samples. The NS, VG and VR stations are at the same elevation above sea level (a.s.l.) – about 83 m a.s.l.

Table 4.1 List of weather stations in the KR which provided the data used in the homogeneity testing and trend analyses.

Weather station	Longitude	Latitude	Elevation a.s.l. (m)	Anemometer height a.g. (m)
BG	20°27′53.44″ E	44°47′54.11″ N	132	24
NS	19°49′47.62″ E	45°19′19.88″ N	84	10
SP	20°57′ E	44°22′ N	121	10
VG	21°29′54.94″ E	44°45′09.56″ N	82	10
VR	21°18′20.01″ E	45°08′39.16″ N	83	10

4.3 Koshava climatology

4.3.1   <u>Wind direction and seasonality</u>

Koshava is a wind that blows from southeast quadrant and mostly, but not always, encompasses southeast (SE) and east-southeast (ESE) directions on a 16-direction wind rose. Wind roses for four seasons (summer-JJA, autumn-SON, winter-DJF, and spring-MAM) and all stations analyzed in this chapter are portrayed in Figure 4.1 with the corresponding numerical values provided in Table 4.2.

Koshava's direction in BG is fairly constant throughout the year. It is restricted to SE and two adjacent directions (ESE and SSE). Fall is the windiest Koshava month in BG when the winds from ESE, SE and SSE directions combined are present in 41.1 % of the time. Koshava winds in BG are more often than calms,

even in the summer season. Most calms occur in summer (7.4 %) whereas the windiest season, accounting for all wind directions, is spring (only 4.8 % of calms). After fall, Koshava in BG is mostly active in winter and spring seasons, respectively. Values presented in Table 4.2 can be further compared against Milosavljević (1950a) and Vujević (1933) studies of winds above BG. Moreover, since their analyses cover the period from before 1945, the climatological results for winds in BG presented in this chapter can be thought of as a continuation of their work for the 1949–2010 period. The main discrepancy between Koshava's occurrence in Table 4.2 and the results by Milosavljević (1950a) is for the SSE direction. Namely, Table 4.2 shows considerably higher frequencies of occurrence of SSE winds compared to Milosavljević (1950a) work (almost 6.6 % higher on an annual basis). Due to small number of days with winds coming in from SSE direction, Milosavljević (1950a) did not consider SSE to be a Koshava direction. The annum results for the most frequent Koshava direction (SE), however, seem to be fairly similar; 13.8 % in Milosavljević (1950a) thesis and 12.7 % in this study. The presented results are also similar to Vujević (1933), but only if Koshava is restricted to SE and ESE directions. For example, Table 4.2 shows that SE and ESE Koshava winds in BG in winter were present in 27.6 % of time whereas Vujević (1933) reported a corresponding value which is only for 0.8 % lower (26.8 %). He also found that calms in BG were less frequent that winds. The observed differences between these results are not necessarily caused entirely by natural variability of wind climate in BG. More likely these inconsistencies might be due to artificial inhomogeneities in the wind data series (see Section 4.4). Lastly, the values in Table 4.2 can be compared against Unkašević's study (Unkašević, 1994) of wind climatology for BG and for the period from 1888 to 1991. Once again, results on an annual basis seem to be very

similar, with the exception of the SSE direction in which case Unkašević (1994) reported smaller percentages of winds blowing in from SSE direction. The difference, however, is smaller compared to Milosavljević's study (Milosavljević, 1950) because her data cover the period prior to 1949 (which had been mostly covered by Milosavljević (1950a) and Vujević (1933)), when SSE winds were rare, as well as the most of the period covered by the present study when SSE winds were common. As a result, the large difference between the SSE winds in Table 4.2 and findings by Milosavljević (1950a) and Vujević (1933) is smoothed out.
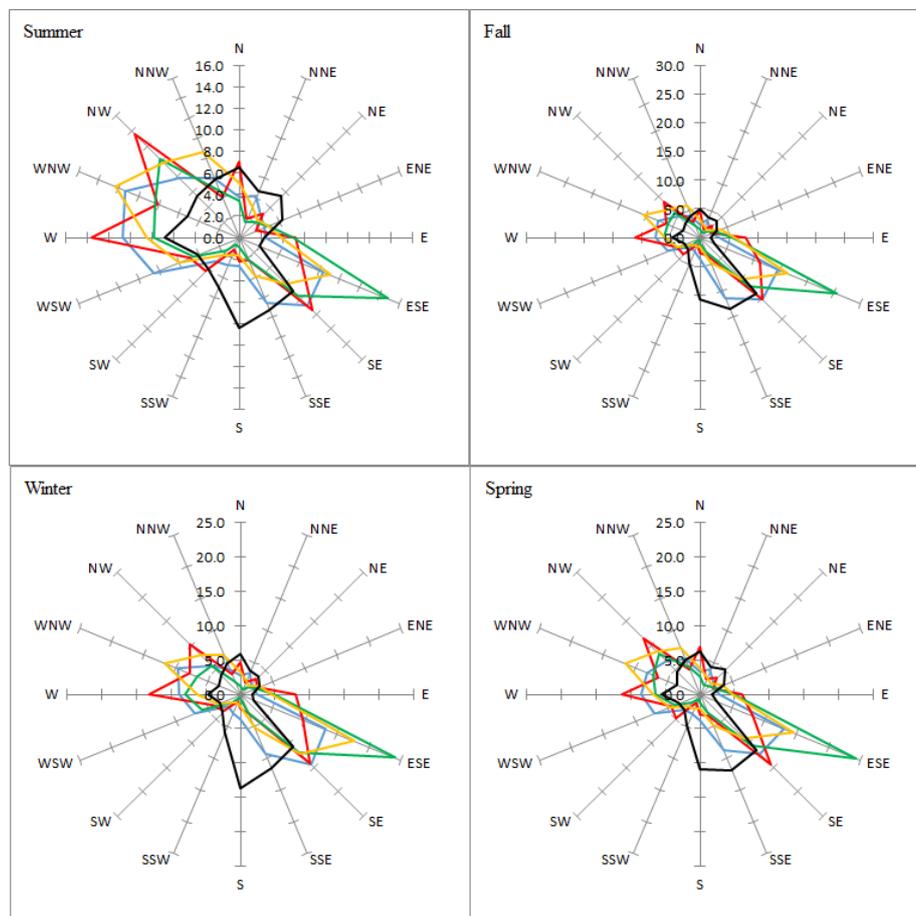
Figure 4.1. Wind roses for the period 1949-2010 and for five weather stations in the KR (Table 4.1). Blue – BG, red – NS, green – SP, yellow – VG, black VR. Corresponding numerical values are given in Table 4.2.

Table 4.2. Frequency (in %) of winds from different directions at five weather stations in the KR in the period January 1, 1949 – December 31, 2010. Corresponding seasonal wind roses are given in Figure 4.1.

		N	NNE	NE	ENE	E	ESE	SE	SSE	S	SSW	SW	WSW	W	WNW	NW	NNW	C
Summer	BG	3.7	4.1	2.8	2.5	2.4	8.3	8.9	6.6	2.7	2.8	3.2	8.5	10.8	11.3	7.8	6.0	7.4
	NS	7.1	1.9	3.1	1.6	5.2	6.2	9.5	2.2	2.3	1.2	4.4	4.9	13.6	8.1	13.6	4.0	11.1
	SP	3.5	1.5	2.0	2.9	4.9	14.8	7.7	2.3	0.9	0.7	1.7	4.5	7.9	8.4	10.3	4.6	21.4
	VG	5.0	3.1	2.4	2.9	3.9	9.0	6.1	3.8	1.7	1.8	2.4	6.0	8.5	12.3	9.8	8.7	12.6
	VR	6.5	4.6	5.5	4.2	2.3	2.1	7.0	7.3	8.4	5.0	4.0	4.1	6.8	5.2	5.5	5.8	15.7
Fall	BG	2.3	3.3	2.3	2.0	3.3	14.5	15.2	11.4	3.7	2.5	2.2	6.1	7.6	7.8	5.2	4.1	6.4
	NS	4.8	1.6	2.8	2.0	7.9	11.3	15.2	3.3	2.6	1.3	4.1	4.4	11.1	6.2	8.7	3.0	9.6
	SP	1.5	1.0	1.4	2.8	5.5	25.4	12.0	2.7	1.0	0.4	1.7	4.3	6.2	6.0	6.2	2.3	19.5
	VG	3.1	2.0	1.8	3.8	5.9	16.4	10.3	4.6	1.7	1.5	1.8	4.2	5.9	10.5	7.2	6.0	13.4
	VR	5.0	3.8	4.1	3.2	1.8	2.8	13.7	13.5	10.8	4.8	3.1	2.9	4.8	3.2	3.6	4.1	14.9
Winter	BG	2.8	3.4	2.3	2.1	2.4	13.2	14.4	9.3	3.7	2.9	2.6	7.0	8.8	9.8	6.0	4.0	5.4
	NS	4.7	1.8	3.2	2.7	7.9	9.7	14.1	3.0	2.0	1.1	3.4	4.2	13.1	7.9	10.2	3.2	7.7
	SP	1.2	0.8	1.4	2.4	4.8	24.1	12.0	3.0	0.8	0.6	1.8	6.0	8.0	6.8	6.0	2.0	18.6
	VG	3.3	2.0	1.7	3.0	4.4	17.7	12.1	5.2	1.7	1.2	1.6	3.5	6.2	11.7	8.0	6.2	10.4
	VR	5.9	3.8	3.7	3.0	1.7	2.1	10.8	11.5	13.7	6.0	3.5	3.2	4.7	3.3	3.9	4.9	14.0
Spring	BG	3.2	3.8	2.6	2.4	2.7	13.1	12.3	8.8	3.7	3.1	3.2	7.0	8.5	8.3	6.7	5.6	4.8
	NS	7.0	2.4	3.3	2.1	6.1	8.2	14.4	3.4	3.0	1.3	4.9	4.5	11.3	6.5	11.6	3.9	6.1
	SP	2.7	1.5	1.6	2.4	4.9	24.2	10.4	2.7	1.3	0.7	1.8	4.0	6.3	7.2	8.3	4.2	15.7
	VG	3.8	2.6	2.1	3.6	4.7	14.6	8.9	4.9	2.1	2.2	2.4	4.7	6.7	11.5	8.8	7.3	9.0
	VR	6.2	4.3	5.1	3.7	1.7	2.7	11.6	11.9	10.9	4.8	3.3	3.3	5.5	3.6	4.5	5.4	11.5
Annual	BG	3.0	3.7	2.5	2.3	2.7	12.3	12.7	9.0	3.4	2.8	2.8	7.2	8.9	9.3	6.4	4.9	6.0
	NS	5.9	1.9	3.1	2.1	6.8	8.8	13.3	3.0	2.5	1.2	4.2	4.5	12.3	7.2	11.0	3.5	8.6
	SP	2.2	1.2	1.6	2.6	5.0	22.1	10.5	2.7	1.0	0.6	1.7	4.7	7.1	7.1	7.7	3.3	18.8
	VG	3.8	2.5	2.0	3.3	4.7	14.4	9.3	4.6	1.8	1.7	2.1	4.6	6.8	11.5	8.4	7.0	11.3
	VR	5.9	4.1	4.6	3.5	1.9	2.4	10.8	11.0	10.9	5.2	3.5	3.4	5.4	3.8	4.4	5.1	14.0

Koshava at the NS station is dominantly from the SE direction – 13.3 % over the year. Other directions are less represented, but easterly Koshava directions are more frequent than southerly. Inspecting Table 4.2 and Figure 4.1, it therefore seems that Koshava directions in NS are SE and ESE (22.1 % over the year). Adopting this rule, it can be concluded that the fall and winter are the windiest Koshava seasons in NS with Koshava being active for 26.5 % and 23.8 % of the time, respectively. Similar to the BG and VR stations, summer Koshava winds were rare.

The ESE and SE are Koshava directions at the SP stations, as it can be inferred from Table 4.2 and Figure 4.1. Although Koshava in SP is most often in the fall (37.4 %), winter (36.1 %) and spring (34.6 %) seasons, it is interesting to note that Koshava is also very active during the summer (22.5 %). Therefore, compared to all other stations analyzed in this study, the SP station has the largest number of Koshava days in the summer. Another interesting observation is that the SP station also has the largest percentage of calms in the summer (21.4 % of the time) and the largest number of calms in the year (18.8 %). Thus, Koshava winds and calms combined account for almost 50 % of the time during the summer period in SP. The BG station is the windiest site in the KR (Table 4.2).

Table 4.2 and Figure 4.1 suggest that Koshava's direction at the VG station are ESE and SE with 23.7 % of combined frequency of occurrence per annum. Winter is the windiest Koshava season with the wind being active for 38.8 % of the time. The fall and spring seasons follow but Koshava's activity in these two seasons is approximately 10 % lower than during the winter season. Koshava's occurrence in the summer seems to be about 10 % below the fall and spring seasons' values.

During the summer and winter seasons, Koshava at the VR station seemed to come in dominantly from the south (SSE in particular) whereas it has more easterly directions in the other two seasons. Therefore, it looks like Koshava directions at the VR station are SSE, S and SE. Koshava's occurrence from these three directions is fairly uniformly distributed, i.e. around 11 % of the time per each of these three directions. Therefore, Koshava in VR is active for 32.7 % of the year, which is almost two and a half times more than calms. Seasonally, Koshava is most active in the fall (38 %) and then closely followed by winter (36 %) and spring (34.4 %) seasons.

The above discussion indicates that Koshava wind does not maintains the same direction throughout the KR. It seems, nonetheless, that SE is the ubiquitous Koshava direction in the whole KR. The physical reasons for this directional variability are discussed later in Chapter 5. Furthermore, depending on the weather station under consideration, Koshava's activity peaks at different seasons in the year. These variabilities are summarized in Table 4.3. Because Koshava shows considerable variability in its direction from one station to another, the homogeneity and trend analyses presented in this chapter have been performed for the entire southeast quadrant (E, ESE, SE, SSE and S wind directions). An additional reason is the observed level of inhomogeneity for the wind direction series (see Section 4.4). Due to the inhomogeneities in the wind direction data series caused by the change of the instrumentation and environment, winds from one direction can be artificially shifted to adjacent wind direction.

Table 4.3. Prevailing Koshava directions and seasonality at different weather stations in the KR.

Weather station	Koshava's direction	Koshava's most active season
BG	SE, ESE, SSE	Fall
NS	SE, ESE	Fall
SP	ESE, SE	Fall
VG	ESE, SE	Winter
VR	SSE, S, SE	Fall

4.3.2 Wind speed

The wind speed climatology for the weather stations in the KR is given in Table 4.4. Based on Koshava directions in Table 4.3, the mean seasonal and annual Koshava speeds can be determined from Table 4.4.

The mean annual Koshava speed in BG is 3.6 m s^{-1} with the highest speeds occurring in the winter season (4 m s^{-1}) and the lowest in summer (2.6 m s^{-1}). The fall and spring seasons have the same mean Koshava speed of 3.7 m s^{-1}, which is very close to the annual value. The strongest winds occur from the ESE direction and SE directions, respectively, and in the winter and spring seasons in particular. Milosavljević (1950a) reported the mean annual ESE Koshava speed of 4.2 m s^{-1} which is for 0.3 m s^{-1} higher than the corresponding value from Table 4.4. The winds from the SE direction, however, seem to be increasing since the value in Table 4.4 is for 0.6 m s^{-1} higher than what Milosavljević (1950a) found in his study (3.2 m s^{-1}). Unkašević (1994) reported similar results. Namely, the mean annual ESE winds in her study are for 0.5 m s^{-1} higher whereas the SE and SSE winds are for 0.4 and 0.1 m s^{-1} weaker than the corresponding values in Table 4.4, respectively.

Table 4.4. Mean wind speed (in m s^{-1}) of winds from different directions at five weather stations in the KR in the period January 1, 1949 – December 31, 2010.

		N	NNE	NE	ENE	E	ESE	SE	SSE	S	SSW	SW	WSW	W	WNW	NW	NNW
Summer	BG	2.5	2.2	2.0	1.9	2.0	2.7	2.8	2.4	2.0	1.7	1.8	2.2	2.4	2.5	2.6	2.6
	NS	3.1	2.4	2.2	2.0	2.1	2.4	2.6	2.1	2.1	2.0	1.9	2.1	2.4	2.6	3.0	2.9
	SP	2.4	2.3	1.9	2.2	2.2	2.4	2.4	2.3	2.0	1.8	1.7	2.0	2.5	3.1	2.9	2.8
	VG	1.9	1.3	1.2	1.2	1.6	2.8	2.4	2.0	1.7	1.2	1.4	1.6	1.9	2.2	2.2	2.1
	VR	2.8	2.1	2.1	2.1	1.9	4.3	7.0	5.5	3.3	2.5	2.2	2.5	2.8	3.1	3.0	3.0
Fall	BG	2.6	2.1	1.9	2.0	3.1	3.8	3.9	3.2	2.5	1.9	1.7	2.1	2.3	2.3	2.5	2.6
	NS	3.0	2.7	2.4	2.4	2.6	3.7	4.0	3.3	2.5	2.1	2.0	2.1	2.5	2.8	3.0	3.2
	SP	2.4	1.9	1.7	2.5	3.2	3.1	3.1	2.8	2.2	1.8	1.6	1.8	2.4	2.9	2.8	2.5
	VG	1.8	1.3	1.1	1.4	1.8	4.9	3.8	2.7	1.9	1.3	1.4	1.4	1.9	2.2	2.4	2.4
	VR	2.7	2.1	2.1	1.8	2.1	7.7	9.8	7.8	4.0	2.6	2.1	2.2	2.5	3.0	3.0	2.8
Winter	BG	2.7	2.2	2.1	2.2	3.1	4.3	4.3	3.5	2.7	1.9	1.9	2.4	2.4	2.4	2.7	2.6
	NS	3.4	3.0	2.5	2.4	2.8	4.2	4.8	4.4	2.7	2.5	2.3	2.5	2.9	3.2	3.3	3.5
	SP	2.3	2.0	2.2	3.0	3.3	3.3	3.4	3.1	2.4	1.9	1.7	2.2	2.8	3.4	3.1	2.8
	VG	1.9	1.3	1.3	1.4	1.7	5.3	4.2	3.1	1.7	1.2	1.4	1.6	1.9	2.7	2.8	2.7
	VR	2.8	2.2	2.1	1.8	1.8	7.3	11.0	8.2	4.7	3.2	2.4	2.4	2.6	3.0	3.1	2.9
Spring	BG	3.0	2.4	2.2	2.2	3.1	4.3	3.8	3.1	2.7	2.1	2.0	2.5	2.7	2.6	2.8	3.0
	NS	4.0	3.5	2.8	2.7	2.9	4.2	4.6	3.5	2.7	2.4	2.4	2.5	2.9	3.3	3.5	4.0
	SP	2.9	2.4	2.4	2.7	3.5	3.5	3.2	3.3	2.6	2.3	2.1	2.5	2.9	3.6	3.2	3.2
	VG	2.3	1.5	1.4	1.4	1.9	5.0	3.7	2.9	2.5	1.8	1.7	1.8	2.2	2.7	2.8	2.9
	VR	3.3	2.7	2.4	2.2	2.1	7.2	9.4	7.4	4.2	3.0	2.4	2.7	3.0	3.4	3.4	3.6
Annual	BG	2.7	2.2	2.1	2.0	2.9	3.9	3.8	3.1	2.5	1.9	1.9	2.3	2.5	2.4	2.6	2.7
	NS	3.4	3.0	2.5	2.4	2.6	3.7	4.1	3.4	2.5	2.2	2.1	2.3	2.7	3.0	3.2	3.4
	SP	2.5	2.2	2.1	2.6	3.1	3.2	3.1	2.9	2.3	2.0	1.8	2.2	2.6	3.3	3.0	2.8
	VG	2.0	1.4	1.3	1.3	1.8	4.7	3.6	2.7	2.0	1.4	1.5	1.6	1.9	2.5	2.5	2.5
	VR	2.9	2.3	2.2	2.0	2.0	6.7	9.5	7.4	4.1	2.8	2.3	2.5	2.7	3.1	3.2	3.1

Koshava at the NS station is the strongest in the winter season (4.5 m s^{-1}) and closely followed by the spring season (4.4 m s^{-1}). The mean annual and fall speeds are the same and equal to 3.9 m s^{-1}. The most vigorous Koshava winds are coming in from the SE direction during the winter season. The summer Koshava winds in NS are weak and, as in the BG case, are equal to 2.6 m s^{-1}.

At the SP station, a small variability of mean Koshava speeds is observed from the fall to the spring seasons. Spring seems to be the season associated with the strongest Koshava winds (3.4 m s^{-1}). The SE and ESE Koshava winds have the similar speeds on both annual and seasonal bases. It can be concluded that the SP station, although not being the windiest Koshava site, has the steadiest Koshava speeds throughout the year.

Koshava is very pronounced wind at the VG station. Namely, the mean annual speed of the Koshava wind in VG is 4.2 m s^{-1}. The strongest winds occur in the winter seasons when the mean speed is equal to 4.8 m s^{-1}. Koshava winds in spring and fall are also strong (4.4 and 4.3 m s^{-1}, respectively). One again, the summer Koshava winds have the mean speed of 2.6 m s^{-1}. After the VR station (see below), the VG station is characterized with the strongest Koshava winds in the whole KR.

Traditionally, Koshava is the strongest at the VR station. For example, the mean summer Koshava speed in VR (5.2 m s^{-1}) is higher than the mean Koshava speeds in any of the seasons at the other four weather stations in the KR. The strongest Koshava winds in VR occur during the winter (8 m s^{-1}). The mean wind speeds of 7.2 and 7 m s^{-1} are observed for the fall and spring seasons, respectively. The mean annual speed at the VR station is 7 m s^{-1}. Note that the mean speed of the SE winds is as high as 9.5 m s^{-1}. The ESE direction has not been considered as a

Koshava direction in the previous sub-section and Table 4.3, although data in Table 4.4 suggests it should be taken into account. Namely, the mean annual speed of ESE winds is 6.7 m s^{-1} and the mean speeds above 7 m s^{-1} are recorded for the fall, winter and spring seasons.

It can be concluded from the above discussion that although Koshava is mostly active in the fall season (with the exception of the VG station), the strongest Koshava winds typically occur in winter. The most dominant directions are not always associated with the strongest Koshava winds For instance, the most frequent Koshava direction in VR are SSE and S, but the highest wind speeds were recorded from the SE direction. On average, the smallest Koshava speeds occur in SP and the highest in VR. Koshava speeds in BG and NS are very similar. This spatial distribution of the mean Koshava speeds suggests that the east parts of the KR have higher velocities than the rest of the region. The meteorological causes for this are discussed later in Chapter 5.

Figure 4.2 shows the mean annual wind speeds for the three measurement terms (7:00, 14:00, 21:00), as well as the daily mean (DM) for the Koshava wind. The highest wind speeds were observed at the VR station throughout the day. On average, wind speed measurements at this station are 2 times higher than the wind speeds observed at the other four stations. Additionally, wind speeds at the stations VR, VG and NS are all observed to be higher than wind speeds at the BG station. It is probable that the large surface roughness of BG leads to the decreased wind speeds noted at this station. The SP station generally had the lowest wind speeds. An interesting pattern can be observed when the diurnal wind variations are analyzed. Generally, wind speeds tend to increase from the early morning (7:00) to the afternoon (14:00) at all stations (the one exception

being the winds observed at the VR station). The observed increase of wind speed in the afternoon correlates with the increased surface temperature at this time of day (Dai and Deser, 1999). In the early afternoon, the air near the surface is warmer than the air aloft and thus the sensible heat flux is orientated upward. This positive flux results in the increased instability of the atmosphere, augmenting the turbulence and the downward mixing of momentum – consequently increasing wind speeds. The reverse trends noted at the VR station are more difficult to explain, however, though the explanation may have to do with the topography of VR's surrounding area. A mountain located east of the city postpones the sunrise and it might shift the surface temperature peak to occur later in the afternoon.
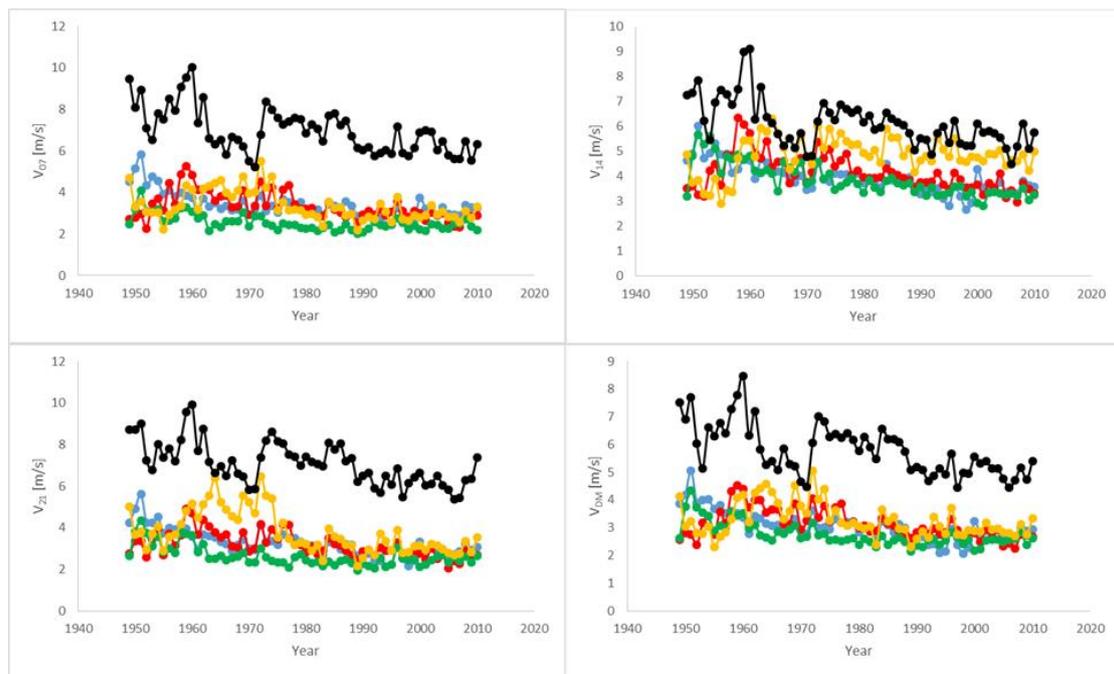
Figure 4.2. The mean annual Koshava speeds for the three measurement terms (07:00, 14:00, 21:00) and DM values. Weather stations: blue – BG; red – NS; green – SP; yellow – VG; black – VR.

The rank of percentile that corresponds to 5 m s^{-1} value has been calculated for the DM values. The VR station had the smallest value (0.518). Therefore, almost 50% of the time Koshava wind speeds were above 5 m s^{-1}. The rank of the 5 ms^{-1} value at the BG, NS, SP, and VG wind speed series was 0.845, 0.846, 0.898 and 0.79, respectively. This certainly identifies the VR region as the windiest one compared to the other four regions.

4.4 Homogeneity of wind series

All wind series were examined using both the basic and the modified form of the ReDistribution Method and results for all weather stations are shown in Figure 4.3.

After conducting a basic RDI analysis on the BG dataset, the series seemed to be relatively inhomogeneous, returning high RDI values for wind direction observations over longer periods (the longest period of such data are featured for the period 1986-2006), while wind speed had some minor anomalies in early 1950s and early 1990s. This type of homogeneity assessment discovered problems mostly concerning numerous changes in wind direction series. At some points, RDI values were found to be quite high (approximately 0.2), indicating 'noisy' datasets.

On the other hand, the output results of the modified form of the ReDistribution Method returned a practically homogeneous wind speed series, while the wind direction series was found to have distinct inhomogeneities in 1956, 1962, 1968, 1973, 1984, 1989 and 2001. These anomalies in the wind direction series influenced the distribution of winds on the wind rose. This clearly indicates that some changes in the instrument environment took place. The inhomogeneity of

2001 seems to reveal a bigger problem with wind direction data. The cause was probably not only a change in the instrument environment, but also an instrument misalignment of a newly added piece of equipment.

When the basic RDI analysis was applied to the NS series, a few anomalies were demonstrated. The greatest anomaly was observed to be in 1978, returning RDI peaks of both direction and speed series in 1982. The cause of this anomaly seems to be a change in the instrumentation, as well as a change in the method of measurement. At that time, the station began to employ an anemograph, and since it began to run synoptic observations, it began recording 16 wind directions instead of 8. Prior to 1978, it might be noted that RDI values were slightly higher, which confirms the described cause of inhomogeneity. The inhomogeneity in wind speed series in 1960 that resulted in the RDI peak value in 1964 also seems to be caused by a change in the wind speed measurement method, taking a 10 minute mean speed as a value instead of 10 minute gust speed. Another anomaly, occurring simultaneously with the wind direction anomaly, comes from different instrument sensitivity, thus resulting in "low speed" being recorded more frequently as opposed to "calm".
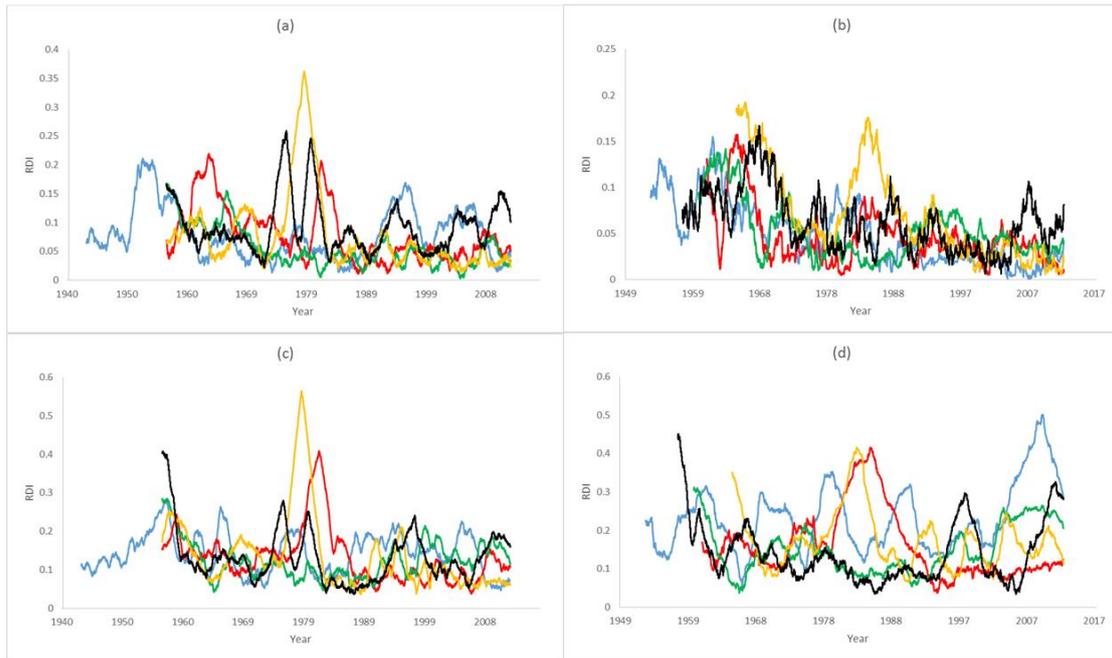
Figure 4.3. Homogeneity of wind speed (a, b) and wind direction (c, d) series using ReDistribution method in its base (a, c) and modified (b, d) versions. Weather stations: blue – BG; red – NS; green – SP; yellow – VG; black – VR.

The modified RDI analysis of the data only confirms these results. The same anomaly in 1978 can be noted, but only in the wind direction series. Again, the change in the distribution of wind directions refers to the addition of 8 more wind direction categories via the 'starry' wind rose, but winds from the southeast quadrant have stayed equally frequent. Since there are no significant anomalies in the wind speed series, the anomaly from 1978 is thus confirmed to affect the low wind speeds only. The anomaly in wind speed from 1960 is greatly reduced.

The SP series, analyzed using the basic RDI method, was observed to have an anomaly in 1953, while slightly higher RDI values were introduced in 1990s. The cause for these spikes in RDI values seems to have been a relocation of the measurement site as well as the introduction of an anemograph, replacing a more

simple wind vane with anemometer. It is not clear, however, what caused the rise of the RDI values from the 1990s, since sufficient metadata about the instruments used was not recorded.

The modified RDI analysis revealed anomaly of the series that can be observed in the 1990s. The change in wind direction distribution may be due to either the use of a newly installed and more sensitive wind vane or, a less likely possibility, to a lower instrument height. The latter possibility, however, is not supported by the fact that wind speed distribution remains unchanged, which should not occur if the instrument was simply set-up at a lower height. More sensitive wind roses tend to change wind direction series from having a more focused, narrower direction, to having a wider range of directions. As a result, the wind direction noted in this decade was much more variable, and the wind originated from one major direction far less frequent. Nevertheless, a sum of the frequencies of wind directions from the SE quadrant has remained similar.

When applying the basic RDI analysis to the VG data series one anomaly of a very high magnitude (RDI value 0.565) in 1979, which is thought to have been caused by station relocation in 1975. Anomalies noted in 1958 and 1969 are thought to have been due to changes in instrumentation, while wind direction anomalies in 1991 and 1995 in wind direction only were due to are thought to have been caused by minor changes in the instrument environment.

Concerning the wind speed subset of the VG dataset, the modified *RDI* analysis introduces higher RDI peaks, which could indicate problems with the distribution of wind directions. However, problems with the wind direction data associated with these RDI peaks are all thought to be due to variations between the two adjacent directions, ESE and SE. In fact, total frequencies from the two

direction quadrants with significant winds, southeast and northwest, maintain their sums and ratio throughout the series.

The VR series also indicates some problems with homogeneity. The basic RDI analysis clearly indicates simultaneous anomalies of both the speed and direction series in 1953, 1972, and 1976. Similar anomalies can be observed in the wind direction data of 1993 and 2006, but wind speed remains relatively more homogeneous. Since the metadata show no relocation of the measurement site, all anomalies are thought to be caused by changes in the instrumentation used, whether it be changes in its position and microenvironment or misalignment and recalibration.

The modified RDI analysis returned more information of these anomalies. Within the wind speed dataset, anomalies are noted in only 1953, 1993 and 2006, all years when different instruments were introduced. On the other hand, anomalies from 1972 and 1976 are not observed within this data subset, meaning that these were probably caused by changes in the instrument's close environment. Changes of wind direction distributions are similar to those from other stations. The redistribution observed in 1953 is thought to be caused by the introduction of the 16 wind direction rose instead of the 8 direction rose.

4.5 Koshava trends

The trend analysis of the Koshava wind has been performed on two categories of Koshava's speeds: (1) all wind speeds and (2) wind speeds above 5 m s^{-1} (named K5 winds). The mean reason for this separation of wind speeds in two sets is the observed level of inhomogeneities (see Section 4.5). Since small wind speeds are more susceptible to inhomogeneities, the thought is that the trends of the K5

winds will more closely represent the natural (climatological) trends of the Koshava wind. The K5 winds are also of particular importance to the wind energy section and thus the observed trends of these winds could have a practical implication in the industry.

4.5.1 Wind speed

Results of the Mann-Kendall test and values of the Sen's slope are given in Table 4.5. At all stations, wind speeds in the morning have strong negative trend over the 62-year study period. Negative trend of the K5 winds is stronger compared to the case when all wind speeds are considered. Statistically significant negative trends for wind speeds at 14:00 have been detected at all stations-except for the VG station where the Mann-Kandall test failed to show any significant trend. Besides the VG station exception, the slopes calculated for the afternoon Koshava winds have higher absolute values compared to those of the morning Koshava winds. A separate analysis of the K5 winds again reveals a strong negative trend, but this time at all stations. The evening Koshava winds (21:00) also experienced a significant negative trend at all stations considering both wind speed regimes.

The DM values, as expected, all show a significant negative trend, with the exception of VG station, where the trend is significant only to $a = 0.01$. The weaker, but still significant trend for the DM values of the VG station is caused by the absence of any trend of Koshava's afternoon winds. The average slope when all DM wind speeds are included is -0.020 m s^{-1} year^{-1}, while the average value of the slope for K5 winds is -0.024 m s^{-1} year^{-1}. This pattern indicates that the stronger wind speeds were declining more rapidly than the near-calm wind speeds.

Table 4.5. Trend analysis of the mean annual Koshava speeds in the period 1949-2010: Mann-Kandall test statistic, Z, significance of the trend, H_1, Sen's slope, Q (m s^{-1} year^{-1}), and offset of the linear trend line, B (m s^{-1}).

Station	Term	All wind speeds				K5 winds			
		Z	H_1	Q	B	Z	H_1	Q	B
BG	07:00	-5.52	4	-0.021	4.01	-7.42	4	-0.026	8.34
	14:00	-6.85	4	-0.026	8.33	-6.80	4	-0.026	8.33
	21:00	-6.60	4	-0.025	4.00	-6.73	4	-0.029	8.43
	DM	-6.45	4	-0.021	3.74	-7.06	4	-0.025	7.37
NS	07:00	-4.62	4	-0.017	3.81	-4.66	4	-0.026	9.12
	14:00	-4.90	4	-0.024	4.81	-5.42	4	-0.024	8.88
	21:00	-5.15	4	-0.019	3.75	-4.51	4	-0.027	9.08
	DM	-4.94	4	-0.017	3.68	-5.07	4	-0.022	7.82
SP	07:00	-4.59	4	-0.011	2.82	-5.30	4	-0.024	8.20
	14:00	-7.57	4	-0.029	4.81	-6.76	4	-0.024	8.48
	21:00	-4.35	4	-0.013	2.89	-4.83	4	-0.022	8.10
	DM	-5.61	4	-0.014	3.13	-6.56	4	-0.022	7.16
VG	07:00	-3.98	4	-0.016	3.69	-4.48	4	-0.031	9.66
	14:00	-0.04	0	0.000	4.86	-3.40	4	-0.21	9.17
	21:00	-4.69	4	-0.027	4.46	-3.74	4	-0.027	9.55
	DM	-3.19	3	-0.013	3.54	-3.64	4	-0.023	8.33
VR	07:00	-5.03	4	-0.036	7.98	-5.70	4	-0.033	11.46
	14:00	-4.99	4	-0.031	7.13	-4.35	4	-0.022	10.24
	21:00	-5.44	4	-0.037	8.21	-5.53	4	-0.031	11.60
	DM	-5.43	4	-0.034	6.83	-5.53	4	-0.029	9.94

The overall strongest negative trend is observed at the VR station for the DM values when all wind speeds are considered (-0.034 m s^{-1} year^{-1}), whereas the strongest negative trend of the K5 winds is also detected at the VR station, but for the morning Koshava winds (-0.033 m s^{-1} year^{-1}). A positive trend has not been detected at any of the stations. Moreover, there is only one non-negative trend and it is recorded for the 14:00 Koshava winds at the VG stations. This trend is

clearly caused by the small wind speeds or, even more likely, inhomogeneities in the wind data time series since the K5 winds in the same term possess a strong negative trend.

4.5.2   Wind activity trends

The annual number of days with the Koshava wind for the most active Koshava directions (based on Figure 4.1) and the whole SE quadrant are presented in Table 4.6. Considering all wind speeds, the VG and BG stations are the locations where Koshava displays the greatest amount of activity. When only the K5 winds are considered, the VR and VG stations seem to display the greatest amount of activity.

A trend analysis of the annual number of days with the Koshava wind is given in Table 4.7. When analyzing the SE sector as a whole, only the SP and VG stations have statistically significant negative and positive trends, respectively. Excluding these two stations, it seems that a redistribution of the Koshava wind has taken place in such a way that the central (SE) direction has a decrease of the Koshava activity, and the peripheral directions have increase of the Koshava activity.

This tendency might be due to: (1) introduction of 16 direction wind rose instead of 8 direction wind rose and/or (2) installation of more sensitive wind vanes (see Section 4.4) or (3) natural long-term variability of Koshava's direction. The results are quite different when only the K5 winds are considered. Taking the entire SE sector as a whole, statistically significant negative trends have been recorded at all the stations, except the VG station, where a positive, but statistically insignificant, trend has been detected.

Table 4.6. The annual number of days with the Koshava wind.

Station	Wind direction	Average yearly number of Koshava days considering all wind speeds	Average yearly number of days with K5 winds
BG	SE quadrant	146.66	24.64
	SE	45.37	9.96
	ESE	44.87	9.62
	SSE	32.95	4.01
NS	SE quadrant	125.42	22.36
	SE	48.61	11.99
	ESE	32.22	6.31
SP	SE quadrant	127.45	15.74
	ESE	52.65	6.18
	SE	34.15	4.68
VG	SE quadrant	150.83	38.31
	ESE	80.75	28.19
	SE	38.33	8.24
VR	SE quadrant	135.22	69.93
	S	39.90	9.44
	SSE	40.30	24.91
	SE	39.28	31.05

Table 4.7. Trend analysis of annual number of days with the Koshava wind in the period 1949-2010: Mann-Kandall test statistic, Z, significance of the trend, H_1, Sen's slope, Q (days year^{-1}), and offset of the linear trend line, B (days).

Station	Direction	All wind speeds				K5 winds			
		Z	H_1	Q	B	Z	H_1	Q	B
BG	E	-1.00	0	-0.020	9.47	-3.48	4	-0.011	0.67
	ESE	-2.81	3	-0.636	58.21	-5.65	4	-0.250	15.25
	SE	-4.06	4	-0.567	64.97	-5.48	4	-0.242	16.12
	SSE	4.69	4	0.626	13.30	1.13	0	0.027	2.05
	S	4.49	4	0.202	4.89	-0.76	0	0.000	0.33
	Q	-1.59	0	-0.187	153.73	-6.54	4	-0.513	39.90
NS	E	2.03	2	0.117	19.47	-1.66	1	-0.009	1.38
	ESE	5.56	4	0.863	6.64	2.49	2	0.105	2.49
	SE	-5.12	4	-0.710	65.54	-5.35	4	-0.261	18.75
	SSE	2.24	2	0.111	6.00	-0.89	0	0.000	1.00
	S	-3.34	4	-0.104	11.83	-4.41	4	-0.014	0.84
	Q	1.53	0	0.175	119.86	-4.36	4	-0.262	28.98
SP	E	-1.97	2	-0.099	18.09	-3.80	4	-0.053	3.99
	ESE	-4.37	4	-0.860	83.36	-6.39	4	-0.156	10.19
	SE	-1.63	0	-0.185	37.20	-6.19	4	-0.118	7.30
	SSE	3.97	4	0.250	8.00	-1.68	1	-0.015	2.18
	S	5.19	4	0.103	2.50	3.02	3	0.000	0.33
	Q	-4.05	4	-0.552	145.24	-8.24	4	-0.385	26.41
VG	E	6.32	4	0.667	-1.50	5.54	4	0.021	-0.18
	ESE	-1.15	0	-0.208	94.48	-0.42	0	-0.042	28.83
	SE	0.87	0	0.235	26.00	2.01	2	0.077	1.64
	SSE	2.03	2	0.075	3.99	-0.32	0	0.000	0.33
	S	3.08	3	0.049	1.48	-0.90	0	0.000	0.00
	Q	4.57	4	1.048	119.50	0.54	0	0.051	34.86
VR	E	2.23	2	0.056	5.11	-1.28	0	0.000	0.00
	ESE	0.32	0	0.009	5.69	-0.45	0	0.000	1.33
	SE	-2.85	3	-0.474	55.56	-2.37	2	-0.333	43.00
	SSE	0.98	0	0.109	35.14	1.95	1	0.191	15.34
	S	4.48	4	0.429	26.02	0.54	0	0.013	8.39
	Q	0.57	0	0.063	133.01	-3.07	3	-0.260	75.70

Table 4.7 further shows that the NS and VG stations possess different trend signs for annual number of Koshava days when all wind speeds are considered and when only K5 winds are taken into consideration. However, the positive trends for the near-calm wind speeds are not statistically significant. Overall, it can be observed that the trends of Koshava's activity are much more diversified than the trend of Koshava's speed (where more or less all stations recorded very strong negative trends).

The following analysis takes into account the spatial and temporal consistency of the K5 winds. Two conditions were placed on the K5 winds. Firstly, the K5 winds had to be detected at a minimum three out of the five stations-spatial consistency. Secondly-for temporal consistency-a three-term (one day) of the minimum wind activity was required to consider that wind to be the K5 wind. Though, when a sequence of Koshava activity exceeded three terms, an allowance was made for short interruptions (no more than two consecutive terms) of winds blowing in from other directions. Below, this principle is numerically presented on a sample exported from the dataset:

0 0 0, 1 1 1, 1 0 0, 1 1 1, 1 1 1, 0 1 1, 0 0 0, 0 1 0.

Only K5 winds are denoted by 1 – all other wind directions or winds with a speed of less than 5 m s^{-1}, are represented by 0. Three terms make one day and the end of a day is presented with a comma in the above scheme. According to the criteria, the Koshava wind started at 07:00 in Day Two and lasted four more days. The underlined zeroes are regarded as the K5 winds. Their occurrence is thought to have been caused by local atmospheric and environmental influences, and it is believed that their existence can be disregarded. Another argument for disregarding these two terms of interruption is the nature of the formation of the

Koshava wind. As mentioned earlier (Section 1.2), the Koshava wind is formed by the large-scale pressure systems which create very persistent pressure gradients. Such pressure gradients do not exhibit significant hourly oscillations.

Results are depicted in Figure 4.4. The negative trend in the period 1949-2010 is statistically significant ($H_1 = 4$) and Sen's slope is equal to -0.640 days year^{-1} (the intercept, B=100.78 days). Even within a 95 % confidence interval (depicted by the red dotted lines), trends are still negative. The 5-year moving average (indicated by the green line) shows that the occurrence of K5 winds had a pronounced positive trend until the second half of the 1950s. The average then seems to fluctuate within the same range until 1980, when a decline in K5 wind activity can be detected.
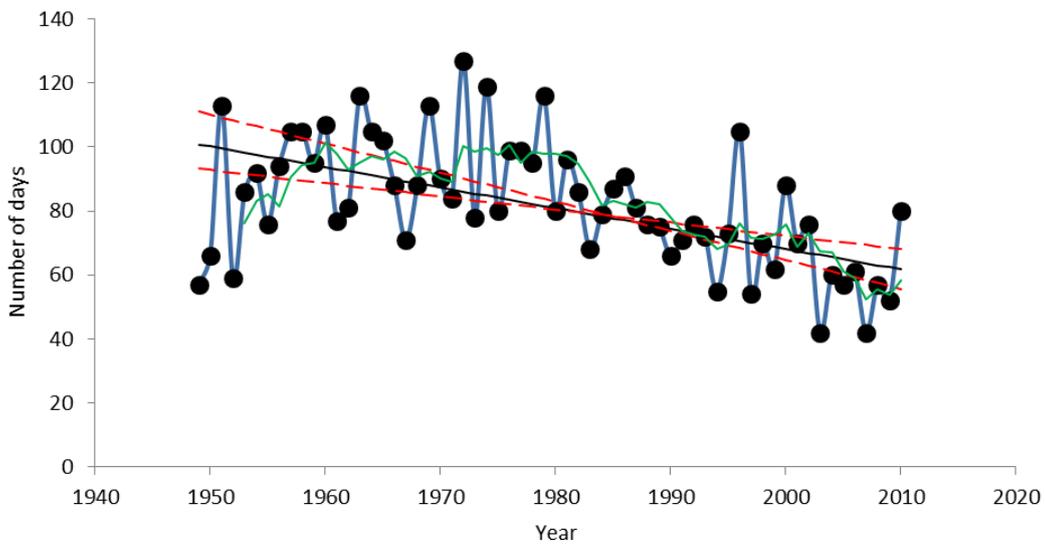
Figure 4.4. Annual number of days with K5 winds based on the group criteria (blue line). The black line is Sen's slope, the red dashed lines are trends at the 95 % confidence intervals and the green line is the 5-year moving average.

The year displaying the greatest amount of activity was 1972, with 127 days of K5 winds. After 1996, no year with more than 100 days of K5 winds can be observed. The trend after 1980 is statistically significant ($H_1 = 4$) with slope value equal to -1 day year^{-1}. The trend before 1960 is also significant ($H_1 = 2$) and has a large slope value, $Q = 4.217$ days year^{-1}. The observed trends in Figure 4.4 can be better understood when compared to individual trends observed at each station (Figure 4.5).
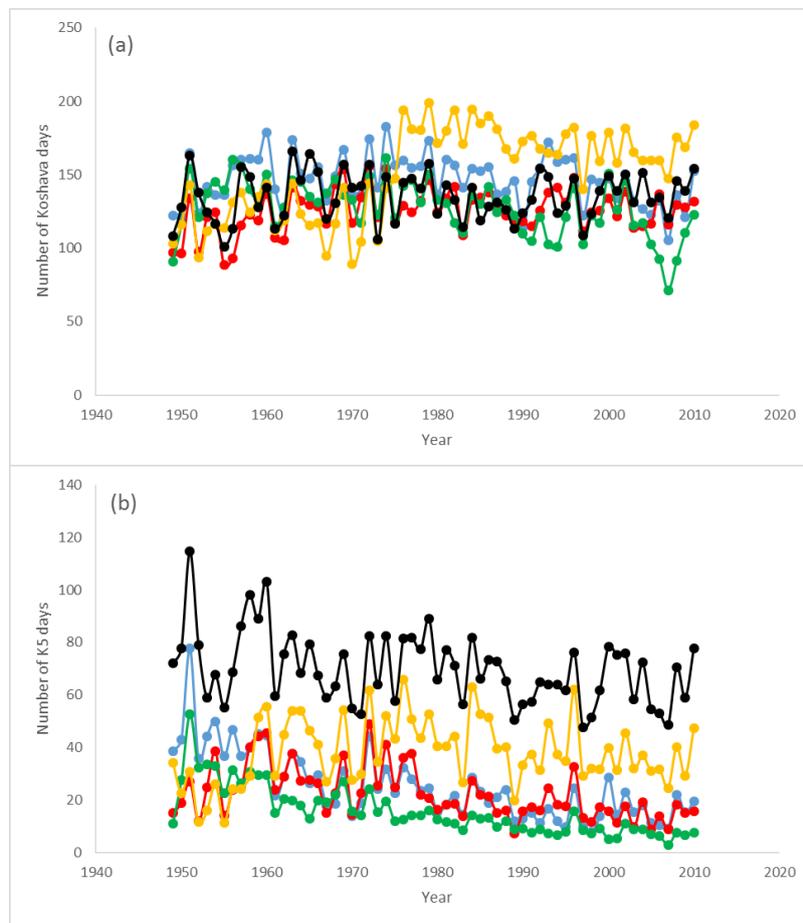
Figure 4.5. Annual number of days with the Koshava wind: (a) all wind speeds, (b) K5 winds. Weather stations: blue – BG; red – NS; green – SP; yellow – VG; black – VR.

The K5 winds in Figure 4.5 have the upward trends at the NS and VG stations from 1949 to the end of 1960s. Therefore, the positive trend observed in Figure 4.4 seems to be solely caused by the positive trends at these two stations. The negative trend in Figure 4.4 that followed from the 1970s can be attributed to the downward trend that was observed at all five stations.

Koshava is a persistent wind that usually blows for several days at a time. Milosavljević (1950a) and Unkašević *et al.* (2007) noticed that Koshava in March usually lasts for 2 to 4 days, but can be active for as long as 18 to 22 consecutive days. The total number of periods when Koshava was active, sorted into ordinal length categories is given in Figure 4.6. On average, 2-day Koshava periods are 2.5 times more frequent than 1-day Koshava events and 1.7 times more frequent than 3-day Koshava periods. At the same time, 3-day periods were found to be 1.5 times more often than 1-day events. The VG station seemed to have the most persistent Koshava winds. This pattern is particularly evident when the ≥6-day events are examined. Although the highest average wind speeds are observed at the VR station, this station is not found to have the most persistent wind activity.
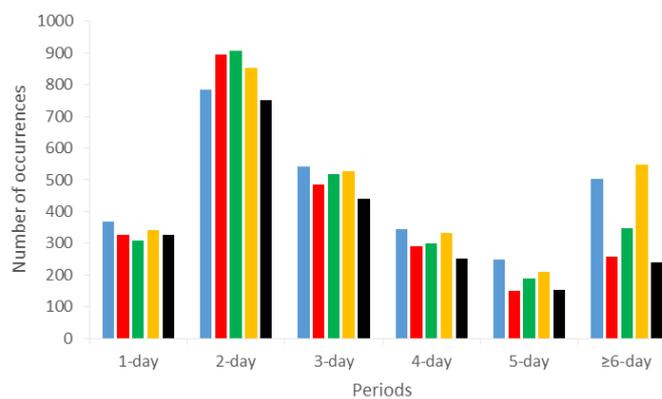
Figure 4.6. The total number of Koshava periods for each station in the KR. Weather stations: blue – BG; red – NS; green – SP; yellow – VG; black – VR.

Table 4.8. Trend analysis of annual number of Koshava episodes in the period 1949-2010. Symbols as in Table 4.7.

Station	Period length	Z	H_1	Q	B
BG	1-day	-0.98	0	0.000	6.00
	2-day	0.70	0	0.000	12.50
	3-day	-1.38	0	-0.026	9.87
	4-day	0.41	0	0.000	6.00
	5-day	-0.99	0	0.000	4.00
	≥6-day	-1.77	1	-0.043	9.43
NS	1-day	0.74	0	0.000	5.00
	2-day	1.31	0	0.033	12.68
	3-day	2.13	2	0.040	6.10
	4-day	3.36	4	0.053	2.95
	5-day	1.53	0	0.000	2.50
	≥6-day	0.89	0	0.000	4.00
SP	1-day	-1.82	1	-0.026	5.65
	2-day	-0.04	0	0.000	15.00
	3-day	0.28	0	0.000	8.00
	4-day	-0.22	0	0.000	5.00
	5-day	-0.23	0	0.000	3.00
	≥6-day	-3.98	4	-0.080	8.10
VG	1-day	0.76	0	0.000	5.50
	2-day	0.03	0	0.000	14.00
	3-day	1.75	1	0.028	7.33
	4-day	1.07	0	0.000	5.00
	5-day	1.15	0	0.000	3.00
	≥6-day	2.53	2	0.053	7.26
VR	1-day	-0.47	0	0.000	5.00
	2-day	-1.93	1	-0.063	14.09
	3-day	0.00	0	0.000	7.00
	4-day	0.24	0	0.000	4.00
	5-day	-0.88	0	0.000	2.00
	≥6-day	-1.17	0	0.000	3.50

In a 365 day year, Koshava was active for 38.4 %, 26.8 %, 31.2 %, 40.8 %, and 24.9 % of the year, at the BG, NS, SP, VG, and VR stations, respectively. Therefore, it can be said that, on average, Koshava is active in 32.4 % of the time in the year in the study area. Out of this 32.4 %, 1-day, 2-day, 3-day, 4-day, 5-day and ≥6-day events have occurred in 1.5 %, 7.4 %, 6.7 %, 5.4 %, 4.2 %, and 7.3 % of the time, respectively.

It should be noted that the values in Table 4.6 are slightly higher. This difference is because results in Table 4.6 also include wind events that were shorter than 1 day. A trend analysis of the periods of Koshava activity was also performed and results are shown in Table 4.8. Many Koshava periods are without any trend (Q = 0). The other periods usually have statistically not significant trends. The only exceptions are the SP station where the ≥6-day events have significant negative trend ($H_1 = 4$) with Sen's slope of -0.08 events per year and the NS station where the 4-day episodes are also declining with 99.9 % statistical confidence.

4.5.3 Comparison between Koshava trends and trends of westerly and northwesterly winds

After Koshava, westerly and northwesterly (W&NW) winds are the most dominant wind directions over Serbia (see Table 4.2). It is interesting therefore to investigate potential similarities and/or contrasts between the Koshava and W&NW winds. Note that northwesterly winds are here represented with WNW and NW directions; thus the W&NW are winds coming in from W, NW and WNW directions.

From the climatologically point of view (Table 4.2 and Table 4.4), the W&NW winds are most frequent in NS during the summer (35.5 %) and least frequent in VR in the fall season (11.6 %). These westerlies are more common in VG than in

BG and SP, although the difference between VG and BG is not that pronounced. This observation is most probably caused by the orography and the location of these weather stations in respect to the orography. Namely, the BG and VG stations are at similar latitudes and both are exposed to the westerlies; BG station directly exposed whereas the VG station through the Danube River basin (see Figure 1.1). The SP station is located in central Serbia and is somewhat sheltered from westerlies by Suvobor, Kosmaj and Rudnik mountains. Therefore, the W&NW winds at SP are not as common as at BG and VG. This orography hypothesis is additionally supported by the observation that the WNW and NW directions at the VG station are more common than W (because of the Danube River channeling), whereas W and WNW are the most common wind directions in BG than NW (see also Section 5.4 for further discussion on the orography hypothesis). The dominance of Koshava in VR attenuates the W&NW winds. On an annual basis, the frequency of occurrence of W&NW winds in BG, NS, SP, VG and VR is 24.6 %, 30.5 %, 21.9 %, 26.7 % and 13.6 %, respectively. The strongest W&NW winds blow in NS, SP (especially at 14:00) and VR with the mean annual wind speeds of 3 m s^{-1}, followed by the BG and VG stations where the mean annual W&NW speeds are found to be 2.5 and 2.3 m s^{-1}, respectively (Figure 4.7). On a seasonal basis, the strongest W&NW winds occur in NS in summer (3.5 m s^{-1}). Comparing Figure 4.7 to Figure 4.2 and inspecting Table 4.4, it can be concluded that on average Koshava is stronger than the W&NW winds. The W&NW winds peak in the summer season when Koshava is the least frequent. Milosavljević (1950a) and Unkašević (1994) noticed similar seasonality of winds over BG. The present study expands these findings to the whole KR.

The trend analysis of the W&NW winds is given in Table 4.9. It can be seen that the westerlies are either pronouncedly decreasing (BG, SP and VR) or possess

very weak and statistically not significant trend (NS and VG). The strongest negative trend is observed at the VR station (Z = -4.79). The only positive trend is recorded at the VG station (Q = 0.002 m s^{-1} year^{-1}), but it is not statistically significant even at a = 0.1 (i.e. the 90 % confidence level).
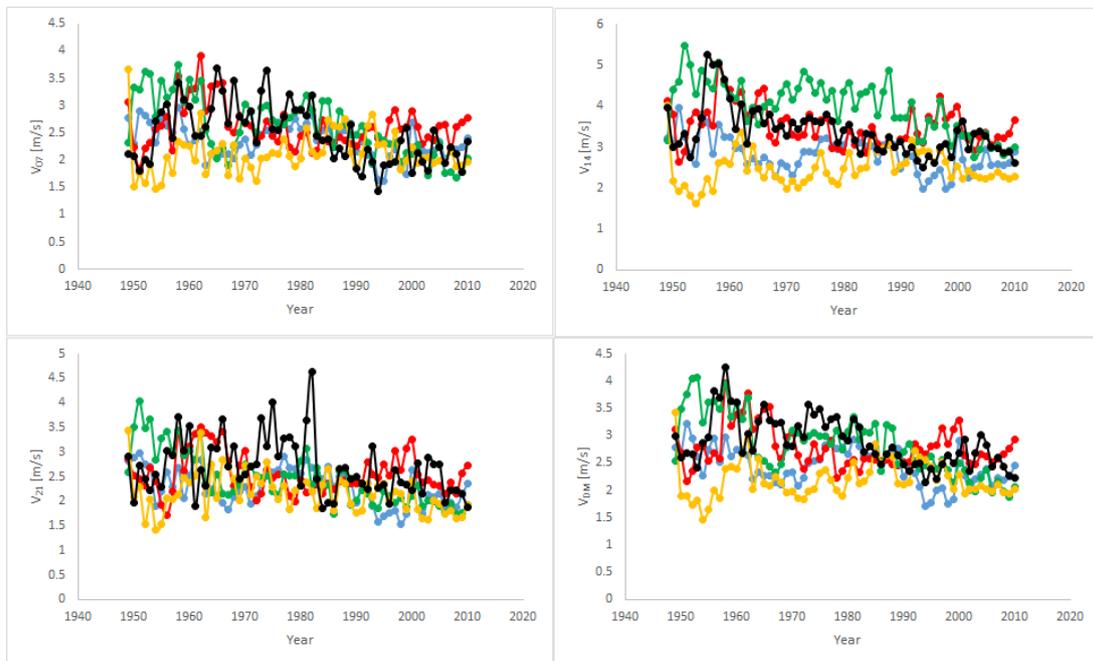
Figure 4.7. The mean annual speed of W&NW winds for the three measurement terms (07:00, 14:00, 21:00) and DM values. Weather stations: blue – BG; red – NS; green – SP; yellow – VG; black – VR.

A comparison of Koshava trends in Table 4.5 (all speeds and DM values) against the N&NW trends presented in Table 4.9 reviles that Koshava's weakening is more distinct then the observed long-term attenuation of the westerlies. The only exception of this rule is the SP station where N&NW winds were declining more rapidly than Koshava.

Table 4.9. Trend analysis of the mean annual speed of W&NW winds (DM values) in the period 1949-2010: Mann-Kandall test statistic, Z, significance of the trend, H1, Sen's slope, Q (m s^{-1} year^{-1}), and offset of the linear trend line, B (m s^{-1}).

Station	Z	H$_1$	Q	B
BG	-3.61	4	-0.009	2.75
NS	-1.28	0	-0.003	2.79
SP	-6.66	4	-0.026	3.64
VG	0.80	0	0.002	2.07
VR	-4.79	4	-0.015	3.33

Sen's slopes for the Koshava speeds at the BG, NS and VR stations are 5.7, 2.3 and 2.3 times larger than the corresponding values of the W&NW wind. The trends at the VG station have opposite sign – negative for Koshava and weak positive for the N&NW winds.

It can be concluded from the previous discussion that the overall negative trend of the Koshava wind is not an isolated case. The second most dominant wind direction over Serbia (the W&NW winds) also experienced an overall decline of wind speeds in the analyzed 62-year period.

4.6 Causes of Koshava trends

4.6.1   Large-scale circulation changes

Changes in the synoptic circulation patterns might be one of the factors causing the observed Koshava trends. In order to investigate this, zonal and meridional components of the total wind at 500 hPa and 850 hPa pressure levels were obtained from the NCEP/NCAR reanalysis data set (Kalnay *et al.*, 1996). The analysis has been only performed for dates when Koshava was recorded at the five surface stations listed in Table 4.1. This way, large-scale circulation patterns

typical for Koshava wind were isolated. Additionally, to obtain the average annual values, data were spatially averaged over the KR (from LON 20°E to LON 23°E and from LAT 44°N to LAT 44.5°N) and time averaged afterwards. The results are depicted in Figure 4.8. The meridional component at 500 hPa level shows a negative trend of -0.015 m s^{-1} year^{-1}, while the zonal component has a fairly small positive trend of 0.007 m s^{-1} year^{-1}. Koshava is a shallow wind that usually blows within the lowest 2000 m of the troposphere (Vukmirović, 1985b; Unkašević *et al.*, 1999). The analysis of the wind components at 850 hPa level (approximately 1500 m a.g.) would, therefore, be more meaningful. It was found that the both wind components at the 850 hPa level have experienced the same decline of velocity (Q = -0.012 m s^{-1} year^{-1}). The attenuation of the total wind in the 1949-2010 period was 1.05 m s^{-1} (Q = -0.017 m s^{-1} year^{-1}).

The negative trend of the synoptic winds at 850 hPa is around 57 % of the observed average attenuation of the K5 winds (-0.030 m s^{-1} year^{-1}). This percentage is even higher, 68 %, after the small Koshava wind speeds are considered. This indicates that the declining trends of the Koshava's speed are largely caused by the slowdown of circulations that have larger spatial scales than the Koshava wind.

A decrease in the frequency of occurrence as well as the strength of the Siberian high and West-MCs can be attributed to this negative trend of the synoptic winds and therefore partially to the negative trend of the surface Koshava winds. As mentioned earlier in Section 4.1, the weakening of the Siberian high (-2.5 hPa decade^{-1}) in the period of 1978-2001 was reported by Panagiotopoulos *et al.* (2002). Similar negative trends of the Siberian high were also observed by D'Arrigo *et al.* (2005), Jeong *et al.* (2011) and Mokhov and Khon (2005). These changes in the

Siberian high intensity influenced many meteorological variables outside of the Siberian high region (Thompson and Green, 2004; Chernokulsky *et al.*, 2013; Hasanean *et al.*, 2013).
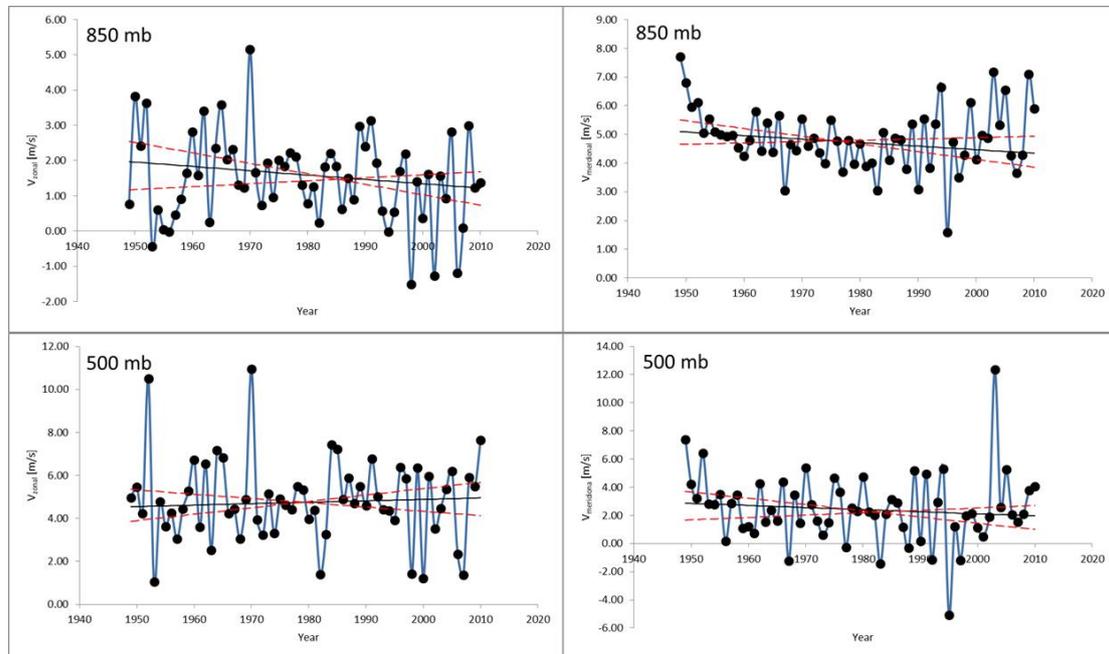
Figure 4.8. Changes of zonal (left panels) and meridional (right panels) wind components at 850 hPa (upper panels) and 500 hPa (lower panels) in the KR from 1949 to 2010. The black line is Sen's slope, the red dashed lines are trends at the 95 % confidence intervals. Data source is NCEP/NCAR reanalysis 1 dataset (Kalnay *et al.*, 1996).

The other pressure systems that drive the Koshava wind, the MCs, have also experienced negative trends in both strength and activity during the last century (Trigo *et al.*, 2000; Maheras *et al.*, 2001; Flocas *et al.*, 2010; Nissen *et al.*, 2010; Nissen *et al.*, 2013). Therefore, it can be concluded that the weakening of these two pressure systems over the course of the last several decades attenuated the zonal pressure gradients above the Balkan region and thus resulted in the weakening of the Koshava wind.

4.6.2 Temperature influence

Several studies showed that temperature trends can be highly correlated to the wind speed trends (Klink, 1999; Pirazzoli and Tomasin, 2003; Dadaser-Celik and Cengiz, 2013). Dadaser-Celik and Cengiz (2013) noticed a strong negative correlation of wind speed trends and air temperature in the west regions of Turkey. On the other hand, Pirazzoli and Tomasin (2003) showed that temperature variations were positively correlated with wind speeds in the central Mediterranean region. Long-term trends of temperature at one region can either diminish or augment the pressure gradients above that and neighboring regions (Klink, 1999; Guo *et al.*, 2011).

Study of the temperature trends in the KR has been performed and the results are depicted in Figure 4.9. The region taken into consideration is the same as the region considered for the synoptic wind analysis in the previous sub-section. It should be noted, however, that the analysis was performed for all days, and not only for days with the Koshava wind.

The surface temperature experienced a strong negative trend (H_1 = 4) in the period from 1949 to 2010. The Sen's slope is equal to -0.025 K year^{-1}. The 5-year moving average shows that the surface temperature had been sharply decreasing until the middle of 1970s, followed with a more or less constant temperature and an increase after the year 1999. Relation between Koshava speed trend and the observed temperature trend can be explained with the aid of Figure 1.1. The high pressure and cold air are situated east and northeast of the KR. Decrease of the temperature in the KR would therefore decrease the temperature difference between the KR and the source region of the Koshava wind (east Romania, Moldavia, and Ukraine), leading to the weakening of pressure gradients. As a

result Koshava wind speeds would be decreased. This conclusion is also in accordance with findings of Croitoru *et al.* (2012) and Brázdil *et al.* (1996). Croitoru *et al.* (2012) noticed that west regions of Romania (also situated in the KR) had negative temperature trends in the period from 1901 to 2000 and east parts of Romania (source region for the Koshava wind) experienced a positive trends in temperature.
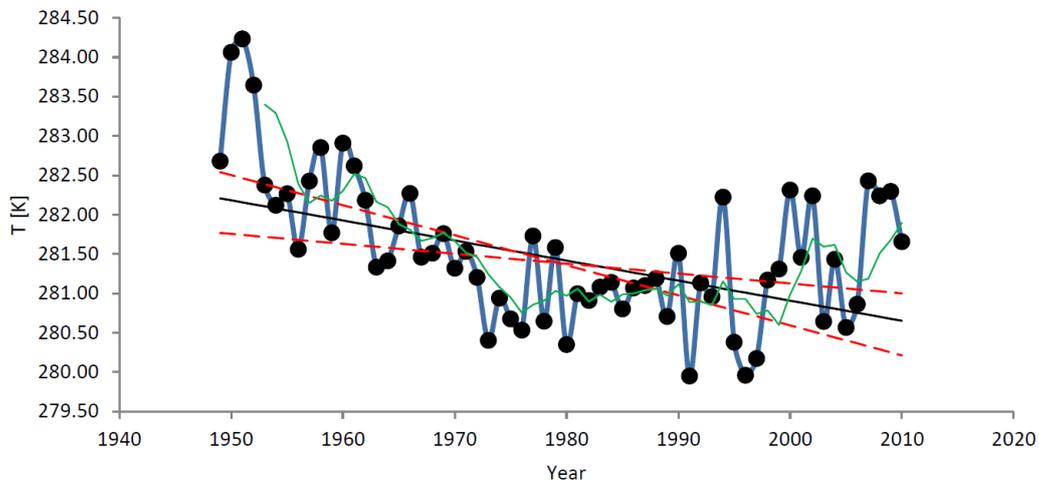
Figure 4.9. Changes of DM temperature in the KR from 1949 to 2010.The black line is Sen's slope, the red dashed lines are trends at the 95 % confidence intervals. Data source is NCEP/NCAR reanalysis 1 dataset (Kalnay *et al.*, 1996).

4.6.3   Roughness changes

Changes in surface roughness can significantly influence the wind speeds (Klink, 1999; Vautard *et al.*, 2010). Vautard *et al.* (2010) concluded that 25 to 60 % of the observed negative wind speed trends in the Northern Hemisphere are due to the increasing surface roughness. Surface roughness increase can result from urbanization, change of land use and forestation. Urbanization in countries that

are in the KR (Serbia, parts of Romania and parts of Bulgaria) has been constantly increasing. Based on the United Nations estimates, the percentage of the urban population in these countries has grown from 24.5 % in 1950 to 58.6 % in 2010 (Unated Nations, 2006). Forest areas, however, have increased only for a few percentages in the last decade (The World Bank, 2013) and generally forests occupy around 30 % of the land in the KR.

The only real urban station in this study was BG station. It showed the second largest downward trend of wind speed considering both wind speed regimes and the largest negative trend of K5 wind activity. However, because these trends are not considerably different than the trends at other four stations, it can be assumed that the above two factors (i.e. changes in synoptic pressure systems that cause Koshava and temperature changes in the KR) had larger influences.

4.6.4 Data quality

Detailed discussion on data homogeneity was given in Section 4.4. Several break points appear in every series of both wind direction and speed data. Anomalies in 1950s are generally due to the introduction of the practice of using 16 wind directions instead of 8. The anomalies that are due to station relocation are clearly represented, especially in the NS series in 1978 and the VG series in 1975. Most of the other anomalies are due to an instrument replacement or minor changes of instrument's close environment.

The modified form of the ReDistribution Method performed over the significant wind speed series greatly reduced the number of anomalies. All anomalies due to changes in instrument's close environment disappeared, while anomalies caused by relocation, misalignment and instrument replacement were still present. Changes in wind direction distribution patterns, however, were mostly

caused by redistributions of a neighboring wind direction. The frequencies of winds within quadrants, especially southeast quadrant, are mostly left to natural variations.

The near-calm wind speeds are substantially more inhomogeneous than the higher wind speed. This observance is because the small wind speeds are much more susceptible to changes in measuring instrumentation and procedures (DeGaetano, 1998). Homogeneity testing revealed that wind direction series have been more inhomogeneous than wind speed series. K5 winds generally have negative trends with larger absolute values compared to trends when all wind speeds are considered. This finding suggests that the quality of the data did not have a significant influence on the observed wind trends (Vautard *et al.*, 2010; for high wind speeds in particular).

4.7 Application to wind energy sector

Wind trend analysis is particularly important in the wind energy sector (Holt and Wang, 2012). Herein, the effects that the Koshava trends might have to the wind energy sector are studied for the VR station. The VR station was selected because it has the highest annual wind speeds compared to the other four stations and because the significant wind potential of the VR region has been identified in other studies (Gburčik *et al.*, 2006; Đurišić *et al.*, 2007).

First, Koshava's DM wind speeds at 10 m level (V_{10}) were extrapolated to 80 m height (V_{80}) using the power law (e.g. Archer and Jacobson, 2003):

$$V_{80} = V_{10} \left(\frac{80}{10} \right)^{\alpha}, \qquad\qquad (4.1)$$

where a is the power exponent that depends upon the surface roughness and stability of the atmosphere. In neutrally stable atmosphere and for open terrain exposures, a is approximately 0.143. In absence of wind speed measurements at two different heights, the above approximation is reasonable (Pryor and Barthelmie, 2003), and more conservative compared to calculated values at many sites (Sisterson *et al.*, 1983). Errors in wind resource assessments that rely upon the extrapolation of wind speeds are inevitable, and thus this study argues that it is better to underestimate wind resources, but to overestimate it.

In the second step, parameters of the Weibull distribution were evaluated for each year using the series of V_{80} wind speeds. The Weibull distribution is a good approximation for the wind speed distribution:

$$f(V_{80}) = \frac{k}{A} \left(\frac{V_{80}}{A}\right)^{k-1} e^{-\left(\frac{V_{80}}{A}\right)^{k}}. \qquad (4.2)$$

Here, A (m s^{-1}) is the scale parameter proportional to the mean wind speed and k is the shape parameter. Different values of the shape parameter can have marked effects on the behavior of the distribution. A large value of k (around 3) indicates constant (steady) winds, whereas the small values of k (around 1) signifies unsteady winds. The trend analysis for the Weibull parameters was performed and results are given in Figure 4.10.

The shape parameter has the statistically significant negative trend ($H_1 = 4$) with the slope value of -0.044 m s^{-1} year^{-1}. This observation is in accordance with the previously obtained result that the mean annual wind speeds at VR station have been declining. The trend of A has steeper slope than the trend of the surface wind speed, indicating that wind speeds at 80 m might have experienced a stronger downward trends. On the other hand, the shape parameter was almost

without trend ($Q = 0.001$ year^{-1}) and has a value of 1.86. Because how skewed the Weibull distribution is depends only on the shape parameter, it follows that the asymmetry of the distribution did not change over time (i.e. it stayed positively skewed since $k < 2.6$).

At last, the power density per unit area at 80 m height (P_{80}) was determined using the European Wind Atlas methodology (Ib and Petersen, 1989). The P80 was calculated from the Weibull parameters using the equation:

$$P_{80} = \frac{1}{2}\rho A^3 \Gamma\left(1 + \frac{3}{k}\right),$$

(4.3)

where, ρ is the air density (assumed to be 1 kg m^{-3}) and Γ is the gamma function. Trend analysis results are depicted in Figure 4.11.
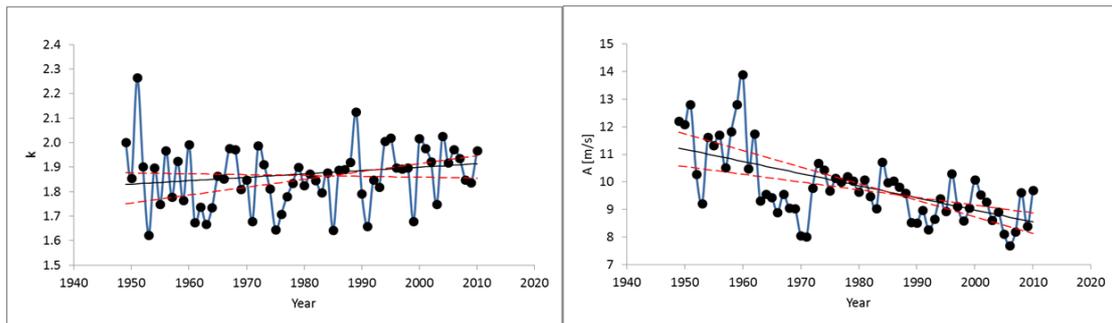
Figure 4.10. The Weibull parameters for Koshava wind at 80-m level in the period 1949-2010 at the VR station. The black line is Sen's slope, the red dashed lines are trends at the 95 % confidence intervals.
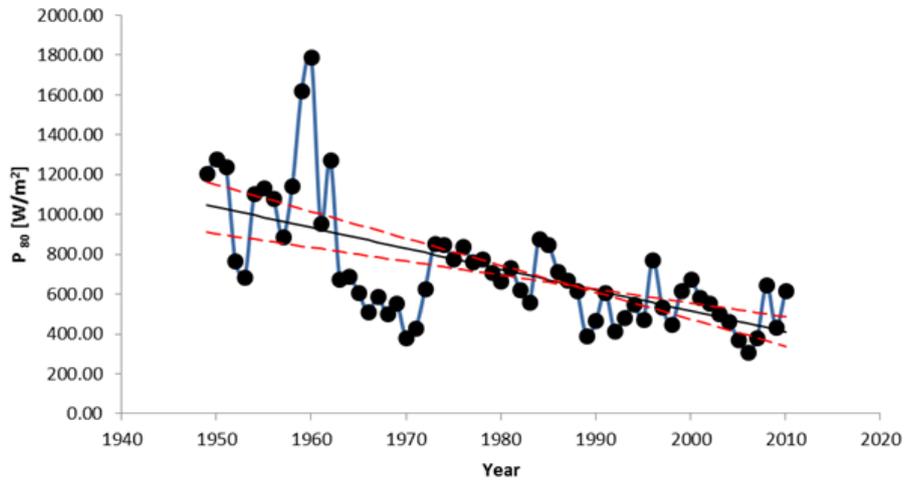
Figure 4.11. The wind power density per unit area of Koshava wind at 80-m level in the period 1949-2010 at the VR station. The black line is Sen's slope, the red dashed lines are trends at the 95 % confidence intervals.

The P_{80} has statistically negative trend at 99.9 % confidence level with Sen's slope equal to -10.463 W m^{-2} year^{-1}. Koshava at the VR station was active in about 37 % (3241.2 hours) of the time in a year (Table 4.2 and Figure 4.1). Keeping in mind that both k and the number of days when Koshava was active have small trends (almost trendless; see Table 4.7 for Koshava activity), the slope of wind energy trend at 80 m (E_{80}) can be calculated. It follows that the decline of the E_{80} is -33.913 kWh year^{-1}. For example, with the feed-in tariffs that are presently active in Serbia (92 € for each MWh from the wind), the wind farm developers would lose around 3.1 € year^{-1} due to the negative trend of the mean annual Koshava wind speeds. This value can be considered as a negligible yearly loss compared to other potential losses such as the losses caused due to year-to-year wind variability, maintenance, failure of equipment and electrical losses.

4.8 Summary and conclusions

A comprehensive analysis of the long-term trends of the Koshava wind was provided in this chapter. The analysis covered a period of 62 years (1949-2010) and is based on meteorological measurements from five synoptic weather stations located in Serbia. The Koshava wind speeds were categorized into two classes: (1) all wind speeds and (2) wind speeds above 5 m s^{-1} (named K5 winds). Trends have been calculated and analyzed for wind speed and the wind activity (including the activity of different Koshava periods). The quality of wind speed and wind direction data has also been addressed through the homogeneity testing. Lastly, a potential effect that the observed trends could have in the wind energy sector has been assessed. The following conclusion can be drawn:

- Small wind speeds have been more inhomogeneous compared to wind speeds larger than 5 m s^{-1} and the wind direction series were more inhomogeneous than the wind speed series.

- Statistically negative and significant (at a=0.001) trends of annual wind speeds have been recorded at all stations. The only exception was VG station in case when all wind speeds were considered, where trend was significant at a=0.01. The average slope of the trend was -0.020 m s^{-1} year^{-1} and -0.024 m s^{-1} year^{-1} for all wind speeds and for K5 winds, respectively. Stronger trend for higher wind speeds indicates that data quality did not have profound influence on the observed trends.

- Trends in the annual number of the days with the Koshava wind show larger spatial irregularity. The K5 winds had negative trends at VR station (at a=0.01) and at BG, NS and SP stations (at a=0.001). A positive, but statistically not significant trend has been observed at the VG station.

Including into analysis the small wind speeds (< 5 m s^{-1}), trends of the Koshava activity at BG, NS and VR stations become statistically not significant.

- On average, Koshava was active in 32.4 % of the time in a year. 2-day and 3-day Koshava events were the most common; recorded in 7.4 % and 6.7 % of the time. 1-day Koshava events were rare (only 1.5 % of time).

- Most Koshava events spanning several days are either have no significant trend or have weak negative trends.

- The westerlies over the KR also experienced negative trends (an exception is positive, but statistically insignificant trend at the VG station). With the exception of the SP station, these trends, however, are weaker (in absolute values) than Koshava's negative trends. This findings indicates that winds in the KR are generally weakening.

- The negative trends of the synoptic winds at 850 hPa and 500 hPa levels, as well as decrease in the temperature gradient between the KR and the source region of the Koshava wind, indicate that the changes in the large-scale weather patterns were dominant factors that caused the negative trends of the Koshava wind. This finding is in accordance with the literature results on the weakening of the Siberian high and West-MCs. Data quality and changes in surface roughness had minor influences.

CHAPTER 5

5. Contributing factors to Koshava wind characteristics

5.1 Introduction

The name Koshava (Košava) has a 17th century Turkish origin as the Turkish Empire ruled the Western Balkan region at that time. The word comes from "koç hava" meaning "fast (or agile) air" in an older version of Turkish. Therefore, Koshava is a well-known wind in the region for a long time. It is a widely accepted postulation that the EAs and MCs are the main synoptic Koshava drivers. This assumption, however, has not been quantified up until now. Namely, the only statistical investigation of the EAs and MCs that generated Koshava was performed by Radosavljević and Vojnović-Kljaić (1985). They analyzed a 6-month period from October 1982 to March 1983 and restricted their study to the BG station. Other studies (see Sections 0 and 2.4) have only qualitatively describe this relationship between Koshava, on one side, and EAs and MCs, on the other side (similar to the description of the Koshava wind provided in Section 1.2). This chapter will quantitatively investigate an *a priori* assumed connection between Koshava wind and its synoptic and mesoscale contributors.

Here, the following questions will be addressed. First, what are the main synoptic and mesoscale contributors to the Koshava wind characteristics? That is, are the

EAs and MCs the only synoptic Koshava drivers? Second, what are the main characteristics of the EAs and MCs that result in Koshava? Third, which gap flow properties are the main mesoscale driving mechanisms for the Koshava wind? In the investigation of these principle questions, the results will further contribute to finding answers to other long-standing question such as: is it possible to predict the occurrence and speed of the Koshava wind based on the characteristics of the synoptic and mesoscale mechanisms that govern it?

5.2 Data

The data used for analysis of contributing factors for the Koshava wind are: (1) mean and maximum hourly wind, MSLP and temperature at 2 m a.g data from the four weather stations located in the KR and the four stations located in the source Koshava region (SKR) (Table 5.1 and Figure 5.1), and (2) the NCEP/NCAR reanalysis 1 dataset (Kalnay *et al.*, 1996).

Wind speed data in electronic form were provided by the Hydrometeorological Service of Serbia. Prior to its digitalization, the data passed a quality control check. The wind data series from the stations in the KR were tested for homogeneity in Chapter 4. Lower wind speeds were found to be more inhomogeneous compared to higher wind speeds. Most of the anomalies in the data series occurred prior to 1980, which was due to the relocation of some of the stations. The data from the stations in the KR were provided with 1-hour temporal resolution, while the data from the stations in the SKR have 3-hour temporal resolution. Hence, all comparisons/analysis between these two datasets are performed on 3-hour intervals.
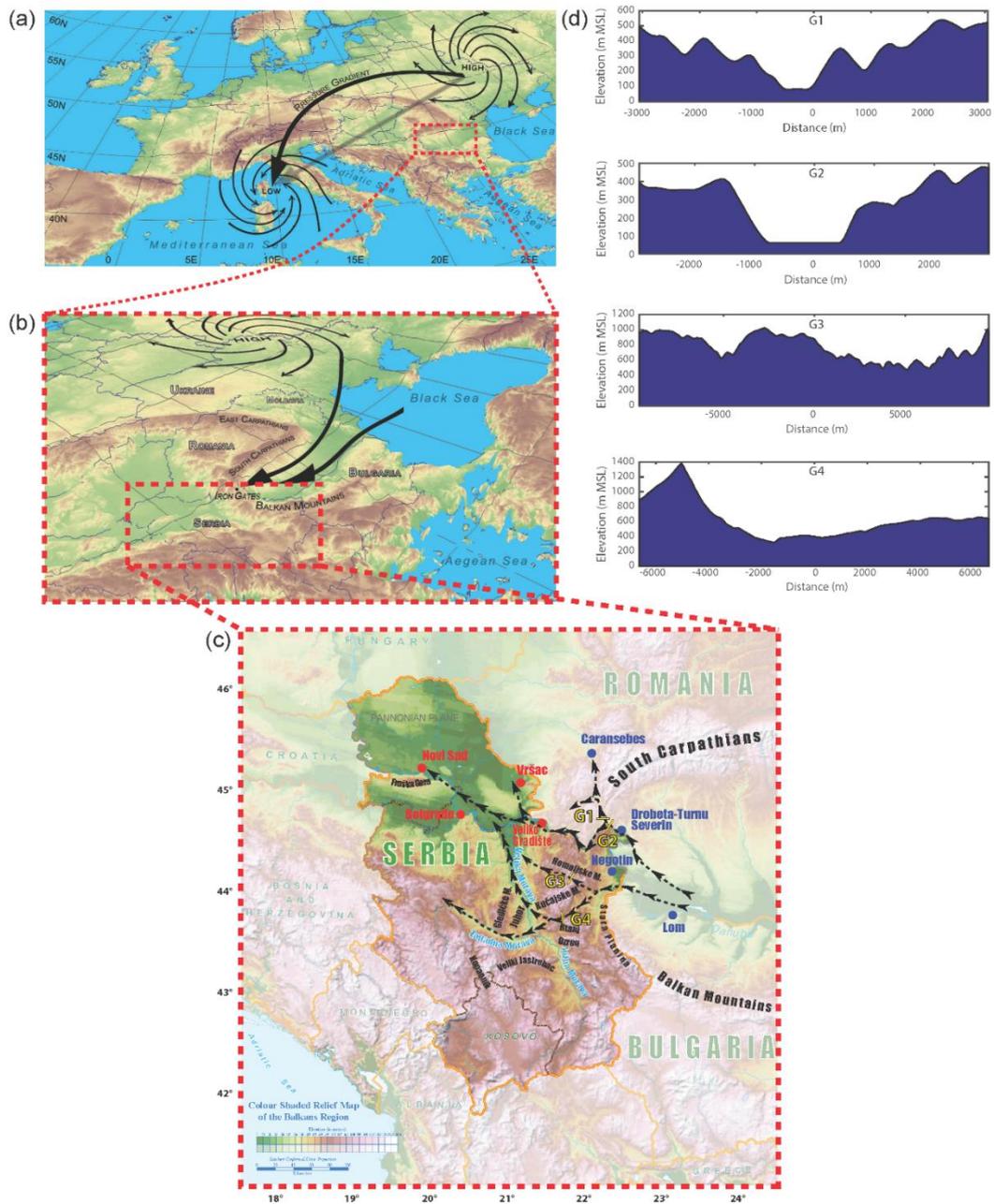
Figure 5.1. Similar to Figure 1.1 with additional details such as the weather stations in the SKR (blue dots in (c)) and (d) vertical cross-section of the gaps that connect the KR with the SKR (see Section 5.4). See text for further details.

Table 5.1. List of weather stations and data records used for the analysis of synoptic and mesoscale Koshava contributors. Weather stations in the KR (BG, NS, VR, VG) are denoted with two-letter abbreviations and weather stations in the SKR (Lom (LOM), Negotin (NEG), Drobeta-Turnu Severin (DTS) and Caransebes (CAR)) are represented with the three-letter abbreviations.

Weather station	Longitude	Latitude	Elevation a.s.l. (m)	Anemometer height a.g (m)	Data coverage (number of observations)
BG	20°27'53.44"E	44°47'54.11"N	132	24	1/1/1971 – 6/30/2014 (373,471)
NS	19°49'47.62"E	45°19'19.88"N	84	10	1/1/1971 – 6/30/2014 (316,026)
VR	21°18'20.01"E	45°08'39.16"N	83	10	1/1/1971 – 6/30/2014 (307,625)
VG	21°29'54.94"E	44°45'09.56"N	82	10	1/1/2011 - 6/30/2014 (29,145)
LOM	23°15'0"E	43°49'1.2"N	33	10	1/1/1973- 11/1/2013 (108,536)
NEG	22°33'0"E	44°13'58.8"N	44	10	1/1/1973- 12/31/2014 (101,097)
DTS	22°37'58.8"E	44°37'58.8"N	80	10	1/1/1973- 12/31/2014 (218,125)
CAR	22°13'1.2"E	45°25'1.2"N	241	10	1/1/1973- 12/31/2014 (245,695)

The wind roses together with wind speed distributions for the stations in the KR are given in Figure 5.2. There are several important features to note. Firstly, Koshava has different directions at different weather stations (see Section 4.3 and Table 4.3 for further discussion). It should be noted here that the wind roses in Figure 5.2 are for the period 1971-2014, whereas the wind roses in Figure 4.1 are

for the period 1949-2010. Therefore, some differences in Koshava's direction can be observed.
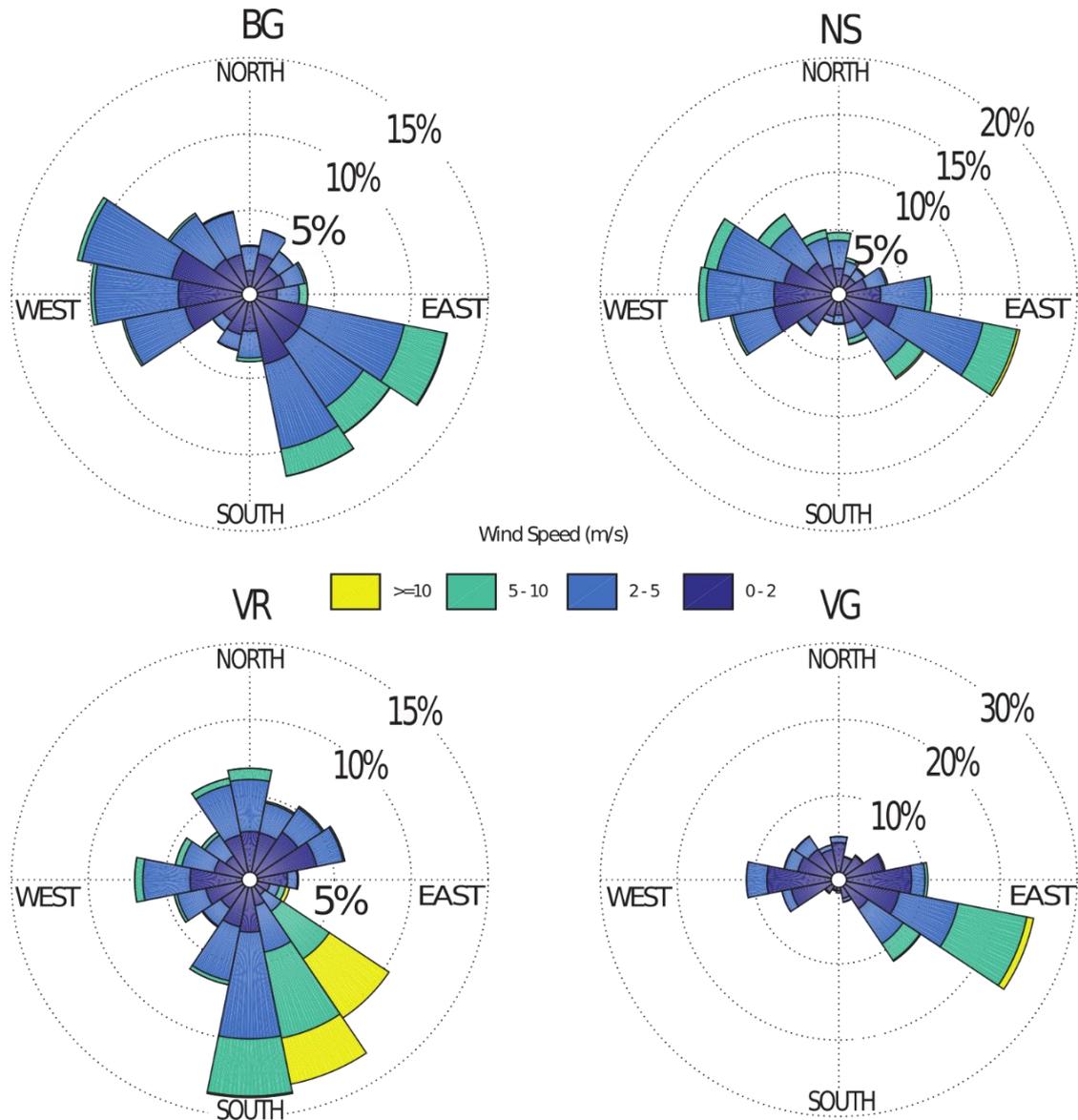
Figure 5.2. Wind roses of direction and intensity for the four weather stations in the KR for the period 1971-2014.

The wind directions associated with the Koshava wind in the period 1971-2014 for each station are: (1) BG [100°-170°], (2) NS [70°-170°], (3) VR [120°-210°], and

(4) VG [100°-150°]. These intervals are in a very good accordance with Table 4.3; however, they are not identical since the corresponding time periods are the same. Secondly, the highest wind speeds were observed at the VR station (about 15 % of the time when Koshava was active, wind speeds were recorded to be above 10 m s^{-1}), followed by the VG station. Thirdly, while Koshava is fairly equally distributed within its directional range at the BG and VR stations, it has a narrower directional distribution at the NS and VG stations. This difference in directional distribution is caused by the orography of the region. Mountains north and south of the VG station channel wind flow restricting the variability of Koshava's directions. Likewise, the mountain to the south of the NS (Fruška Gora, see Figure 5.1c), redirects the flow towards a more easterly direction. Adding more support to this explanation is the observation that at the NS and VR stations, winds from directions blocked by the mountains were rare. Finally, Koshava's speed was rarely below 2 m s^{-1} (less than 4 % of the time for each of Koshava's directions, at all of the considered stations).

Based on these findings, the following procedure has been developed to isolate the Koshava winds from the entire wind datasets. First, Koshava encompasses the wind directions as defined in the previous paragraph. Second, only mean hourly wind speeds above 2 m s^{-1} have been taken into consideration. There are two main reasons for the elimination of wind speeds under 2 m s^{-1}: (1) Koshava is a strong wind, as demonstrated in Figure 5.2 as well as in Figure 4.2, and (2) small wind speeds are more susceptible to inhomogeneity (see Chapter 4). Third, Koshava had to be active for at least 2 days to be taken in to account. This condition is in accordance with the findings presented in Chapter 4 that 1-day Koshava events were rare. Based on these conditions, the basic climatology of the Koshava wind is given in Table 5.2.

The MSLP data for the Northern Hemisphere were acquired from the NCEP/NCAR reanalysis 1 dataset (Kalnay *et al.*, 1996). The data with a 6-hour time interval and a horizontal spatial resolution of 2.5°×2.5° were extracted for the period January 1970 – May 2014. Therefore, the NCEP/NCAR's MSLP data overlap the wind measurement data.

Table 5.2. Climatology of the Koshava wind for the period 1971-2014.

Weather station	Koshava occurrence (days)	Koshava hourly mean speed (m s⁻¹)	Koshava maximum hourly mean speed (m s⁻¹)
BG	1720.25	4.9	10.6
NS	1613.25	4.7	7.6
VR	1995.75	8.6	16.1
VG	154.00	5.9	10.8

5.3 Synoptic scale contributors

5.3.1   The Mediterranean cyclones and Eurasian anticyclones

Total number of lows and highs that occurred in the days when Koshava was active is shown in Figure 5.3. Occurrences of lows and highs were counted in a 2°×2° squares. Strong Koshava cyclones (C0) were mainly located in the Gulf of Genoa (Ligurian and Tyrrhenian Sea) and the west part of Adriatic Sea. Weak cyclones (C10) occurred in the Gulf of Genoa (similar to C0s) and over the eastern Mediterranean and the southern part of Turkey. These areas are located approximately 1000 km from the KR. Strong depressions (C1) were rarely associated with the Koshava wind. Anticyclones, on the other hand, were located in the same geographical region regardless of their strength. Most of them were positioned above northeastern Romania, Moldavia and the south Ukraine. This zone is about 500-900 km northeast from the KR. These findings confirm an *a*

priori assumption that anticyclones and cyclones associated with Koshava are mostly located northeast and southwest of the KR, respectively.

However, Figure 5.3 also shows that the pressure systems can sometimes be located above the KR itself. In these situations, Koshava is caused by a single pressure system – an anticyclone not being accompanied by a cyclone or vice versa. If an anticyclone or a cyclone is positioned above or very close to the KR, then the circulation in the south or southwest part of the anticyclone, or the circulation in the east and northeast part of the cyclone, actually becomes the Koshava wind itself. If, on the other hand, the pressure systems occur a greater distance from the KR, but simultaneously, Koshava is caused by the pressure gradient that is formed between these two pressure systems.

As indicated in Table 5.3, cyclones that trigger Koshava about 52 % of the time were C10s, followed by C0s, about 22 % of the time. The C1s were very rare (making up 3 % of cases). This result can be explained by the fact that closed pressure systems are stronger than open systems, and, secondly, the counterclockwise circulation in cyclones positioned southwest to southeast of the KR contribute to the southeasterly directions of the Koshava wind. On the other hand, A0s were the most frequently observed anticyclone. They were observed about 47 % of the time during Koshava's active periods. The A0s are followed by the A1s, being observed 24 % of the time Koshava was active. Finally, the A10s were recorded approximately 17 % of the time when Koshava occurred.

Table 5.3. Number of days (and %) with cyclones and anticyclones when Koshava was active. Percentages are calculated based on the number of Koshava days from Table 5.2.

Weather station	C0	C10	C1	All C	A0	A10	A1	All A
BG	401.00	899.25	39.50	1339.75	840.25	281.75	417.25	1539.81
	(23.3)	(52.3)	(2.3)	(77.9)	(48.8)	(16.4)	(24.3)	(89.5)
NS	352.25	833.75	33.75	1219.75	765.00	290.75	383.25	1439.00
	(21.8)	(51.7)	(2.1)	(75.6)	(47.4)	(18.0)	(23.8)	(89.2)
VR	347.50	1000.25	38.50	1386.25	823.50	402.75	430.25	1656.50
	(17.4)	(50.1)	(1.9)	(69.4)	(41.3)	(20.2)	(21.6)	(83.1)
VG	39.50	81.25	6.25	127.00	75.50	21.00	38.75	135.25
	(25.6)	(52.8)	(4.1)	(82.5)	(49.2)	(13.6)	(25.2)	(88.0)

Further analysis was undertaken in order to determine which of the two pressure systems had a greater impact on Koshava. Results are portrayed in Figure 5.4, which represents the percentages of Koshava events in which: (1) the presence of both an anticyclone and a cyclone was observed, (2) only an anticyclone was observed, (3) only a cyclone was observed, and (4) neither of the two systems was observed. Both pressure systems were present in about 67 % of all Koshava events. Winds that are influenced by only one of the pressure systems were less frequent. Averaged over all stations in the KR, 21 % of the all Koshava occurrences were paired with an anticyclone without an accompanying cyclone, and only about 10 % of the Koshava episodes were associated with a cyclone without an accompanying anticyclone. Less than 3 % of the Koshava winds occurred without the occurrence of either an anticyclone or a cyclone.
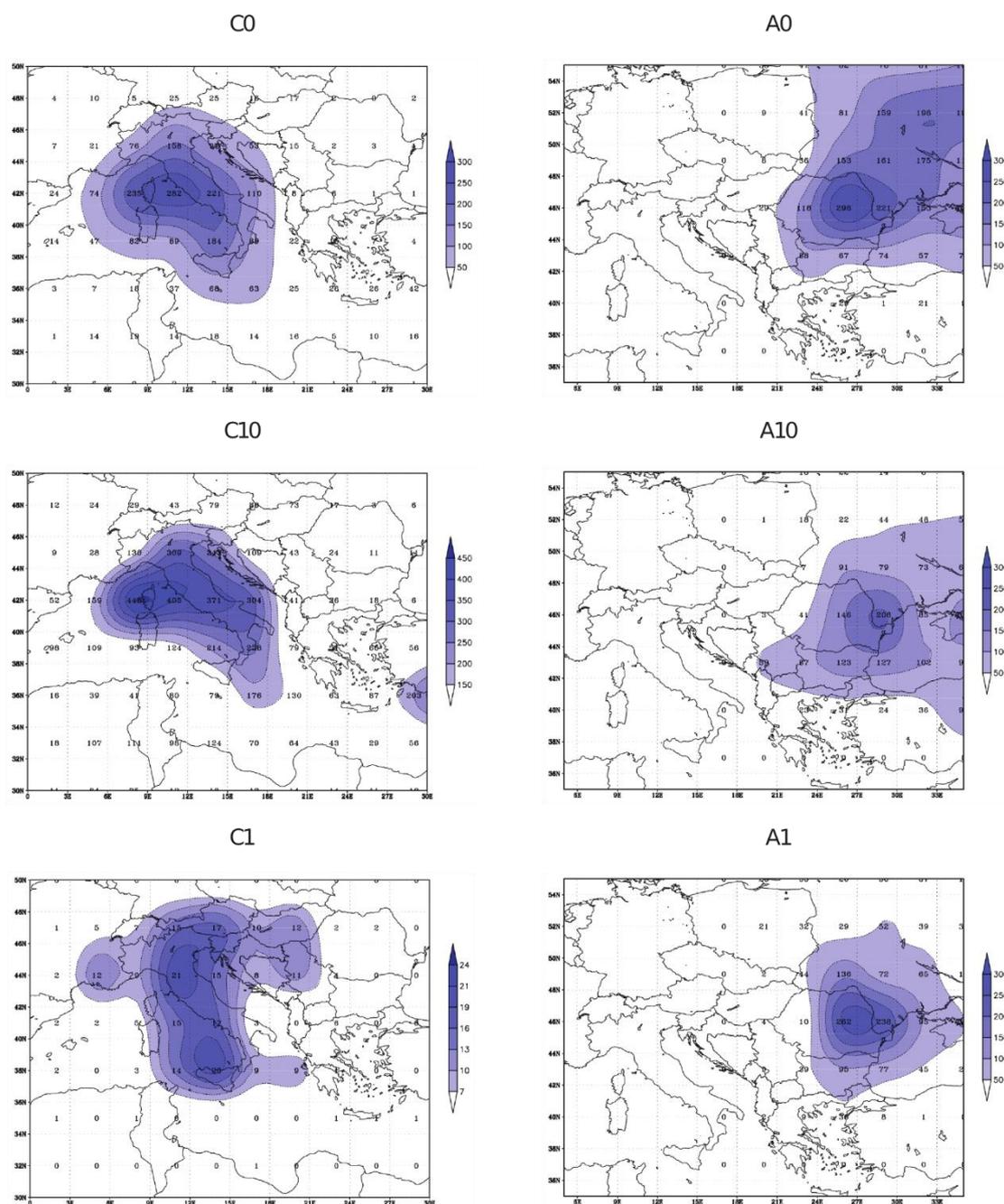
Figure 5.3. Total number of lows (left panels) and highs (right panels) when Koshava was active. C0/A0 – strong closed cyclones/anticyclones; C10/A10 – weak closed cyclones/anticyclones; C1/A1 – strong open depressions/ridges.
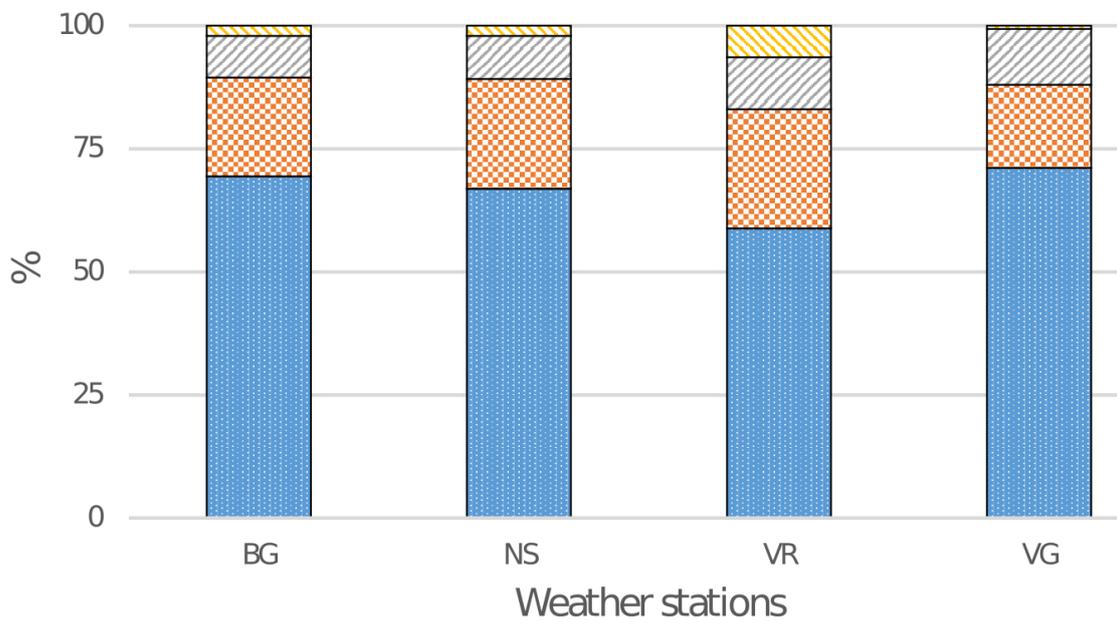
Figure 5.4. Pressure systems associated with Koshava: anticyclone and cyclone present (blue), only an anticyclone present (orange), only a cyclone present (grey), neither of the two pressure systems present (yellow).

Table 5.4 contains the mean hourly Koshava speeds, as well as the maximum mean hourly Koshava speeds for each of the four pressure system scenarios (the simultaneous occurrence of an anticyclone and a cyclone, the occurrence of only an anticyclone, the occurrence of only a cyclone, and when neither an anticyclone nor a cyclone was observed). It can be concluded that Koshava is strongest when both pressure systems occur simultaneously. Besides the NS station, winds driven by only one of the pressure systems have similar mean hourly wind speeds at any given station in the KR. The Koshava events that are not paired with an anticyclone or a cyclone, when they even occur, only achieve low wind speeds. These lower wind speeds may be indicative of Koshava in its dissipation phase.

Table 5.4. Values of the mean hourly (maximum mean hourly) Koshava speeds as the function of the pressure system that was paired with the wind. Values are in m s^{-1}.

Weather station	Anticyclone and cyclone together	Only anticyclone	Only cyclone	None
BG	5.1 (11.0)	4.6 (9.7)	4.6 (9.9)	4.2 (8.6)
NS	4.9 (7.8)	4.0 (5.9)	4.5 (6.7)	3.6 (5.0)
VR	9.2 (16.0)	8.0 (13.3)	8.1 (13.8)	6.6 (11.0)
VG	6.1 (11.1)	5.3 (10.5)	5.3 (9.8)	4.1 (8.0)

The probability density functions (PDFs) of the central pressures of cyclones and anticyclones are presented in Figure 5.5. The red histograms and the red lines represent the pressure systems that caused Koshava, while the blue histograms and the blue lines refer to the pressure system that did not generate Koshava. The area under each of the curves is equal to unity; therefore making it possible to compare Koshava and "no-Koshava" cases. On average, the central pressure of anticyclones that produced Koshava (1027.6 hPa) was 5.1 hPa higher than its "no-Koshava" counterpart (1022.5 hPa). The difference was less pronounced in the case of the cyclones, where the average central pressure of Koshava cyclones (1008.5 hPa) was just 1.6 hPa below the value for the "no-Koshava" cyclones. These results, together with the findings presented in Table 5.3 that state that the high pressure systems were present in 88 % of all Koshava events, indicate that the strong anticyclones are the main trigger for the Koshava wind. This conclusion is reinforced by the fact that the Koshava wind is most active in the winter and spring, when the Siberian High is pronounced (Sahsamanoglou *et al.*, 1991).
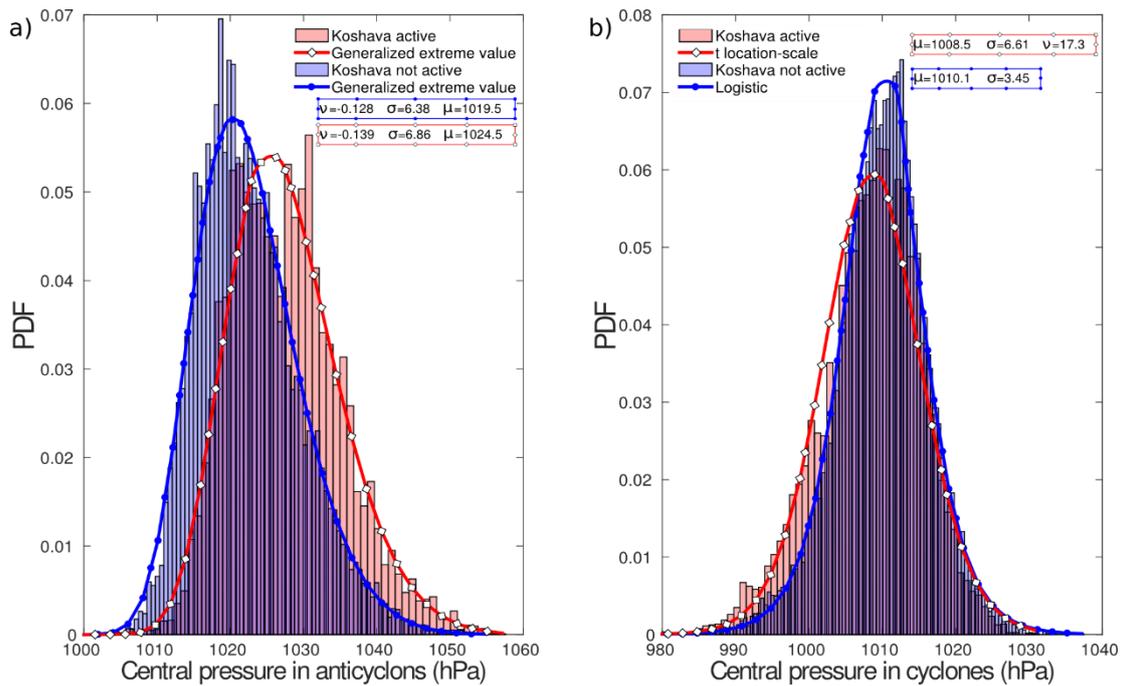
Figure 5.5. PDFs of EAs (a) and MCs (b) central pressures.

The Bayesian Information Criterion (BIC; Schwarz, 1978) is used to determine the best distribution for a given set of data. The parameters of distributions are given in the corresponding figures. Both Koshava and "no-Koshava" anticyclones in Figure 5.5 are best described with the generalized extreme value (GEV) distributions. Since in both cases $\nu < 0$, the distribution corresponds to the Type III (Weibull) GEV distribution. The distributions for Koshava and "no-Koshava" cyclones are the *t* location-scale and logistic distributions, respectively. These two distributions are similar to the normal distribution, but have the heavier tails than the normal distribution and thus are better at modeling outliers.
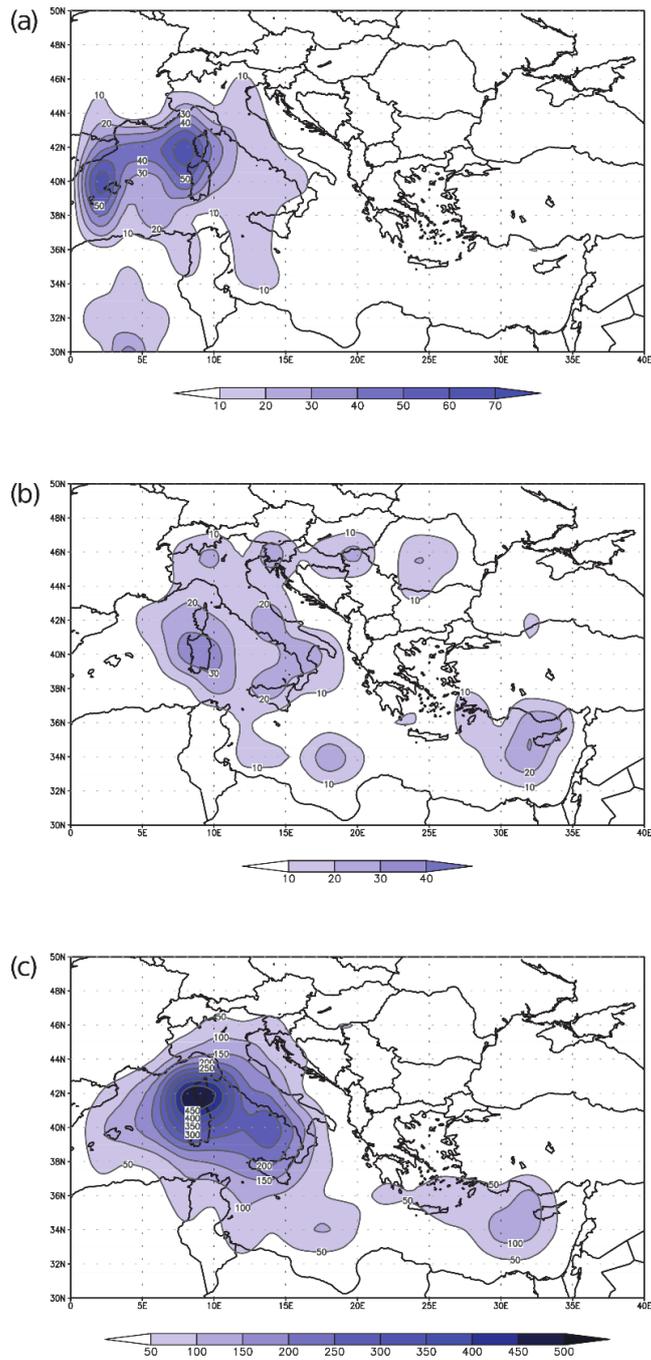
Figure 5.6. Spatial distribution of the Koshava cyclone trajectories. The contours represent the number of: (a) cyclone start positions (cyclogenesis), (b) cyclone end positions (cyclolysis), and (c) cyclone transitions above a given point.

Figure 5.6a shows that the source area of the Koshava MCs is the Gulf of Genoa (together with Corsica and the Balearic Islands). The cyclolysis (Figure 5.6b) occurs south and southeast of their source region: the first region found near Sardinia, Sicily and south of Italy, and the second area being located over the eastern Mediterranean Sea and Cyprus. It follows then, as shown in Figure 5.6c, that the Koshava MCs have southeast trajectories from the Gulf of Genoa to Sardinia and Sicily. Koshava MCs move along southeast trajectories twice as often as they move northeast. This finding is in good accordance with the results previously obtained by Radinović (1987). Horvat *et al.* (2007) also reported that cyclones that form in the Gulf of Genoa typically have southeasterly directions (more than 35 % of Adriatic cyclones originated in the Gulf of Genoa). Similar results were reported by Flocas *et al.* (2010), Trigo *et al.* (1999) and Maheras *et al.* (2001). In the coldest part of the year, when Koshava is most active, cyclones form above large water surfaces. On the other hand, during the summer, cyclones are formed above the warmed continental regions of central Europe. These continental cyclones are not well placed to create the necessary pressure gradient that could cause Koshava.

5.3.2   The mean pressure field and a Synoptic Koshava Index

The MSLP fields averaged for those periods when Koshava was active at all of the stations in the KR, as well as for those days when Koshava was not observed to be active at any of the stations, are presented in Figure 5.7. A typical synoptic situation favorable for the Koshava wind is very different from the synoptic situation observed when the wind was not active. Figure 5.7a shows that the EAs and MCs are located northeast and southwest of the KR, respectively. The isobars above the Balkan and Eastern Europe regions, and hence the KR, have a

meridional orientation. In the SKR, the isobars have northwest-southeast orientation.
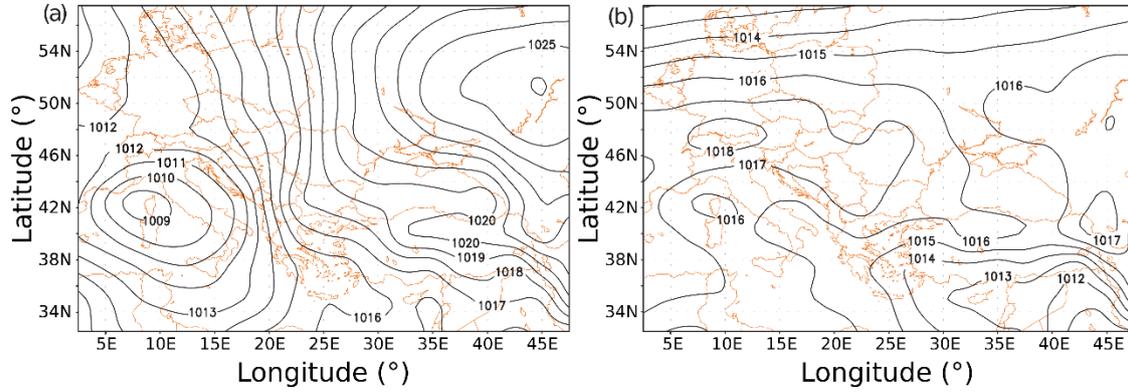
Figure 5.7. MSLP in hPa averaged for days with Koshava (a) and without Koshava (b).

This isobar orientation demonstrates the channeling effect of the Carpathian and Balkan Mountains on airflow, as portrayed in Figure 5.1b. On the other hand, the synoptic chart for days without Koshava (Figure 5.7b) shows the isobars that are zonally orientated over most of Europe. The low and high pressure systems in Figure 5.7a do not exist in Figure 5.7b. This result indicates the existence of the westerly winds in these regions. Therefore, it can be concluded that when Koshava is active, the westerly winds over most of the eastern, southeastern and southern Europe are attenuated or do not exist at all.

Based on the findings presented in Figure 5.7, a synoptic index for the detection of Koshava has been derived. The Synoptic Koshava Index (SKI) is defined as the difference between the area-averaged MSLPs in the anticyclone and cyclone regions:

$$\text{SKI} = \frac{PD_K - \overline{PD}}{\widehat{PD}}.$$

(5.1)

107

Here, PD_K is the pressure difference between the high pressure region (HPR) and the low pressure region (LPR) over Koshava's active periods. In order to obtain a non-dimensional index, the standard score normalization has been employed (Kreyszig, 2011), where $\overline{PD}$ and $\widehat{PD}$ are the mean and the standard deviation, respectively, of the pressure differences between the HPR and LPR for the whole period lasting from January 1, 1971 to May 30, 2014. Their values are 0.27 hPa and 9.65 hPa, respectively. The HPR is located within LON 35°-45° and LAT 45°-55°, while the LPR is found within LON 2.5°-12.5° and LAT 37.5°-47.5°. Both regions have 12 points on a 2.5°×2.5° grid.

Employing Eq. (5.1), while inserting the pressure differences for days without Koshava (PD_{NK}) instead of PD_K, one can obtain the SKI values for days when Koshava was not recorded (called *NKI*). The SKI will be effective in forecasting Koshava's activity if the distributions for the SKI and NKI differ. Results are presented in Figure 5.8. The SKI histogram is shifted to the right from the *NKI* histogram. Thus Figure 5.8 suggests that SKI could be used to predict the occurrence of the Koshava wind. The SKI values are mostly in the range between 5 and 15, while the NKI is in the interval between -10 and 5. The overlap (Weitzman, 1970) between the two histograms exists in the region around SKI = 5. The Rayleigh distribution is the best fit for the SKI data, indicating that SKI rarely takes values less than 0. The total overlap between SKI and NKI distributions is 0.308. The following criteria for interpretation of the SKI is outlined:

$$\text{Koshava occurence} = \begin{cases} \text{unreliable,} & \text{SKI} \leq 10, \\ \text{likely,} & \text{SKI} \in (10,20], \\ \text{very likely,} & \text{SKI} > 20. \end{cases} \quad (5.2)$$

The accuracy of the SKI in the interval (10, 20], which corresponds to a "likely" occurrence of Koshava, is 92.1 %. An additional advantage of the SKI is that the index is based on easily observed and modeled features of the large-scale pressure systems.
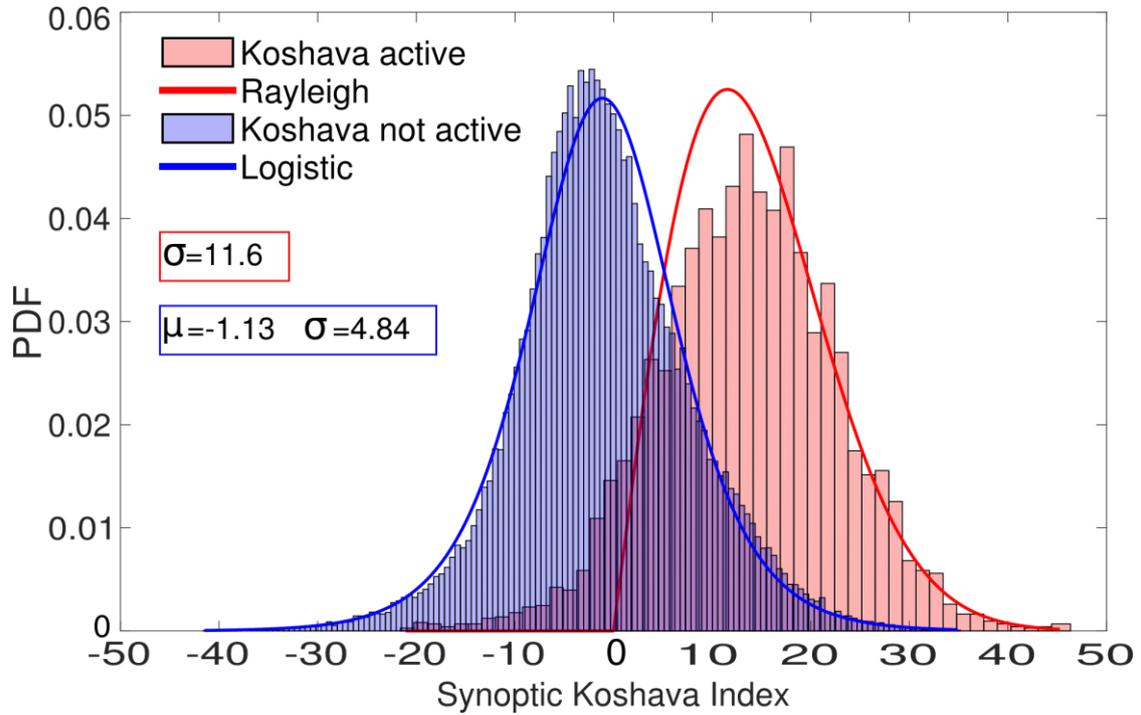
Figure 5.8. PDFs of the SKI (red) and NKI (blue).

5.4 Mesoscale contributors

Koshava is also investigated from the perspective of a gap flow windstorm. Gaps G1, G2, G3 and G4 (Figure 5.1c and d) are connecting the upstream reservoir of cold air (in the Wallachia Valley) with the KR located downstream from the gaps. West regions of the Wallachia Valley are between 35 m (close to the Danube River) and 300 m (north parts) above sea level. The KR has an altitude in the range between 70 m and 100 m a.s.l. Mountains in Serbia with peaks less than

1000 m separate the Wallachia Valley from the KR. The bottom surface of G2 is the Danube River with a relatively constant width (W) of about 1 km throughout the whole winding canyon (from Drobeta-Turnu Severin (DTS) to VG). The height (H) to W ratios for G3 and G4 are small (< 0.1) compared to the H/W ratios of G1 and G2 (> 0.1). With a length (L) of 95 km, G2 is also the longest gap among all four gaps. G1 is 12 km downstream from G2. Thus, the flow that enters G2 will be later distributed between G1 and G2. Furthermore, the flow that enters G1 will be channeled by the orography and a part of that flow will eventually again confluence with the flow that continued through G2 (see Figure 5.1c). The confluence occurs upstream from the VR station. This initial branching and subsequent confluence might be one of the reasons for the long-lasting question why Koshava at the VR station is stronger than it is at the VG station.

Overlaps (Weitzman, 1970) for the PDFs of ΔP and $\Delta \theta$ between the stations in the SKR and the stations in the KR are given in Table 5.5. The smaller the overlap, the better the separation between Koshava and "no-Koshava" events. The best reference station for identifying Koshava wind is the NEG station (two exceptions being LOM – BG for $\Delta \theta$ and DTS – VG for ΔP). The ΔP overlaps for the Koshava stations further downstream from the gaps (BG and NS stations) are similar (around 26 %). The results show that ΔP is more reliable Koshava indicator than $\Delta \theta$ for all Koshava stations. On average, the PDFs of $\Delta \theta$ have 54 % larger overlaps than the PDFs of ΔP. It should be noted, however, that $\Delta \theta$ between the gap (or crest) and the location downstream from the gap (or crest) would be better Koshava indicator than the cross-barrier $\Delta \theta$ (which is used in this study). Drechsel and Mayr (2008) in their study on foehn wind in Alpine Valley found the overlaps for ΔP (18 %) and $\Delta \theta$ (15 %) to be similar. However, they used gap – downstream differences to calculate $\Delta \theta$ and a 3-year long data record. Due to the

lack of stations located inside the gaps, or at the tops of mountain crests that separate the KR from the SKR, it was impossible to calculate gap (or crest) – downstream descent of isentropes. An attempt to calculate ΔP and $\Delta\theta$ from the reanalysis data was done (Appendix A). Due to the coarse resolution of the grid, the results were less accurate than the presented results obtained using observations (especially for $\Delta\theta$ where overlaps were above 75 %).

Table 5.5. Overlaps between PDFs of MSLP and potential temperature differences (ΔP and $\Delta\theta$ respectively) for Koshava and "no-Koshava" events. The differences are calculated between the stations in the SKR and the stations in the KR. Distribution plots for the smallest overlaps (underlined values) are given in Figure 5.9 and Figure 5.10.

	BG		NS		VR		VG	
	ΔP	$\Delta\theta$	ΔP	$\Delta\theta$	ΔP	$\Delta\theta$	ΔP	$\Delta\theta$
LOM	0.329	<u>0.549</u>	0.333	0.551	0.385	0.437	0.333	0.403
NEG	<u>0.261</u>	0.574	<u>0.266</u>	<u>0.549</u>	<u>0.376</u>	<u>0.427</u>	0.281	<u>0.389</u>
DTS	0.328	0.635	0.329	0.609	0.503	0.450	<u>0.222</u>	0.451
CAR	0.684	0.889	0.593	0.769	0.612	0.670	0.763	0.883

Distributions for the cases with the smallest overlaps for ΔP and $\Delta\theta$ are given in Figure 5.9 and Figure 5.10, respectively. The peak of ΔP distributions for the BG, NS and VR stations when Koshava was active is between 1.5 and 5.2 hPa. "No-Koshava" events have ΔPs between -3 and 1 hPa. The positive ΔPs are notably evident in the case of VG station, as well as at the BG and NS stations where a non-negative Rayleigh distribution is the best fit for data (ΔPs sometimes even exceeded 10 hPa). Stations further downstream in the KR have the broader distributions of ΔPs than the VG station. It is because DTS is only about 4 km upstream from the G2, and therefore the convergence of streamlines at the entrance of G2 results in higher velocities and lower MSLPs (Zängl, 2002a; Zängl, 2002b; Gaberšek and Durran, 2004) at DTS compared to the LOM and NEG

stations. On the other side, VG is located about 15 km downstream from the exit of the Danube canyon and thus the pressure drop at VG is less than the pressure drop at the BG and NS stations. This reasoning is additionally supported with the results given in Figure 5.11 which depicts the wind roses at the SKR stations when Koshava was active.
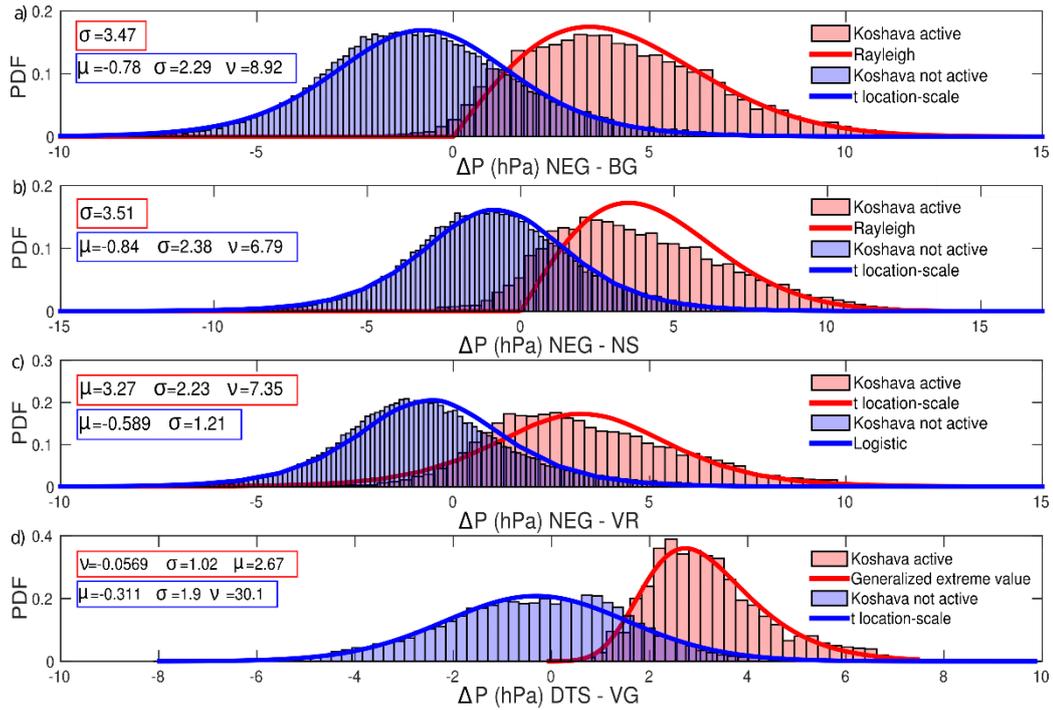
Figure 5.9. Across-mountain MSLP differences between the stations in the SKR and stations in the KR: (a) NEG – BG, (b) NEG – NS, (c) NEG – VR, and (d) DTS – VG. Overlaps between distributions are given in Table 5.5.
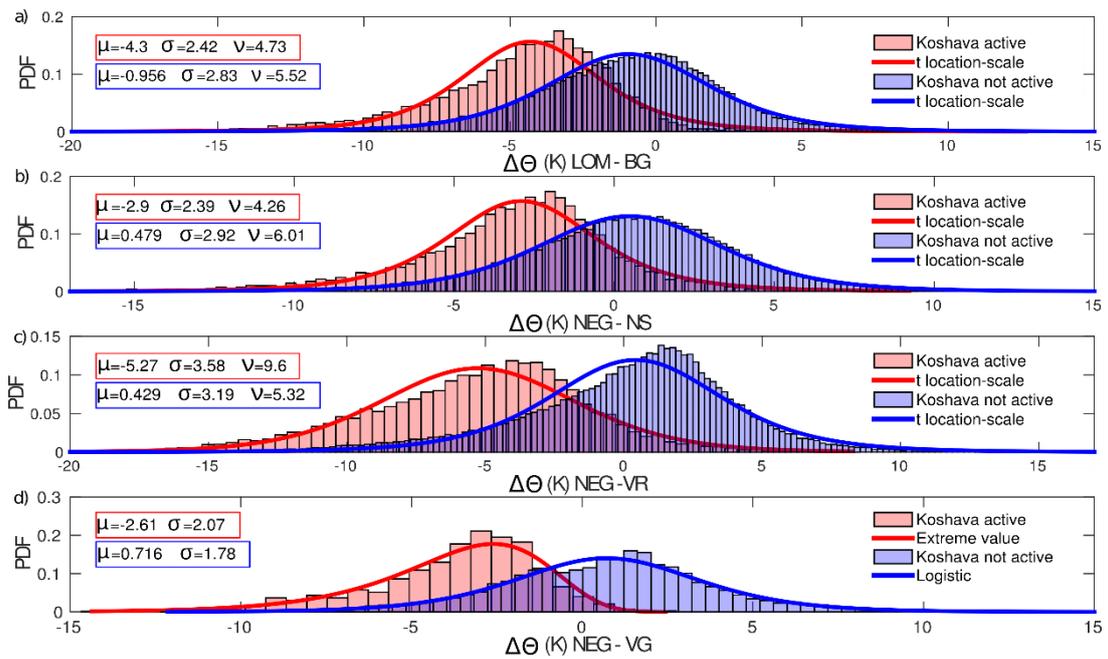
Figure 5.10. Same as Figure 5.9 but for potential temperature differences.
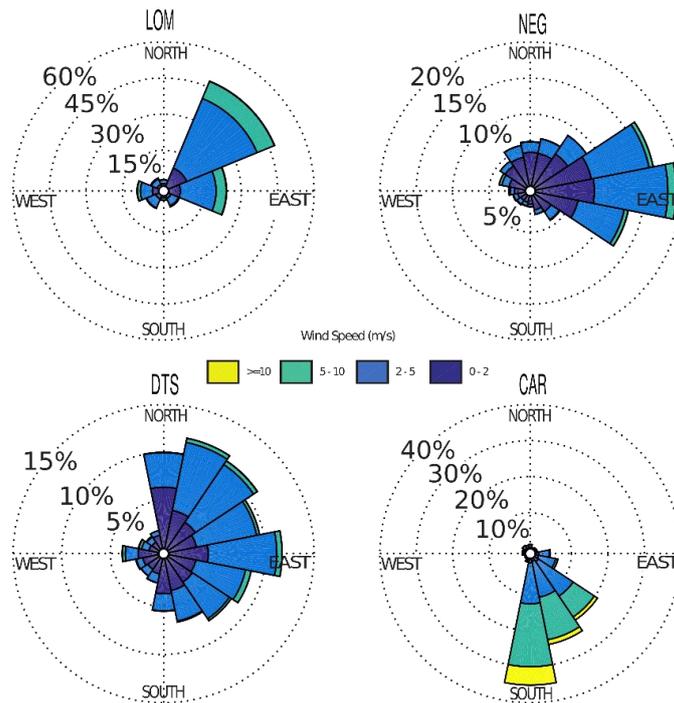
Figure 5.11. Wind roses of direction and intensity for the weather stations in the SKR when Koshava was active.

Potential temperatures in Wallachia Valley have to be lower than in the air in the KR for Koshava to develop, as portrayed Figure 5.10. The $\Delta\theta$ peaks are in the range from -1 to -5 K. Although $\Delta\theta$s for Koshava resembles a typical fingerprint of a foehn wind (Drechsel and Mayr, 2008), the distributions of $\Delta\theta$ for "no-Koshava" events are very broad (-10 to 10 K), resulting in many ambiguous cases. The differences in $\Delta\theta \leq 0$ K not accompanied with the Koshava wind could be due to several meteorological factors. First, strong diabatic heating from the surface can result in superadiabatic lapse rates in the surface layer (Drechsel and Mayr, 2008) in the KR (Vukmirović, 1985b), resulting in $\Delta\theta \leq 0$. Second, same air mass can be positioned above the KR and the SKR simultaneously, thus resulting in $\Delta\theta \approx 0$ K. Peel *et al.* (2007) reported that both regions are in the same Köppen-Geiger climate zone (Csb - temperate climate with dry and warm summers), and therefore on average host air masses with similar physical characteristics (see Section 2.1). Furthermore, altitudes of the Wallachia Valley and the KR are in the similar range. Third, due to the nocturnal radiative cooling, cold air from the South Carpathians and Balkan Mountains sinks into the Wallachia Valley creating the stable layer close to the ground, resulting in $\Delta\theta$ between the SKR and KR being negative (Whiteman, 2003). However, in the absence of the synoptic scale pressure gradients that in turn results in the mesoscale pressure gradient over the mountain range, the difference in $\Delta\theta < 0$ K alone is not sufficient enough to generate Koshava.

Figure 5.12 shows that there is a significant and positive correlation between the mean hourly Koshava velocities at each of the BG, NS and VG stations, and ΔP calculated between DTS and these three Koshava stations ($R > 0.6$). The negative correlation between the ΔP (CAR – VG) and the mean hourly Koshava speed at VG is one more indicator of the channeling and the branching of the flow that

occurs in G2 and G1. Namely, the more the flow is branched into G1 from G2, the larger the MSLP at the CAR station compared to the VG station. At the same time, if the flow is mainly directed towards the CAR station, the wind speed at the VG station will decrease. Koshava speeds at the BG, NS and VG stations are more driven by the across-mountain pressure gradient than by the winds at higher levels. The correlation between either of V925 or V850 winds with the mean hourly Koshava speed at the BG and NS stations is higher than in the case of the other two stations in the KR (the correlations with V500 winds are negligible in all cases). The weak correlations between the Koshava speed and winds at higher levels are in accordance with Vukmirović (1985b) finding that the maximum Koshava speeds occur between 200 and 600 m a.g. He also noted that on top of this layer is a layer of capping inversion (Gaberšek and Durran, 2004; Mayr *et al.*, 2007). This way Koshava is "isolated" from the flow at higher levels (therefore called a low-level jet by e.g. Vukmirović (1985b). The correlation between Koshava and winds at higher levels increases for stations further downstream from the gaps. Finally, the correlations between Koshava speed and $\Delta\theta$ were negligible and therefore not presented in Figure 5.12. Instead, they are discussed in the following section and presented in Figure 5.16.
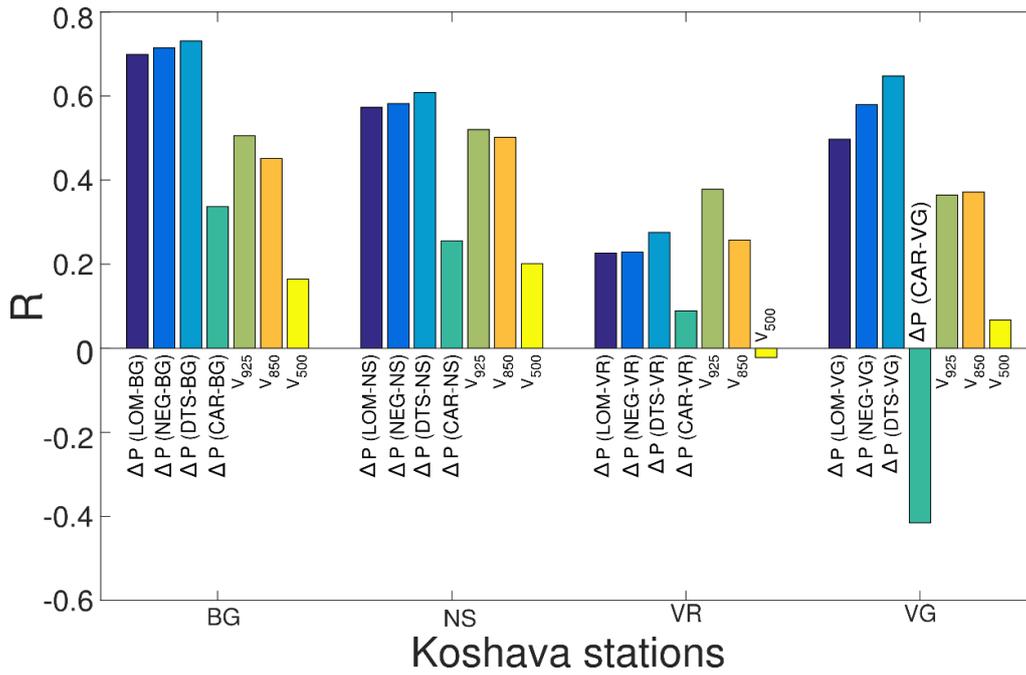
Figure 5.12. Correlation coefficients between the mean hourly Koshava speed at each of the stations in the KR and (1) MSLP differences between the SKR and KR stations and (2) wind speed at 925, 850 and 500 hPa pressure levels.

The local pressure gradients for the stations in the KR are computed from the NCEP/NCAR data as the MSLP differences ΔP_i over $2\Delta\lambda$, and ΔP_j over $2\Delta\varphi$:

$$PG_i = \frac{\Delta P_i}{2R_E\Delta\lambda\cos\varphi}, \qquad PG_j = \frac{\Delta P_j}{2R_E\Delta\varphi}, \qquad (5.3)$$

with R_E representing the Earth's radius (6,371 km). Here, the longitudinal and latitudinal differences are expressed in radians as: $\Delta\lambda = \lambda_{j+1} - \lambda_i$; $\Delta\varphi = \varphi_{j+1} - \varphi_i$, respectively. Therefore, the pressure gradient at a grid point (i,j) is calculated from the four surrounding points. The total pressure gradient is then given by $PG = \sqrt{PG_i{}^2 + PG_j{}^2}$; the units being Pa km^{-1}. The PGs were calculated only for these days when Koshava was active. The results are presented in Figure 5.13. The mean pressure gradient can be calculated from the distribution parameters

116

as: $\overline{PG} = \nu\sigma = 1.18$ Pa km^{-1} (or 1.18 mb per 100 km). It was found that 50 % of the time the pressure gradients were larger than 1.1 Pa km^{-1}. These values are similar in magnitude to the pressure gradients noticed in the "mean" cyclone presented in Figure 5.7. Trigo *et al.* (1999) also concluded that pressure gradients in MCs typically have values between 0.5 and 2 Pa km^{-1}.
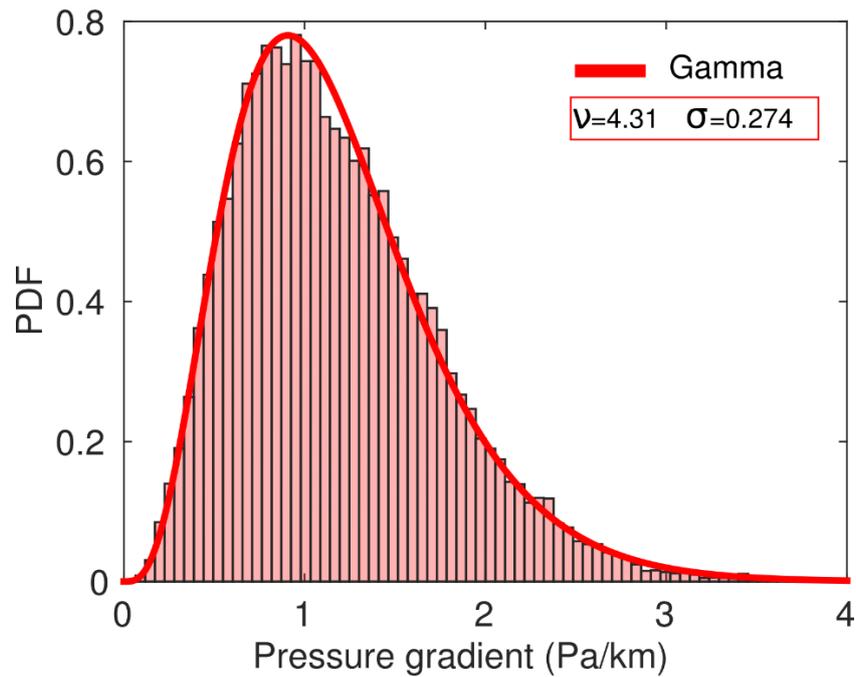
Figure 5.13. PDF of pressure gradients for stations in the KR.

5.5 Probabilistic model of the Koshava wind

The parameters ΔP and $\Delta\theta$ are used to construct the probabilistic model of Koshava's occurrence. The PDFs of ΔP (Figure 5.9) and $\Delta\theta$ (Figure 5.10) are combined in order to obtain the joint probability of the Koshava occurrence, as portrayed in Figure 5.14. The width of the intervals is 1 hPa for ΔP and 1 K for $\Delta\theta$. As previously observed in Figure 5.10, Koshava occurs over wider range of

Δθs, meaning that the wind is more dependent on ΔP than on Δθ. The sharpest distinction between Koshava and "no-Koshava" events is observed at the VG station (Δθ ≤ 0 K combined with ΔP > 1 hPa always generates Koshava). The advantage of using the joint PDFs instead of single PDF is, for instance, evident in the case of the VR station. For ΔP = 3 hPa, the probability of Koshava occurrence increases from 0 % (Δθ > 5 K) to more than 90 % for Δθ < -7 K.
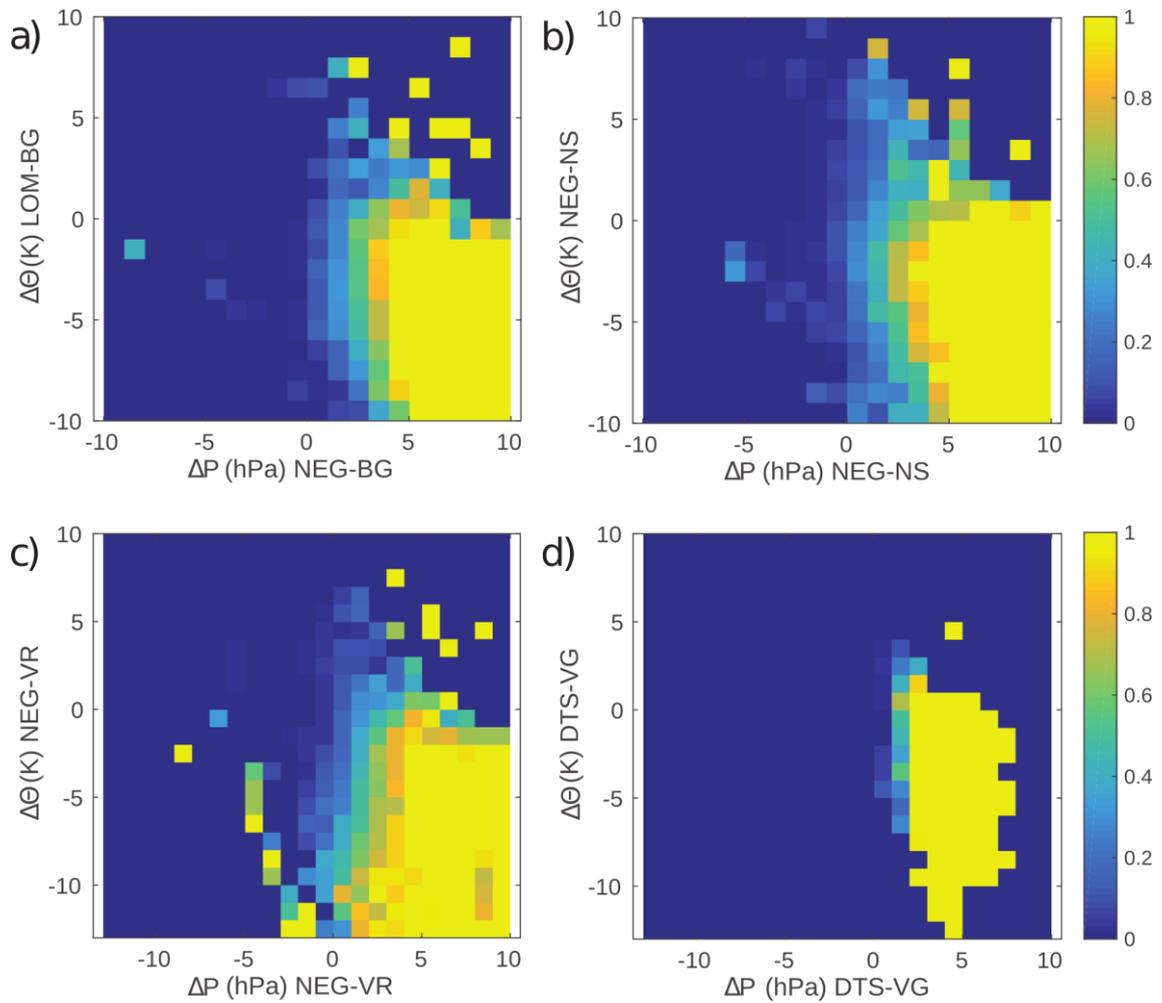
Figure 5.14. Joint probability of Koshava winds based on combined PDFs of ΔP and Δθ.

A probabilistic model for Koshava speed is also constructed. In all cases ΔP was the only statistically significant predictor. Inclusion of other predictors had negligible impact and ultimately resulted in overfitting the model. The probabilistic model for $\bar{V}_K$ is presented in Figure 5.15, where $\bar{V}_K$ is plotted against ΔP and superimposed on top of the joint PDF of $\bar{V}_K$ and ΔP. The width of the intervals for $\bar{V}_K$ and ΔP is 1 m s^{-1} and 1 hPa, respectively.
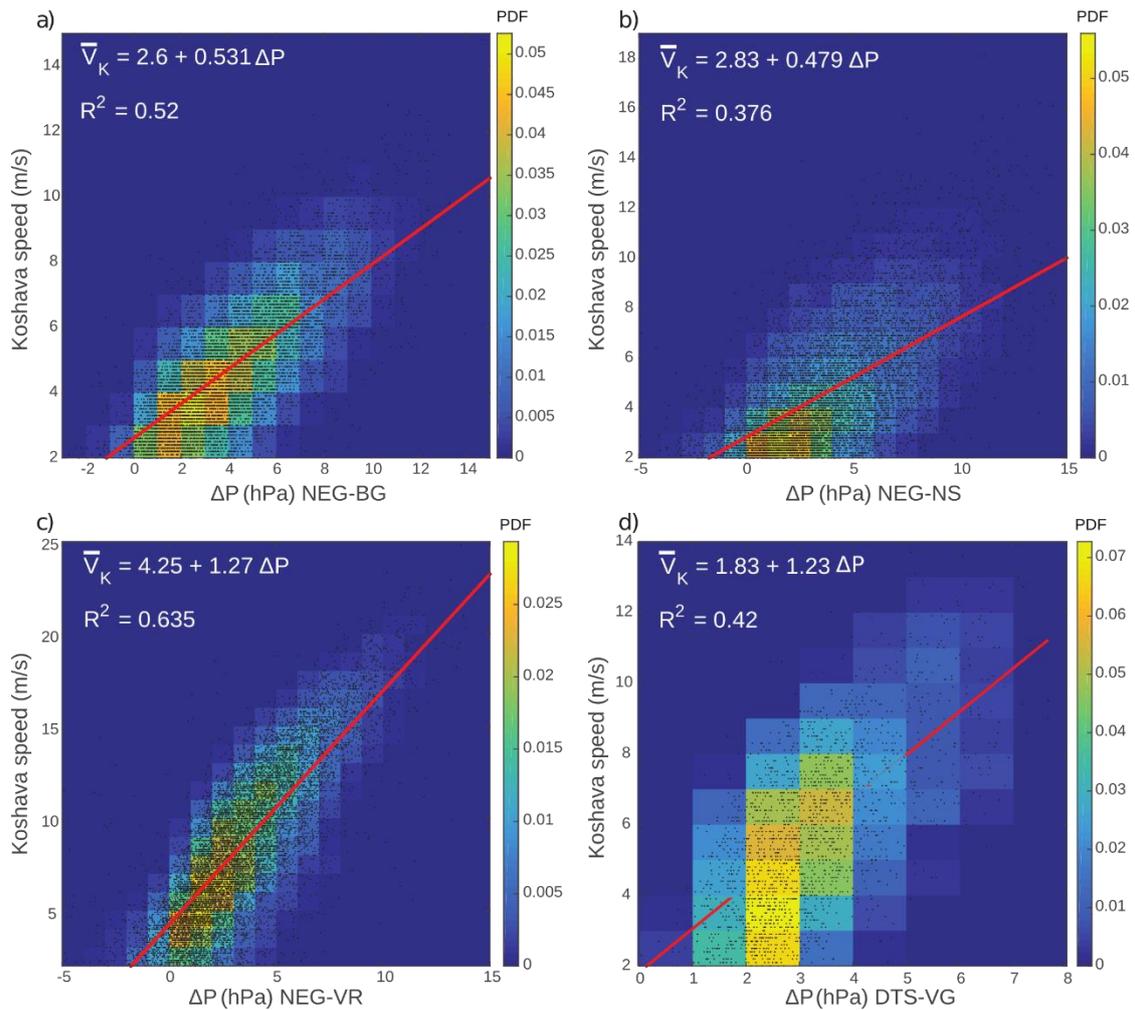
Figure 5.15. Probabilistic model of the mean hourly Koshava speed for stations in the KR: (a) BG, (b) NS, (c) VR, and (d) VG superimposed on top of the joint PDFs of $\bar{V}_K$ and ΔP.

119

Although the linear relationship between $\bar{V}_K$ and ΔP is noticeable at each of the stations in the KR, the strength of the relationship is not pronounced. This weak relation can be seen from the fact that a fixed value of ΔP can result in a wide range of $\bar{V}_K$s. Consequentially, the R^2 values are ranging from 0.376 (NS) to 0.635 (VR), pointing out that the large variation in $\bar{V}_K$ cannot be explained by ΔP alone using the simple linear model. The evaluation statistics is given in Table 5.6.

Table 5.6. Evaluation statistics for the Koshava stochastic equations: R^2 - coefficient of determination; MSE – mean square error; RMSE - root mean square error; FvsC - F-statistics vs. constant model (tests for a significant linear regression relation between $\bar{V}_k$ and the predictor); p-value - p-value for the F-test on the model (at the 5% significance level).

	BG	NS	VR	VG
R^2	0.520	0.376	0.635	0.420
MSE (m^2/s^2)	1.63	3.21	5.92	3.16
RMSE (m/s)	1.28	1.79	2.43	1.78
FvsC	11100	6640	21400	1520
p-value	0	0	0	0

The RMSEs show that the uncertainty in estimated $\bar{V}_K$ is within 2.5 m s^{-1}. Interesting to note is that the VR station has the highest R^2 and RMSE values at the same time. Namely, R^2 represents a relative measure of the fit, while RMSE is an absolute measure of the model (has the same units as the response variable). Therefore, if the main purpose of the model is to predict $\bar{V}_K$, then the model with the lowest RMSE values (model for the BG station) is the most reliable. The strongest observed Koshava speed was recorded at the VR station, $\bar{V}_K$ = 27.5 m s^{-1} for which ΔP was equal to 12.1 hPa. The largest value of ΔP, however, was 17.3 hPa, resulting in $\bar{V}_K$ = 25.2 m s^{-1} at VR station. The probability of occurrence of $\bar{V}_K$ > 15 m s^{-1} at the VR station is only 10.6 %, and even smaller at other three stations in the KR. The strongest and most reliable linear relationship between $\bar{V}_K$

and ΔP is observed at the VR and BG stations (the largest FvsC values in Table 5.6).

The presented model can be compared to the previously developed models by Radosavljević and Vojnović-Kljaić (1985) and Todorović and Paskota (2002) described in Section 2.4. The results can only be compared for the BG station and $\bar{V}_K$. The presented model is similarly accurate as the model proposed by Radosavljević and Vojnović-Kljaić (1985). Namely, the RMSE value for BG (Table 5.6) is for 0.28 m s^{-1} larger than the mean absolute deviation (MAD) value of the model by Radosavljević and Vojnović-Kljaić (1985). Note that RMSE is always larger or in the limiting case equal to MAD. The MAD values of the developed model are not presented in Table 5.6. The RMSE method is more accurate because squaring the errors the negative and positive errors do not cancel out each other, thus adding more accuracy to the result. The model proposed herein is more accurate than the model suggested by Todorović and Paskota (2002). The R^2 value for BG in in Table 5.6 (0.520) is higher than the value they reported (0.414). Equally important to note is the fact that the model developed in this study is based on the comprehensive dataset (1971-2014 for BG, NS and VR and 2011-2014 for VG) whereas their models are based on a single Koshava episode (Todorović and Paskota, 2002) or several months of data (Radosavljević and Vojnović-Kljaić, 1985).

Although not presented here, the accuracy of the model with all the predictors included was found to be only < 5 % higher (depending on the station considered) than the accuracy of the presented model. The complexity of the model, however, increases significantly. Figure 5.16 shows the correlation coefficient between $\bar{V}_K$ and all synoptic and mesoscale predictors.
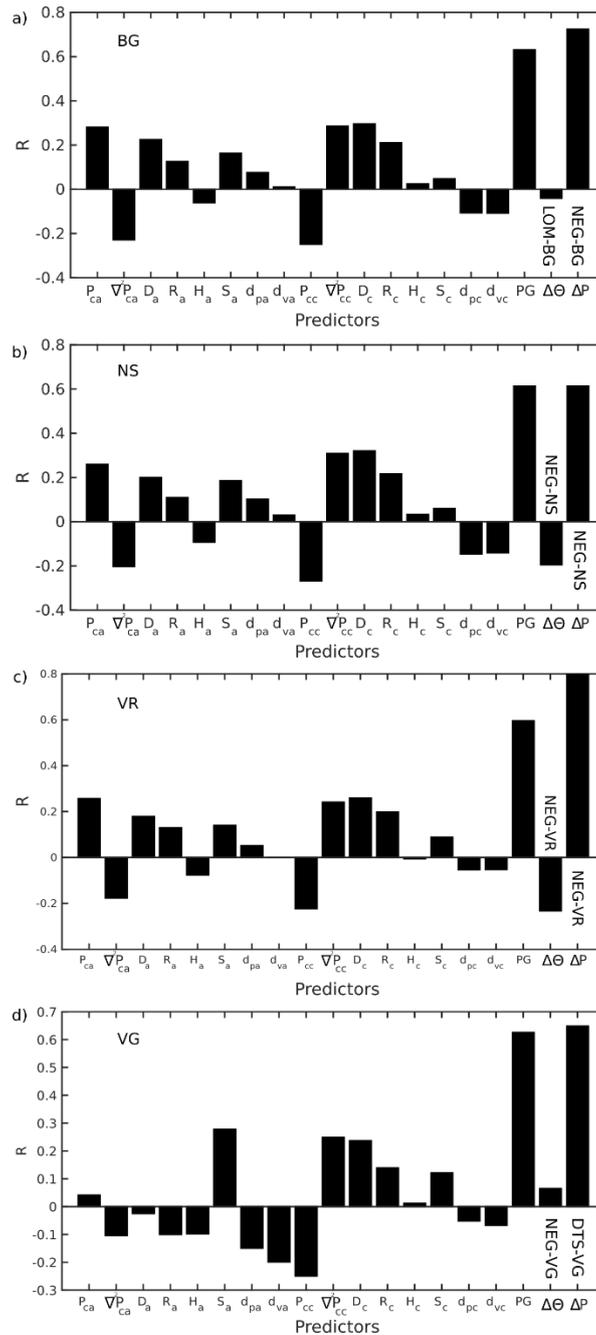
Figure 5.16. Correlation coefficient between the mean hourly Koshava speed at each of the stations in the KR and all synoptic and mesoscale predictors. Symbols are defined in Section 3.5. The first nine predictors corresponds to anticyclone features while the second nine predictors represents cyclone features.

Figure 5.16 is a good demonstration of the statistical rule which states that correlation does not necessarily imply causation. Namely, although the correlation between $\bar{V}_K$ and PG (pressure gradients in the KR) is similar to the correlation between $\bar{V}_K$ and ΔP, the stochastic model constructed using PG instead of ΔP turns out to be considerably less accurate. This finding is a result of the fact that Koshava is a gap and downslope local wind. That is, PGs are pressure gradients in the KR and hence can not drive the air over the mountains between the SKR and KR. ΔPs, on the other hand, are the pressure gradients which govern the wind and force the cold air from Wallachia Valley to flow through gaps and gorges into the KR. Therefore, the stronger the ΔPs, the stronger the Koshava wind. The R values between other synoptic and mesoscale predictors and $\bar{V}_K$ are small and typically below 0.3.

Results from this section show that the occurrence of Koshava is more predictable than its speed. These findings are in accordance with the other studies on predictability of downslope winds (Drechsel and Mayr, 2008; Plavcan *et al.*, 2013). The MCs and the EA are the synoptic contributors responsible for creating the Koshava wind; however, the mesoscale (and local) contributors such as local orography, stability of the atmosphere, surface roughness, and obstacles around the measurement stations determine the dynamics of the wind.

5.6 Summary and conclusions

A comprehensive analysis of the synoptic pressure systems (MCs) and EAs) showed that their characteristics have a profound influence on the occurrence of the Koshava wind. Using the University of Melbourne automatic cyclone tracking scheme, it was demonstrated that closed MCs located in the Gulf of Genoa and Adriatic Sea were the most associated with Koshava (being present in

74 % of all Koshava events). Closed anticyclones causing Koshava were located above Romania, Moldavia and south Ukraine and were observed in 71 % of all Koshava occurrences. Both, the low pressure and the high pressure areas that cause Koshava occur about 500-1000 km distant from the KR. Further investigation showed that in 67 % of all Koshava events, the activity of both pressure systems was recorded. In addition, it was observed that Koshava's mean hourly and maximum hourly wind speeds were largest when both pressure systems were simultaneously active. Koshava occurred independent of MCs and EA only 3 % of the time. The source region of the MCs which caused Koshava was found to be the Gulf of Genoa. From there, the cyclones followed southeast trajectories two times more frequently than they followed northeast trajectories.

Koshava is a gap flow wind. Four gaps in the mountain region between Serbia and Romania connect the Wallachia Valley (i.e. SKR), situated in Romania and Bulgaria) with the KR. Local characteristics of the Koshava wind are dominantly determined by mesoscale contributors such as orography, across-mountain MSLP (ΔP) and potential temperature ($\Delta\theta$) differences. Data from four stations located in the SKR (LOM, NEG, DTS, CAR), and from four stations in the KR (BG, NS, VR, VG) were used to calculate the above-mentioned differences. The PDFs of ΔP and $\Delta\theta$ distinguish Koshava from "no-Koshava" events quite well. It was found that ΔP is more influential on Koshava than $\Delta\theta$. On average, the overlap between the PDFs of ΔPs is 0.257 and the overlap between the PDFs of $\Delta\theta$s is 0.479 (54 % of difference). The correlations between Koshava wind, on one side, and winds at 925, 850 and 500 hPa levels, on the other side, were small (always below 0.55). Moving away downstream from the mountain region and deeper into KR, the correlations tend to increase. The mean pressure gradient in the KR when the

wind was active is 1.18 Pa km^{-1}, which is in the range of the pressure gradients observed in the MCs that caused the wind.

The Synoptic Koshava Index (SKI), defined as the difference between the area-averaged mean sea level pressures in the anticyclone and cyclone regions, is shown to be a good indicator of the Koshava occurrence. The SKI values are mostly in the interval from 10 to 25 when Koshava occurred. The index has values ranging from -10 to 10 when Koshava was not active. The occurrence can be predicted with high accuracy in about 70 % cases.

The accuracy of the mean hourly Koshava speed ($\bar{V}_K$) forecast using the simple linear model constructed in this study is the highest at the BG station (*RMSE* of 1.28 m s^{-1}) and the lowest at the VR station (*RMSE* of 2.43 m s^{-1}). ΔP is the only significant predictor in the model. The linear relationship between $\bar{V}_K$ and ΔP is statistically significant at all stations in the KR.

CHAPTER 6

6. Investigation of an extreme Koshava wind episode and a new methodology for identification of locations favourable for deep snowdrifts

6.1 Introduction

From January 30 to February 4, 2014, large parts of Serbia were affected by an extremely severe windstorm. A strong wind, named Koshava, occasionally had hurricane velocities. In addition to extreme wind speeds, Koshava created snowdrifts several meters deep. This weather disaster impacted everyday life across the country – trees were toppled, many buildings and cars were damaged, and rail and air transports in the northern Serbia were shut down. Furthermore, between 5,000 and 10,000 people were trapped in their vehicles on the snow-covered roads and it was necessary to rescue them from cold (Figure 6.1). Fortunately, no human casualties were reported. Interestingly, this EKE (EKE), had a positive effect on the air quality in cities. Measurements in BG showed that the atmosphere after the EKE was two times cleaner compared to the air quality before the event.

Figure 6.1. Snowed vehicles on roads in northern Serbia. Source: The Ministry of Defence of the Republic of Serbia.

As demonstrated in the previous chapters, Koshava is strongest in the VR region. Figure 6.2 shows that the VR station has 10 to 15 m s^{-1} stronger Koshava gusts than the BG station. The strongest Koshava gust ever recorded was measured in VR on February 11, 1987 (48 m s^{-1} at 10 m a.g). The strongest Koshava speed at the BG station was 35.9 m s^{-1} at 24 m a.g. on October 17, 1976. The measured velocity at 650 m a.g. was 45 m s^{-1}. These two weather stations mostly recorded different storms as being the most extreme. Exceptions are the storms that occurred in February 1979 and February 2014; the latter being the main subject of this study. These results indicate that extreme Koshava events are mostly localized. Lastly, it can be seen that extreme Koshava events were not recorded in the period from the late 1980s to 2014. An absence of extreme Koshava winds in the period from the late 1980s to 2014 is in accordance with the results presented in Chapter 4, which state that Koshava was most active in the period from the 1970s to 1980s.
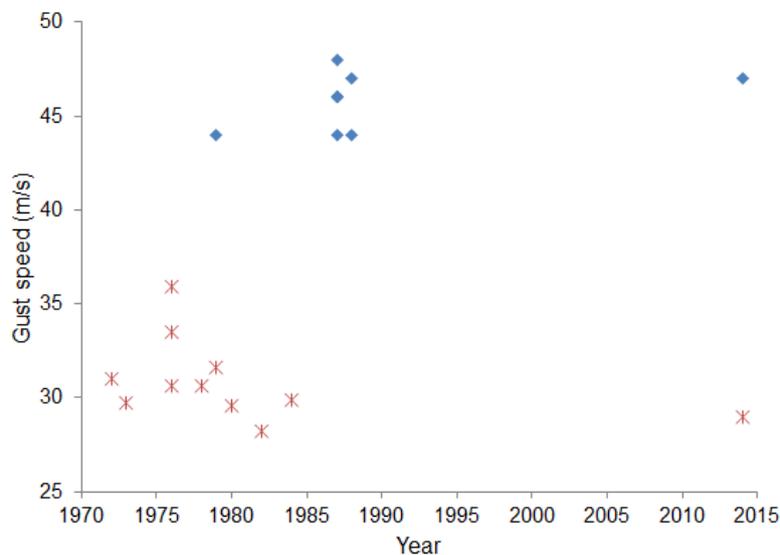
Figure 6.2. Past records of the extreme Koshava gusts at the VR station (blue diamonds) and BG station (red stars).

This chapter investigates the meteorological factors that caused the EKE of 2014. The following questions are addressed: (1) what was the synoptic situation which brought the EKE, (2) how well two numerical models with different configurations forecasted the EKE (see Section 3.6), and most importantly, (3) what caused such high Koshava speeds to occur? Hereafter, when refereeing to dates related to the EKE, the year (2014) will be omitted for simplicity.

The EKE was a blizzard characterized not only with high wind speeds, but deep snowdrifts as well. Thus, the event represents a convenient natural setup for investigation of snowdrifts. Three mechanisms are responsible for transport of snow (Mellor, 1965): creeping, saltation and turbulent diffusion. Creeping process transports the heaviest particles that can not be lifted by the wind, but instead are rolled on the snow-covered surface. Saltation occurs when large wind shears take off particles from the ground which then follow ballistic trajectories before again falling to the ground. The lightest particles can be suspended in the air due to strong vertical mixing and hence be advected without touching the surface. Li and Pomeroy (1997) reported that snow transport depends on wind speed, air temperature and snow water content. They concluded that the average wind speed thresholds for transport of wet and dry snow on Canadian prairies are 9.9 and 7.7 m s^{-1}, respectively. These numbers, however, largely depend on temperature. Other researchers reported smaller values for thresholds (*e.g.* Schmidt, 1981; Tabler *et al.*, 1990).

Historical data show that the EKE is not the first Koshava event associated with snowdrifts in the Pannonian Plane, but the relationship between snowdrifts and Koshava's velocity has not been investigated up to now. The proposed methodology for detection of snowdrift locations is presented in Section 6.5.

6.2 Data

The data used to investigate the EKE are as follows. Wind speed, snow cover and radiosonde measurements in the KR are acquired from the Republic Hydrometeorological Service of Serbia. The MSLP and air temperature at 2 m a.g. data are obtained from the European Center for Medium-Range Weather Forecasting's Meteorological Archival and Retrieval System dataset.

6.3 Synoptics and dynamics of the EKE

The ridge of a deep anticyclone stretched across the Balkan Peninsula on January 27. On January 30 (Figure 6.3a), the pressure difference between the EA and MC was 55 mb and the temperature difference between these two regions was approximately 50°C. The distance between the centres of these two pressure systems was about 2500 km. The pressure gradients above Serbia were extremely large – approximately 5 hPa/100 km. This synoptic situation was favourable for the development of a strong Koshava wind.
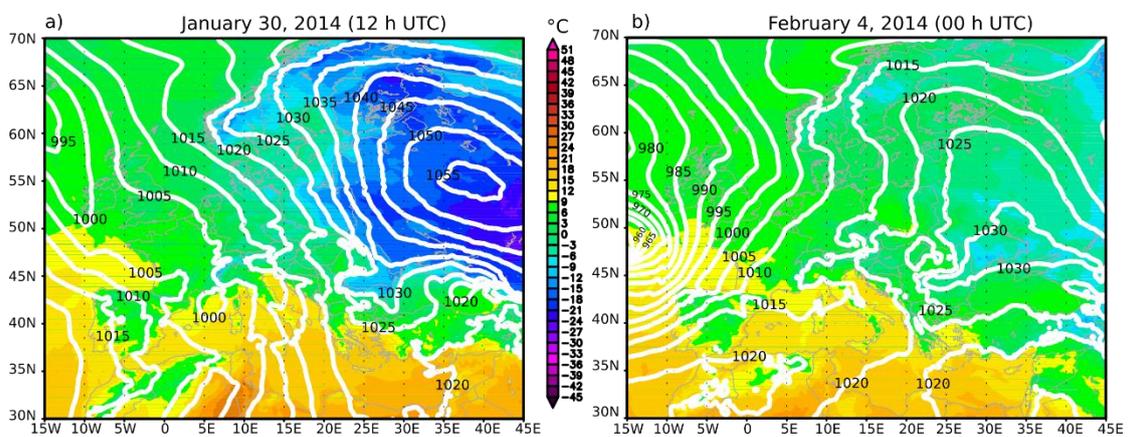
Figure 6.3. MSLP in hPa (white contours) overlaying 2-m air temperature map. EKE started on January 30 (a) and lasted until February 40 (b).

The EKE started in the afternoon of January 30. The central pressure in the anticyclone that caused the EKE was 1055 hPa, which according to the results presented in Figure 5.5 (Section 5.3.1) has an exceedance probability of occurrence of 0.1 %. The MC, situated in the Gulf of Genoa, was not particularly strong as its central pressure was 3 hPa below the average central pressure of the cyclones which typically generate Koshava (see Figure 5.5). Therefore, it can be concluded that the strong anticyclone was the main trigger of the EKE. The center of the anticyclone was slowly moving eastward from the KR during the EKE. Its high-pressure ridge, however, was constantly positioned above Balkan Peninsula and therefore maintained strong pressure and temperature gradients above most of the Balkans. The disappearance of the anticyclone (Figure 6.3b) led to the cessation of the EKE.

The SKI parameter, defined as the normalized area-averaged MSLP difference between the anticyclone and cyclone regions (see Section 5.3.2), is presented in Figure 6.4a. The SKI values above 25 are noticeable during the EKE, while the values above 35 can be observed for the days with the strongest Koshava winds. The high values of SKI demonstrate a strong pressure difference between the anticyclone and cyclone regions, which indubitably generated the strong Koshava velocities. Figure 5.8 shows that the SKI values above 35 have a probability of occurrence below 1 % (less than 0.3 % chance of the SKIs above 40). The case study of EKE suggests that the SKI is a reliable prognostic Koshava parameter.

As demonstrated in Chapter 5 (Section 5.4), the major Koshava's contributors on the mesoscales are the across-mountain MSLP and potential temperature differences (ΔP and $\Delta\theta$, respectively) between west parts of the Wallachia Valley

(i.e. SKR) and the KR. ΔP between DTS and VG reached 10 hPa during the EKE, whereas the $\Delta \theta$ value between these two stations was below -7°C. According to the results portrayed in Figure 5.9, the probability of occurrence of such a large pressure difference is 0.01 %, while the joint probability of ΔP and $\Delta \theta$ values combined is practically zero (0.0012 %; see Figure 5.14).

Due to these large pressure and temperature differences, northern and northeastern parts of Serbia experienced a blizzard that caused significant damage to infrastructure and posed a threat to human safety. A strong and cold Koshava wind with daily mean speeds of 6 to 12 m s^{-1} and occasional gusts between 12 and 25 m s^{-1} was blowing during the EKE. In the early morning of February 1, Koshava gusts in BG reached 29 m s^{-1}. Radiosonde measurements in BG conducted on February 2 (00 UTC) recorded the maximum Koshava speed of 34 m s^{-1} at a height of 497 m a.g (Figure 6.4b). The strongest Koshava speed, however, was measured in VR on February 1, when a gust at 10 m a.g. reached 47 m s^{-1}. This value is the second largest Koshava gust ever recorded. The 2014 EKE was the first severe Koshava event after more than 25 years (see Figure 6.2).
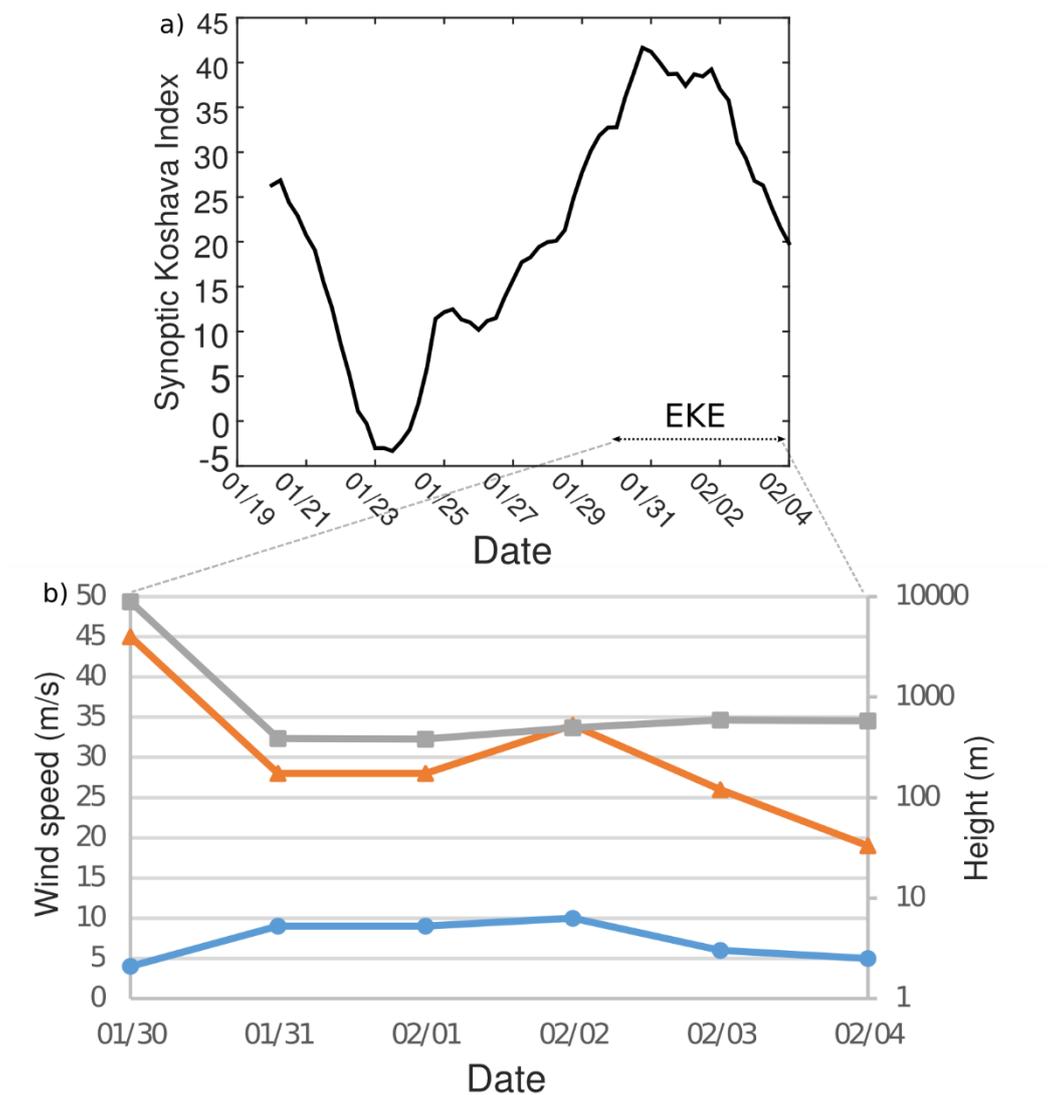
Figure 6.4. (a) SKI before and during the EKE. (b) Daily mean (the blue line with circles) and maximum (the orange line with triangles) Koshava speeds during the EKE at the BG station (primary y-axis). The grey line with squares represents the height of maximum Koshava speed.

Emagrams in Figure 6.5 indicate that the Koshava layer at the BG station was considerably deeper than at the VR station. The Koshava winds above BG occurred in a layer stretching from the surface up to 350 hPa. The Koshava layer

at the VR station was much shallower; reaching only up to 900 hPa. Despite the differences in the thickness of the Koshava layer, the maximum Koshava speeds occurred at similar heights (950 to 900 hPa) at both stations. Figure 6.4b shows that the maximum Koshava speed at the BG station was measured in a layer between 389 m (January 31) and 594 m a.g. (February 3). This observation is in accordance with the finding by Vukmirović (1985b) that Koshava is strongest in a layer between 500 and 600 m a.g. The strongest Koshava speed in BG on February 2 occurred at the bottom of an elevated inversion, which was also previously noticed by Unkašević *et al.* (1999). Koshava layer was characterized either with a deep surface inversion (Figure 6.5b) or an elevated inversion layer above adiabatic and conditionally stable layers close to the surface (Figure 6.5b). The elevated inversion was due to the advection of the warm air in the front of the MC (Vukmirović, 1985b).

Atmospheric stability indices in emagrams show the absence of the atmospheric instability during the EKE. However, both environmental helicity (EH) and storm relative environmental helicity (SREH) had very high values. The helicity represents a measure of the vertical transfer of energy by the shear of the horizontal wind vector, *i.e.*:

$$\text{SREH} = -\int_0^h \boldsymbol{k} \cdot (\boldsymbol{V} - \boldsymbol{C}) \times \frac{d\boldsymbol{V}}{dz} \, dz, \qquad (6.1)$$

where vector $\boldsymbol{V}$ is the environmental wind vector, $\boldsymbol{C}$ is the storm's translation velocity, $\boldsymbol{k} \times \frac{d\boldsymbol{V}}{dz}$ is the horizontal vorticity, and $\boldsymbol{k}$ in the unit vector in in the vertical (z) direction. The SREH values at the VR station were around 370 m² s⁻²,

which is comparable to the figures favorable for the development of strong tornadoes.
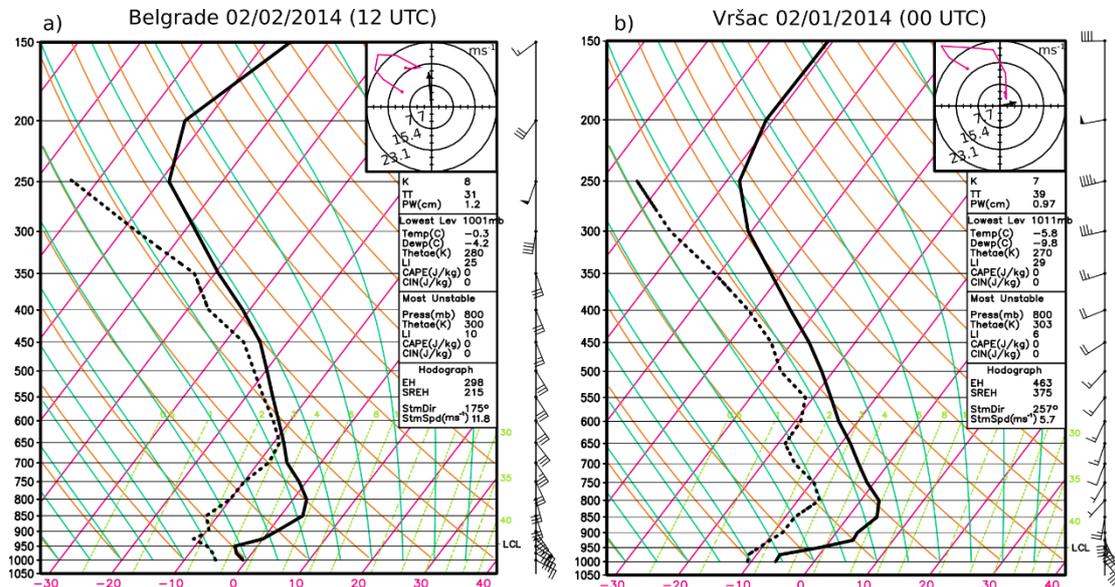
Figure 6.5. Emagrams for (a) BG and (b) VR. Parameters in the boxes are: K – K index in °C; TT – total totals index in °C; PW – precipitable water for the entire sounding in cm; Temp – temperature on ground in °C; Dewp – dewpoint on ground in °C; Thetae – equivalent potential temperature in K; LI – lifted index in °C; CAPE – convective available potential energy in J kg^{-1} ; CIN – convective inhibition in J kg^{-1} ; EH – environmental helicity in m^2 s^{-2}; SREH – storm relative environmental helicity in m^2 s^{-2}; StrmDir – storm direction in degrees; StrmSpd – storm speed in m s^{-1}. For further explanation of the parameters see Doswell III and Schultz (2006).

It is interesting to compare vertical sounding of the atmosphere in the KR (Figure 6.5) with the sounding of the atmosphere in the SKR. Emagram for NEG, which is situated in the SKR, is shown in Figure 6.6.

Figure 6.6. Emagram for NEG. Symbols as in Figure 6.5.

Accumulation of cold air in front of the mountains is highly pronounced. Compared to the BG station, the near-surface air temperature at NEG was 3-4 °C lower. An adiabatic temperature gradient is present up to 950 hPa height, followed by the capping temperature inversion up to 800 hPa and an isothermal layer from 800 to 750 hPa. The near-surface relative humidity at NEG was 100 %, where as the relative humidity at the BG station was low. This difference in relative humidity between the SKR and KR is because the air masses have been stripped out of the moisture as they come over the mountains.

The near-surface winds at the NEG station were blowing from east; again indicating the advancement of cold air from the anticyclone region. This result is

in accordance with the wind rose for NEG when Koshava was active, presented in Figure 5.11 (Section 5.4). The predominant wind direction at NEG is from east.

Wind speeds at NEG were smaller than at BG and considerably weaker than at VR. The vertical wind shear in the KR is much stronger than in the SKR. This result definitely indicates that Koshava can be thought of as a low-level jet. Westerlies were present at the top of the troposphere in both KR and SKR. Finally, the pressure difference between the NEG and BG stations was 9 hPa.

6.4 Numerical modelling of the EKE

Figure 6.7 and Table 6.1 show the models' forecasted wind directions (D) more precisely than the mean hourly wind speeds ($\bar{V}$) and wind gusts ($\hat{V}$). The most accurate wind direction forecasts were at the VR station. A constant 20° to 25° offset between the forecasted (~130°) and the observed (~110°) wind directions at the VG and NS stations is evident. The forecasts at BG were the least accurate, probably due to the complex urban environment around the BG station. The higher accuracy of wind direction forecasts compared to wind speed forecasts is due to the strong and persistent pressure gradients that drove Koshava unidirectionally. The discrepancies between modelled and observed wind directions are most likely caused by poor resolution of small-scale orography and lack of proper representation of urban environments in the models.

The models were not fully capable of capturing high fluctuations of the observed wind speeds and gusts. The most precise $\bar{V}$ forecasts were at the BG and NS stations, i.e. the stations that are further downstream from the mountain regions of central and eastern Serbia.

A general tendency of NMM_QNSE to predict higher $\bar{V}$ and $\hat{V}$ values than the other four models is noticeable. Small variations between NMM and NMMB simulations indicate that initial and boundary conditions, as well as the grid resolution, had little impacts on the forecasts' accuracy. The largest discrepancies between modelled and observed values of $\bar{V}$ are found at the VR station, where the observed $\bar{V}$s were approximately two times higher than the modelled values in the first 90 hours of simulation. The largest deviations between NMM_QNSE's outputs and forecasts of the other four models were in cities (the BG and NS stations). NMM produced the most accurate forecasts of $\bar{V}$ at the VG station. The fluctuations of mean wind speed were best modelled at the BG and VR stations (high CC values). The superiority of the QNSE scheme for numerical modelling of stable conditions, however, has not been confirmed in this study. It can be concluded that numerical modelling of stable PBLs is not at a satisfactory level and more research is needed.
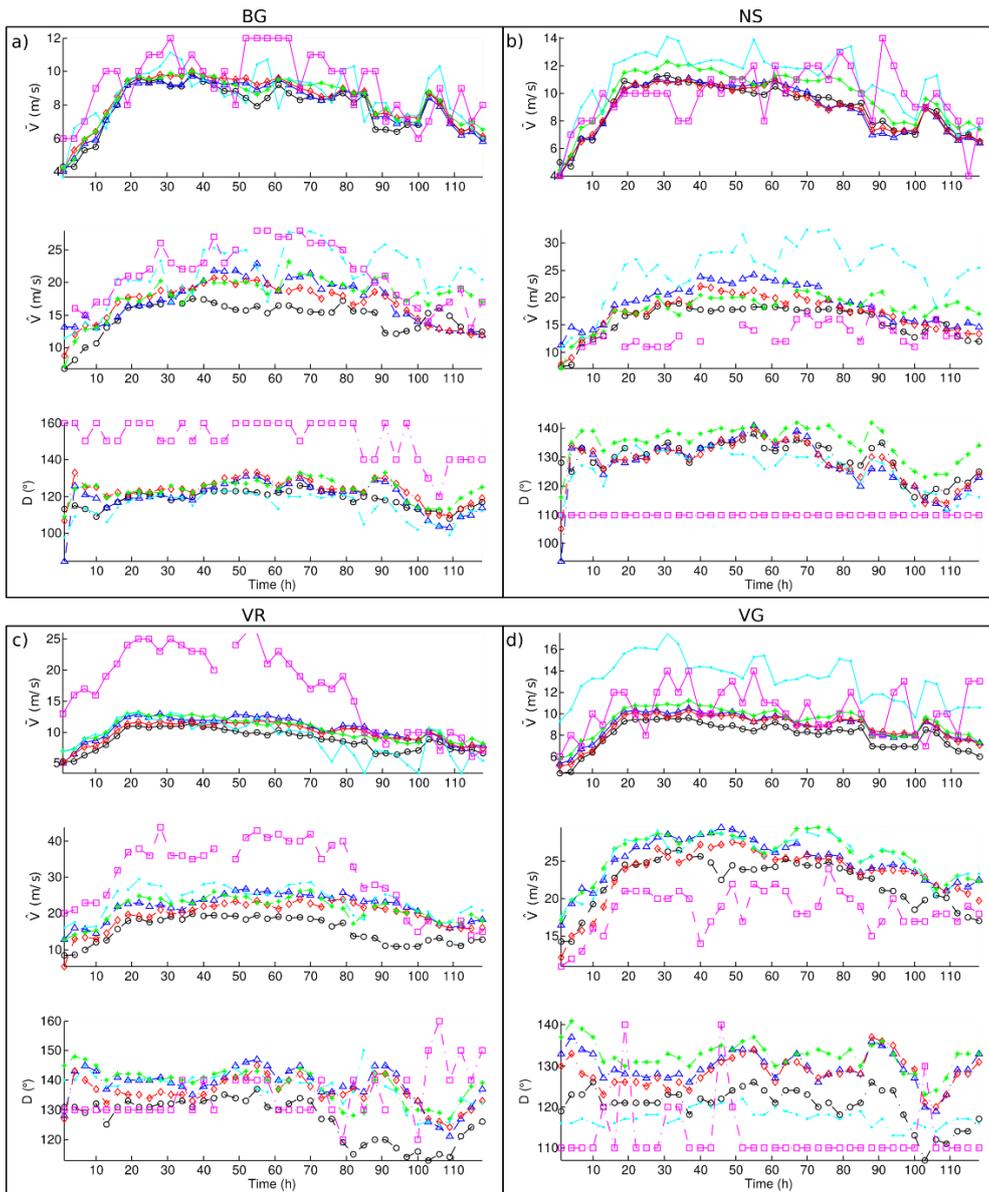
Figure 6.7. Comparison of simulated mean hourly wind speed ($\bar{V}$), gust ($\hat{V}$) and wind direction (D) time series against observations (magenta lines with squares) the BG, NS, VR and VG stations. The utilized models are summarized in Table 3.1: NMM (green lines with stars), NMMB_1 (blue lines with triangles), NMMB_2 (red lines with diamonds), NMM_QNSE (cyan lines with dots) and IFS (black lines with circles). See Table 6.1 for the verification statistics.

Table 6.1. Bias (i.e. Absolute Difference), Mean Absolute Difference (MAD), Root Mean Square Difference (RMSD) and Correlation Coefficient (CC) between forecasts and observations during the EKE. The corresponding time series are portrayed in Figure 6.7.

		NMM			NMMB_1			NMMB_2			NMM_QNSE			IFS		
		$\bar{V}$	$\hat{V}$	D	$\bar{V}$	$\hat{V}$	D	$\bar{V}$	$\hat{V}$	D	$\bar{V}$	$\hat{V}$	D	$\bar{V}$	$\hat{V}$	D
BG	Bias	-1	-3	-28	-1.3	-4.1	-32	-1	-4.5	-28	-0.8	0.2	-37	-1.5	-6.5	-34
	MAD	1.4	3.8	28	1.6	4.1	32	1.4	4.5	28	1.5	3.2	37	1.7	6.6	34
	RMSD	1.7	4.5	30	1.8	4.7	34	1.6	5.1	30	1.8	4.1	38	2	7.3	35
	CC	0.7	0.7	nan	0.7	0.9	nan	0.7	0.9	nan	0.6	0.5	nan	0.7	0.6	nan
NS	Bias	0.1	7.8	25	-0.8	5.5	18	-0.8	4.1	18	1.2	12.1	16	-0.8	2.9	19
	MAD	1.5	7.8	25	1.7	5.5	18	1.6	4.2	18	1.8	12.1	16	1.6	3	19
	RMSD	1.9	8.3	26	2.2	6.6	20	2.1	4.9	17	2.3	12.9	17	2.1	3.9	20
	CC	0.5	0.4	nan	0.5	0.1	nan	0.5	0.2	nan	0.6	0.5	nan	0.5	0.2	nan
VR	Bias	-6.9	-9.8	3	-6.8	-9.2	3	-7.4	-11.6	1	-8.2	-7.4	2	-8.5	-15.8	-8
	MAD	7.3	10.8	10	7.2	10.1	10	7.7	12.1	8	8.5	8.9	10	8.7	15.8	10
	RMSD	8.5	12	12	8.4	11.5	13	9	13.6	11	9.3	10.1	12	9.9	17	15
	CC	0.8	0.7	nan	0.8	0.8	nan	0.7	0.7	nan	0.8	0.7	nan	0.8	0.9	nan
VG	Bias	-1.1	7.5	20	-1.5	6.6	17	-1.6	5	15	2.8	7.2	4	-2.4	3.9	7
	MAD	1.6	7.5	21	1.8	6.6	18	1.9	5	17	3.2	7.2	8	2.6	4	10
	RMSD	2.2	7.9	21	2.4	7.1	19	2.5	5.6	18	3.6	7.6	9	3.1	4.6	12
	CC	0.4	0.6	nan	0.5	0.6	nan	0.6	0.7	nan	0.4	0.6	0.1	0.4	0.7	nan

The wind gusts are not directly calculated by WRF, but computed in post-processing. The Unified Post Processor (UPP; version 2.2) is used to post-process the NMM and NMMB outputs. UPP computes surface wind gusts ($\hat{V}$) by mixing down momentum from the PBL height (z_{PBL}) level (Mankin, 2015):

$$\hat{V} = V_{sfc} + \Delta V \tag{6.2}$$

where

$$\Delta V = \left(V_{PBL} - V_{sfc}\right) \cdot \left(1 - \min\left(0.5, \frac{z_{PBL}}{2000}\right)\right). \tag{6.3}$$

Here, V_{PBL} is the wind speed at z_{PBL} and V_{sfc} is the surface wind speed. The assumption behind this method is that the gusts are caused by air parcels brought down from the top of the PBL by turbulent eddies. The reliability of calculated gusts, therefore, depends on the accuracy of calculated turbulent kinetic energy and other PBL features. Applicability of the method is particularly questionable for the stable PBL (hence small turbulent eddies) and extremely large helicities, both observed during the EKE. However, analysis of different methods for calculations of wind gusts is beyond the scope of this study (*c.f.* Sheridan, 2011).

The RMSD values of estimated gusts are as high as 12.9 m s^{-1} (NMM_QNSE's forecasts at the VR stations). The discrepancies between observed and simulated gusts are smallest at the BG station where NMM_QNSE captured gusts fairly well. In other cases, gusts were largely either over-predicted (NS and VG) or under-predicted (VR). The presented results demonstrate that more research is needed in the field of wind gust modelling.

Table 6.1 further shows that the NMM forecast of $\bar{V}$ have the smallest RMSDs. Since RMSD is the absolute measure of the model's accuracy, the model with the

lowest RMSD is the most reliable model for forecasts of extreme Koshava speeds. Figure 6.8 is shows a spatial distribution of the mean daily wind speeds in the KR based on the NMM simulations. The strongest Koshava speeds (> 17 m s^{-1}) occurred in east Serbia (the VR region) and west Romania (the region around CAR). High wind speeds were also found in the Morava River basin (14-21 m s^{-1}). The high intensity of the Koshava wind in the above-mentioned areas is due to the wind channeling effect created by the local orography. Strong winds were also blowing along the gorges in the South Carpathians. Koshava weakened moving downstream from these regions, but strong winds were still present around BG and NS.
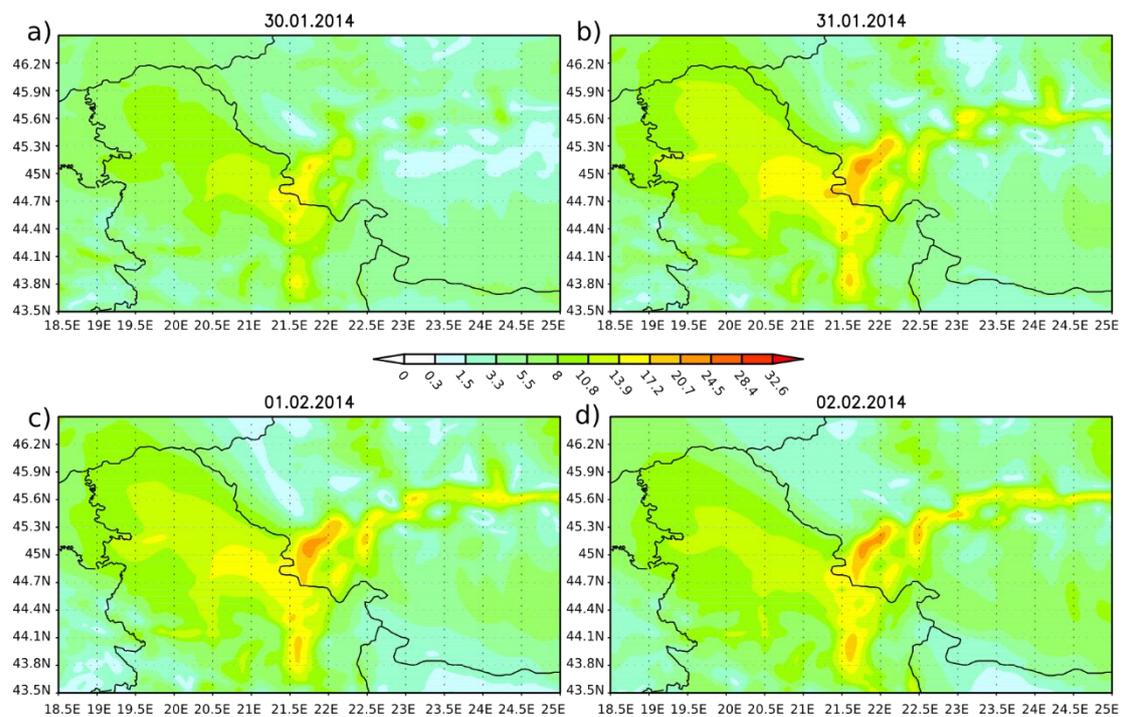
Figure 6.8. NMM forecasts of the mean daily wind speeds during the EKE. Model start at January 30 (00 h UTC).

Extremely high Koshava speeds were present from January 31 to February 2, when the mean daily wind speeds above the whole Pannonian Plane were greater than 10 m s^{-1}.

Figure 6.9 shows that the strong Koshava gusts on January 31, February 1 and February 2 occurred over the whole Pannonian Plane including south Hungary and east Croatia. The pronounced gustiness of the Koshava wind demonstrates its turbulent nature. The thermal convection during the EKE was negligible, thus the main source of turbulence was the strong wind shear, earlier discussed and shown in Figure 6.5. The strongest gusts occurred in the VR and CAR regions (> 30 m s^{-1}).
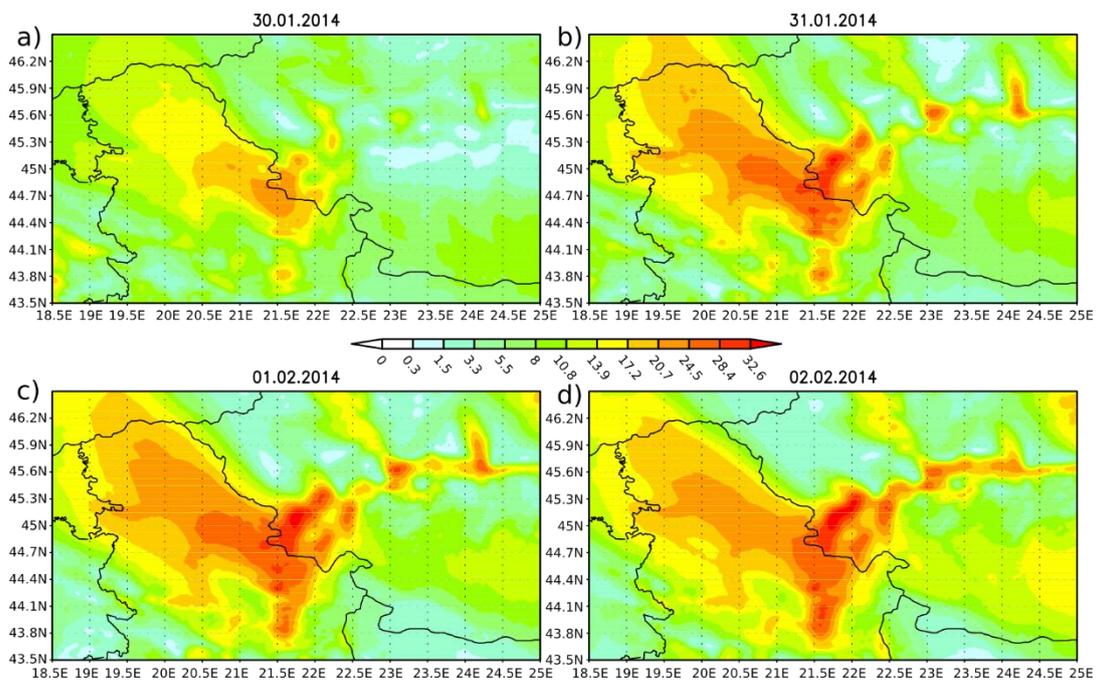
Figure 6.9. Same as Figure 6.8 but for daily wind gusts.

It should be noted that Figure 6.8 and Figure 6.9 in particular should be interpreted cautiously as the evaluation statistics presented in Table 6.1

demonstrate that NMM greatly under-predicted $\bar{V}$s in the VR region. At the same time, NMM under-predicted gusts in BG and VR and over-predicted them in NS and VG to a large extent. The figures, therefore, might be used to identify regions with high Koshava speeds or extreme gusts, but not to report the exact values of these two variables.

6.5 Snowdrifts

There was no significant precipitation during the EKE in most regions of Serbia. Light snow was falling only in the Timočka Krajina region (Zarić, 2014). Occasional snowstorms occurred in the mountain region of eastern Serbia (on Crni Vrh). The maximum height of the previously formed snow cover was 37 cm and it was measured in Timočka Krajina and on Crni Vrh. The depth of snow cover in most of the Pannonian Plane was between 9 and 18 cm (Zarić, 2014). On February 3, after four days of blizzard, the ground in south and eastern parts of the Pannonian Plane was mostly bare, because strong Koshava blew all the snow that existed there before the EKE. The blown snow created deep snowdrifts (snow dunes) in certain regions of the Pannonian Plane. For example, snowdrifts in the central region of the Pannonian Plane, near Feketić village in particular, were several meters deep.

This section introduces a novel method for identifying locations favourable for deep snowdrifts in flat areas. The effects of wind on a snow cover are most visible in open flat terrains (Jones *et al.*, 2011), which Pannonian Plane certainly is. The method is based on a hypothesis that there is a relationship between the location(s) of deep snowdrifts and spatial distribution of the horizontal wind speed gradients. Figure 6.10 schematically portrays the physical background of the proposed method.
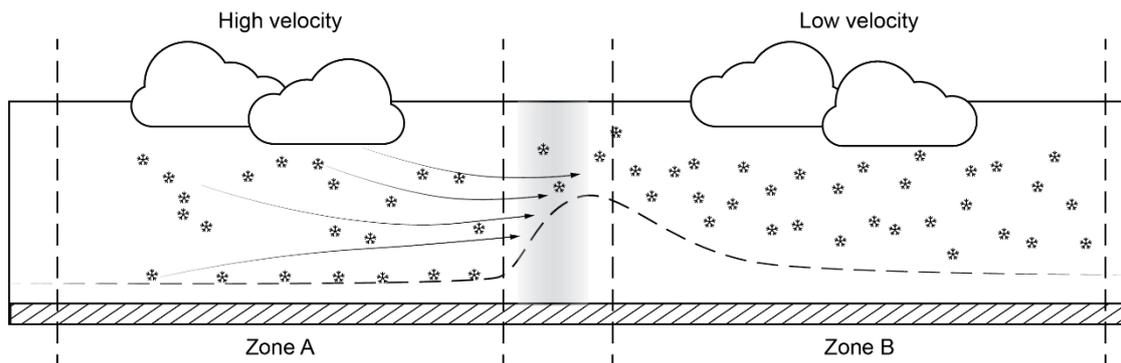
Figure 6.10. Schematic representation of the proposed method for identification of locations with deep snowdrifts. High velocity Zone A is located upstream of low velocity Zone B. Quasi-horizontal dashed line indicates the snow cover. The shaded zone in the middle of the figure (bounded with two vertical dashed lines) is a region with strong negative horizontal wind speed gradient. See text for further details.

Namely, consider two zones – a high velocity Zone A located upstream of a low velocity Zone B, as indicated in Figure 6.10. Assume flat terrain with uniform low roughness (e.g. grass or bare soil) and without any obstacles in both zones. Also recall that snow transport includes three mechanisms of movement (Mellor, 1965): creeping, saltation and turbulent diffusion (see Section 6.1). Assuming very high wind speeds above Zone A, e.g. similar to the Koshava speeds during the EKE, all three modes of snow transport have to be taken into consideration.

First, due to high wind speeds above Zone A, any snowflakes falling from cloud (most likely a Nimbostratus cloud) will have inclined trajectory towards the low velocity Zone B. Thus snow cover at Zone B will be deeper than at Zone A due to the small wind speeds above Zone B.

Second, consider the creeping mechanism of snow transport. Again due to high wind speeds above Zone A, the rolling of heavy snow particles on the surface

will take place from Zone A to Zone B. As the wind speed decreases moving downstream from Zone A and towards Zone B, the creeping mechanism of snow transport also weakens. Therefore, it should be expected that this mode of snow transport will create the deepest snow accumulations somewhere in the upstream region of Zone B or in the transitional region between Zona A and Zone B.

Third, saltation mechanism will act similarly to the creeping mode of snow transportation in sense that snow particles will be lifted from the high velocity zone and deposited in the low velocity zone. Since the snow particles are now lifted from the surface and carried by the wind, it is logical to expect that they might be transported a bit further downstream to Zone B than the heavy snow particles transported through the creeping process. Saltation is derived from eroded snow (Jones *et al.*, 2011). In order for the snow erosion to occur, the shear stress exerted on the snow cover by the wind must exceed the strength of snow crystal bonds and any cohesive forces (for example, surface tension due to wetness in the snow cover). Several authors reported (Grey and Male, 2004), that the threshold wind speed for saltation to occur is between 4.3 m s^{-1} and 18 m s^{-1}, depending on the snow surface hardness. The saltation process also depends on temperature and it was found that typical threshold wind speed values are between 7 m s^{-1} and 9 m s^{-1} (Li and Pomeroy, 1997). These wind speeds were most certainly exceeded during the EKE.

The above discussion supported by scientific literature indicates that transport of snow will take place from Zone A to Zone B. If so, where is the most likely location of the deepest snowdrifts? The assumption of the proposed method is that the deepest snowdrifts will occur in the transition region between Zone A

and Zone B and in the upstream region of the low velocity Zone B. Namely, these two regions are characterized by strong negative horizontal wind speed gradient, i.e. the regions where the wind significantly slows down.

The Pannonian Plane and EKE are an ideal natural setup to test the proposed method. The zones where wind speed markedly weekend over Pannonian Plane had to be identify and compared with the reported locations of deep snowdrifts.

The horizontal gradient of wind speed (∇V) is determined as:

$$\nabla V = \frac{\partial V}{\partial x}\boldsymbol{i} + \frac{\partial V}{\partial y}\boldsymbol{j}, \tag{6.4}$$

where x and y are zonal and meridional directions with associated unit vectors $\boldsymbol{i}$ and $\boldsymbol{j}$, respectively. The intensity of the gradient is afterwards calculated as:

$$\|\nabla V\| = \sqrt{\left(\frac{\partial V}{\partial x}\right)^2 + \left(\frac{\partial V}{\partial y}\right)^2}. \tag{6.5}$$

Figure 6.11a represents the normalized values of the cumulative horizontal wind speed, while Figure 6.11b shows the normalized horizontal gradients of the mean wind speed. In both cases, normalization is with respect to a maximum value. The reported locations of deep snowdrifts during the EKE are indicated with the blue polygons.
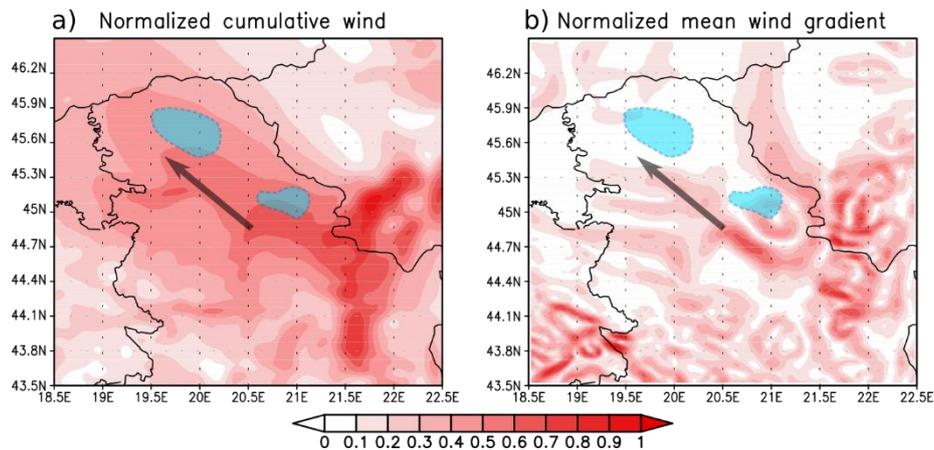
Figure 6.11. (a) Normalized cumulative wind speed and (b) and normalized mean wind speed gradients during the EKE. Reported locations of deep snowdrifts are indicated with blue polygons. Black arrows represent the prevailing wind direction. See text for further details.

Figure 6.11 seems to indicate that the deepest snowdrifts are observed in the low-velocity zones (with respect to the upstream speed) and, in particular, in the regions of the low-velocity zones close to the upstream high-velocity zones. For instance, deep snowdrifts in the central Pannonian Plane were the most pronounced in the area where the cumulative horizontal wind speed during the EKE dropped from 0.5 to 0.4. Large wind speed gradients in Figure 6.11b indicate locations of the decreasing wind speed. These locations are prone to deep snowdrifts. A good example is the region with reported deep snowdrifts situated in the southeast Pannonian Plane.

The above methodology is tested only for the case of the 2014 EKE and is limited to the flat terrains with more or less uniform surface roughness. Most certainly more research is needed in order to further validate the proposed method. Some suggestions for the further research on this subject are given in Chapter 7.

6.6 Summary and conclusions

This chapter analyses a case study of an EKE (EKE) that occurred from January 30 to February 4, 2014. The mean daily Koshava speeds during the EKE were generally above 10 m s^{-1} with gusts exceeding 30 m s^{-1}. Similar Koshava event had not occurred during the past 25 years. Meteorological factors leading to this EKE were: (1) large pressure gradients across the Balkan Peninsula caused by an extremely deep EA with the central pressure above 1055 hPa combined with (2) large temperature gradients between the anticyclone and cyclone regions – all of which resulted in (3) extremely large across-mountain pressure and potential temperature differences between the Wallachia Valley and the KR. The extreme wind speeds occurred together with deep snowdrifts, thus causing a blizzard. The atmosphere in the Koshava layer was either stable with surface inversion or adiabatic with capping elevated inversion.

Four numerical simulations of the EKE were performed (two using WRF-NMM and two using NMMB) and benchmarked against the observations and the global IFS' analysis. The models captured Koshava's directions more accurately than its mean speeds and gusts. The strongest Koshava speeds occurred in the VR region. Higher accuracy of direction forecasts is due to the strong pressure gradients that drove the wind. The low accuracy of modelled speeds and gusts is probably due to the lack of planetary boundary layer schemes capable of properly replicating stable stratifications. More research is needed in the field of numerical modelling of stable boundary layers.

A new technique for identifications of snowdrifts based on horizontal wind speed gradients is proposed and results demonstrate that deep snowdrifts occur in the zones of (1) small accumulated wind speed and/or (2) pronounced

negative horizontal gradients of wind speed. The methodology is restricted to the flat regions with uniform surface roughness. More research is needed to validate the proposed method.

CHAPTER 7

7. Concluding remarks and future work

The work presented in this thesis is aimed towards better understanding of the Koshava wind. This chapter presents a summary on the findings of the work and it suggests directions for future development.

7.1 Discussion summary and conclusions

Koshava is the most dominant local wind over Serbia and one of the most vigorous winds in Southeast Europe. The pressure systems which drive the wind are an anticyclone located over Eastern Europe and/or Western Asia and a low pressure system positioned over the Mediterranean Sea. Due to the seasonality of these synoptic pressure systems, Koshava typically occurs in the cold part of the year and spring and rarely in summer.

The scientific research on the Koshava wind started in the first half of XIX century with the works of Vujević (Vujević, 1933) and Milosavljević (Milosavljević, 1950). Most of this research has been centered about the climatological characteristics of the wind, such as mean wind speed, seasonality, mean wind directions and relation between Koshava and other meteorological variables. All this work is nicely summarized in Unkašević and Tošić (2006). Important to note is that most of the previous studies analyzed Koshava over BG and not the whole KR. Some important aspects of the Koshava wind have not been analyzed up to now.

This thesis analyzes some of the dynamical characteristics of the Koshava wind. Certain climatological aspects of the wind are addressed as well. The main objectives of this thesis are: (1) analysis of long-term Koshava trends, (2) inspection of quality of measured wind data in the KR (KR), (3) determination of causes of Koshava's trends, (4) investigation of synoptic pressure systems which generate Koshava, (5) study of mesoscale and sub-mesoscale factors that drive Koshava, (6) construction of stochastic model for determination of mean Koshava speed, (7) analysis of an EKE (EKE) and what are the meteorological factors which develop strong Koshava winds, (8) investigation of vertical profiles of meteorological variables during the EKE (9) evaluation of capabilities of numerical models to simulate extremely strong Koshava winds, and (9) introduction of new methodology for detection of locations suitable for deep snowdrifts in flat terrains.

The homogeneity analysis revealed that the small wind speeds are substantially more inhomogeneous than the higher wind speed. Homogeneity testing furthermore showed that wind direction series have been more inhomogeneous than wind speed series. The anomalies in wind data in the 1950s are due to the introduction of wind roses with 16 wind directions instead of 8. The anomalies that are due to station relocation are clearly represented in wind time series. Most of the other anomalies either due to an instrument replacement or minor changes of instrument's close surrounding.

Negative and statistically significant trends of the mean annual Koshava speed have been detected at all weather stations in the KR in the period 1948-2014. The average negative slope of the trend is -0.020 m s^{-1} year^{-1} for all Koshava speeds and -0.024 m s^{-1} year^{-1} for Koshava speeds above 5 m s^{-1} (i.e. strong Koshava

winds). Stronger trend for higher wind speeds suggests that the above discussed inhomogeneity of wind data did not play an important role in the observed trends. Trends in the annual number of the days with the Koshava wind are statistically weaker than the wind speed trends. Namely, most trends (except at the VG station) are negative, but not as statistically pronounced as the mean annual Koshava speed trends. The westerlies over the KR were also weakening, but the calculated negative trends were not as steep as Koshava's trends.

The negative trends of the winds at 850 hPa and 500 hPa levels accompanied with the decrease in the temperature gradient between the KR and the source region of the Koshava wind, shows that the changes in the large-scale weather patterns were dominant factors that caused the negative trends of the Koshava wind. This result is in accordance with the literature results on the weakening of the Siberian high and West-MCs. The observed negative Koshava trends, however, have a negligible impact on the wind resources and wind power sector in Serbia.

It has been demonstrated that 2-day and 3-day Koshava events were the most common; in combination observed in 14.1 % of the time in a year. In a year, Koshava was blowing in about 32 % of the time. It has been shown that 1-day Koshava occurrences were rare.

It was shown that closed MCs located in the Gulf of Genoa and Adriatic Sea were the most associated with Koshava. These cyclones were present in 74 % of all Koshava events. Anticyclones causing Koshava were located above Romania, Moldavia and south Ukraine (EAs (EAs)) and were observed in 71 % of all Koshava occurrences. These pressure systems are about 500-1000 km from the KR.

It was observed that Koshava's mean hourly and maximum hourly wind speeds were largest when both pressure systems were simultaneously active, which occurred in 67 % of all Koshava events. Koshava occurred independent of MCs and EA only 3 % of the time. Cyclones which caused Koshava followed southeast trajectories two times more frequently than they followed northeast trajectories from the Gulf of Genoa.

Koshava is a gap flow wind and local characteristics of the Koshava wind are dominantly determined by mesoscale factors such as orography, across-mountain mean sea level pressure (ΔP) and potential temperature ($\Delta\theta$) differences. The probability density functions (PDFs) of ΔP and $\Delta\theta$ accurately distinguish Koshava from "no-Koshava" events. It was found that ΔP is more influential on Koshava than $\Delta\theta$. On average, the overlap between the PDFs of ΔPs is 0.257 and the overlap between the PDFs of $\Delta\theta$s is 0.479. Koshava is poorly correlated with winds at higher levels. The mean pressure gradient in the KR when the wind was active is 1.18 Pa km^{-1}, which is in the range of the pressure gradients observed in the MCs that caused the wind.

The Synoptic Koshava Index (SKI), defined as the difference between the area-averaged mean sea level pressures in the anticyclone and cyclone regions (PD_K), i.e.:

$$\text{SKI} = \frac{PD_K - \overline{PD}}{\widehat{PD}} \qquad (7.1)$$

where $\overline{PD}$ and $\widehat{PD}$ are the mean pressure difference and its standard deviation, respectively. It has been shown that SKI is a good indicator of the Koshava occurrence. The values of the index are mostly in the interval from 10 to 25 when

154

Koshava occurred and from -10 to 10 when Koshava was not active. The occurrence can be predicted with high accuracy in about 70 % cases.

The accuracy of the mean hourly Koshava speed ($\bar{V}_K$) forecast using the simple linear model constructed in this study is the highest for the BG station and the lowest at the VR station. It was demonstrated that ΔP is the only significant predictor in the stochastic model and linear relationship between $\bar{V}_K$ and ΔP is statistically significant at all stations in the KR.

The mean daily Koshava speeds during the EKE of 2014 were above 10 m s^{-1} with gusts exceeding 30 m s^{-1}. This EKE is the first extreme Koshava event after more than 25 years without any similar event. It has been shown that the meteorological factors leading to this EKE were large pressure gradients across the Balkan Peninsula in combination with large temperature gradients between the anticyclone and cyclone regions. These factors resulted in extremely large ΔPs and $\Delta \theta$s between the Wallachia Valley in Romania and the KR. The extreme wind speeds occurred together with deep snowdrifts. Therefore, the EKE was a blizzard. The atmosphere in the Koshava layer was either stable with surface inversion or adiabatic with capping elevated inversion.

Four numerical simulations of the EKE were performed using WRF-NMM and NMMB mesoscale models. The results are compared against the observations and the global IFS' analysis. The models captured Koshava's directions more accurately than its mean speeds and gusts. Higher accuracy of direction forecasts is due to the strong pressure gradients that drove the wind. The low accuracy of modelled speeds and gusts is probably due to the lack of planetary boundary layer schemes capable of properly replicating stable stratifications. It was

concluded that more research is needed in the field of numerical modelling of stable boundary layers and associated phenomena.

On the example of the EKE, it was demonstrated that deep snowdrifts occur in the zones of small accumulated wind speed and pronounced negative horizontal gradients of wind speed. The proposed methodology, however, is restricted to the flat regions with uniform surface roughness.

This thesis investigated Koshava wind from a new perspective. All results presented in this thesis are a unique contribution to the understanding of this local wind. All of the open questions stated in the research proposal have been addressed and results presented. Some of the applications of the results are discussed and demonstrated. The applications of the results could further be extended to other areas of science and industry. For example, the proposed method for identification of snowdrift locations could be very valuable for the sector of land transport. The stochastic model of mean hourly Koshava speed could be used for Koshava forecasting. The results of the homogeneity analysis might be used by other researches interested in wind analysis in the KR. The observations of the extreme wind speeds during the EKE will serve as a detailed benchmark for the future numerical simulations of both extreme winds and stable atmospheric conditions.

The results presented in this thesis are published in the leading peer-reviewed meteorological journals – International Journal of Climatology and Atmospheric Science Letters (published on behalf of Royal Meteorological Society).

7.2 Future recommendations

Despite the rigorous investigations performed in this thesis, there is always room for further development and improvement. The following recommendations can be made to complement and extend the current study.

The homogeneity analysis performed in this study is based on wind data from several meteorological stations in the KR. The analysis could be extended to the rest of Serbia. Furthermore, it would be interesting to perform the homogeneity testing over the wind data from the source KR (Wallachia Valley) and compared the results with the results from the KR. The homogeneity analysis of other meteorological variables would be of great importance too. These analysis have not been performed. If conducted, the results of these analysis would provide the comprehensive insight into the quality of meteorological data in Serbia.

The trend analysis of the Koshava wind speed and activity could be extended to 1888. The data from 1888 are available, but most of them are not in the digital form and require a considerable effort to digitalize them. Moreover, the homogeneity testing of the wind data from 1888 to 1949 is recommended. It would be interesting to compare Koshava trends in the period 1888-1949 with the results for the period after 1949. Meteorological measurements are of great significance and digitalization of all data stored in archives is highly recommended.

The stochastic Koshava model presented in this thesis is based on the linear regression method. A nonlinear model might be more accurate. Therefore, the extension of the presented linear model to nonlinear regression is recommended. The comparison between the results of the simple linear model (presented

herein) and more complex nonlinear model would be interesting. The nonlinear regression might reveal the importance of other predictors on the mean hourly Koshava speed.

More testing of the proposed stochastic model for mean hourly Koshava speed is needed. Namely, the model is developed based on the large set of data, but really tested for the individual Koshava events. Figure 5.15 includes all Koshava events from 1971, but the data are lumped in one figure. Therefore, it is difficult to perform separate case studies. The proposed model requires more case study tests.

The proposed SKI is shown to be an accurate parameter for prediction of Koshava occurrence. Similarly to the stochastic model of the mean hourly Koshava speed, the SKI requires more testing. One case study test was performed for the EKE and the high accuracy of the SKI is demonstrated. However, the SKI should be further tested for small Koshava winds, intermediate Koshava winds and Koshava winds when one of the pressure systems that drive Koshava is weak. All the cases have been analyzed as a whole, not on a case-by-case basis.

The investigation of the EKE showed that an accurate numerical modelling of stable atmospheric layers is still very challenging. More research in this field is recommended. To be more specific, theoretical and numerical work should be focused on the investigation of turbulence characteristics in stable atmosphere, analysis of gust winds and how to accurately model gusts in numerical models. This thesis provides a comprehensive set of wind data to benchmark the results of numerical models and theoretical investigations.

Lastly, the new methodology for determination of locations favorable for deep snowdrifts in flat terrains requires more testing. The methodology is developed and tested only for the case of EKE. Although, the first results look promising, more testing is recommended. Furthermore, the proposed method assumes uniform surface roughness and does not include the influence of any obstacles that might be on the surface.

References

Alexandersson H. 1986. A homogeneity test applied to precipitation data. *Journal of Climatology* **6**(6): 661–675. DOI: 10.1002/joc.3370060607.

Alexandersson H, Schmith T, Iden K, Tuomenvirta H. 1998. Long-term variations of the storm climate over NW Europe. *The Global Atmosphere and Ocean System* **6**(2): 97–120.

Archer CL, Jacobson MZ. 2003. Spatial and temporal distributions of U.S. winds and wind power at 80 m derived from measurements. *Journal of Geophysical Research: Atmospheres* **108**(D9): n/a–n/a. DOI: 10.1029/2002JD002076.

Auer I, Böhm R, Jurković A, Orlik A, Potzmann R, Schöner W, Ungersböck M, Brunetti M, Nanni T, Maugeri M, Briffa K, Jones P, Efthymiadis D, Mestre O, Moisselin J-M, Begert M, Brazdil R, Bochnicek O, Cegnar T, Gajić-Čapka M, Zaninović K, Majstorović Ž, Szalai S, Szentimrey T, Mercalli L. 2005. A new instrumental precipitation dataset for the greater alpine region for the period 1800–2002. *International Journal of Climatology* **25**(2): 139–166. DOI: 10.1002/joc.1135.

Bakker AMR, Hurk BJJM van den. 2012. Estimation of persistence and trends in geostrophic wind speed for the assessment of wind energy yields in Northwest Europe. *Climate Dynamics* **39**(3-4): 767–782. DOI: 10.1007/s00382-011-1248-1.

Bakker AMR, Van den Hurk BJJM, Coelingh JP. 2013. Decomposition of the windiness index in the Netherlands for the assessment of future long-term wind supply. *Wind Energy* **16**(6): 927–938. DOI: 10.1002/we.1534.

Baule WJ, Shulski MD. 2013. Climatology and trends of wind speed in the Beaufort/Chukchi Sea coastal region from 1979 to 2009. *International Journal of Climatology* n/a–n/a. DOI: 10.1002/joc.3881.

Beare RJ, Macvean MK, Holtslag AAM, Cuxart J, Esau I, Golaz J-C, Jimenez MA, Khairoutdinov M, Kosovic B, Lewellen D, Lund TS, Lundquist JK, Mccabe A,

Moene AF, Noh Y, Raasch S, Sullivan P. 2006. An Intercomparison of Large-Eddy Simulations of the Stable Boundary Layer. *Boundary-Layer Meteorology* **118**(2): 247–272. DOI: 10.1007/s10546-004-2820-6.

Brázdil R, Budíková M, Auer I, Böhm R, Cegnar T, Faško P, Lapin M, Gajič–Čapka M, Zaninović K, Koleva E, Niedźwiedź T, Ustrnul Z, Szalai S, Weber RO. 1996. Trends of Maximum and Minimum Daily Temperatures in Central and Southeastern Europe. *International Journal of Climatology* **16**(7): 765–782. DOI: 10.1002/(SICI)1097-0088(199607)16:7<765::AID-JOC46>3.0.CO;2-O.

Brázdil R, Chromá K, Dobrovolný P, Tolasz R. 2009. Climate fluctuations in the Czech Republic during the period 1961–2005. *International Journal of Climatology* **29**(2): 223–242. DOI: 10.1002/joc.1718.

Brohan P, Kennedy JJ, Harris I, Tett SFB, Jones PD. 2006. Uncertainty estimates in regional and global observed temperature changes: A new data set from 1850. *Journal of Geophysical Research: Atmospheres* **111**(D12): n/a–n/a. DOI: 10.1029/2005JD006548.

Čadež M. 1976. Some Observations on Bora and Föhn Winds. *In: Local wind Bora, M. Yoshino, editor*. University of Tokio Press: Tokio, Japan, 193– 202.

Chernokulsky A, Mokhov II, Nikitina N. 2013. Winter cloudiness variability over Northern Eurasia related to the Siberian High during 1966–2010. *Environmental Research Letters* **8**(4): 045012. DOI: 10.1088/1748-9326/8/4/045012.

Conrad V, Pollak LW. 1962. *Methods in climatology.* Harvard University Press: Cambridge.

Costa AC, Soares A. 2009. Homogenization of Climate Data: Review and New Perspectives Using Geostatistics. *Mathematical Geosciences* **41**(3): 291–305. DOI: 10.1007/s11004-008-9203-3.

Croitoru A-E, Holobaca I-H, Lazar C, Moldovan F, Imbroane A. 2012. Air temperature trend and the impact on winter wheat phenology in Romania. *Climatic Change* **111**(2): 393–410. DOI: 10.1007/s10584-011-0133-6.

Crosman ET, Horel JD. 2010. Sea and Lake Breezes: A Review of Numerical Studies. *Boundary-Layer Meteorology* **137**(1): 1–29. DOI: 10.1007/s10546-010-9517-9.

Ćurić M. 1978. Some mesoscale meteorological phenomena involved by the mountain. paper presented at the Comptes rendus du 15. Congres International de meteorologie Alpine. Publication de l'Institut Suisse de Meteorologie: Grindelwald, Switzerland, 186–188.

Ćurić M. 1980. Dynamische Prozesse beim Verschwinden von Kaltluftseen. *Abhandlungen des Meteorologischen Dienstes der Deutschen Demokratischen Republik* **124**: 223–225.

Ćurić M. 2002. *Dinamička meteorologija*. RHMZ Srbije: Beograd.

Dadaser-Celik F, Cengiz E. 2013. Wind speed trends over Turkey from 1975 to 2006. *International Journal of Climatology* n/a–n/a. DOI: 10.1002/joc.3810.

Dai A, Deser C. 1999. Diurnal and semidiurnal variations in global surface wind and divergence fields. *Journal of Geophysical Research: Atmospheres* **104**(D24): 31109–31125. DOI: 10.1029/1999JD900927.

D'Arrigo R, Jacoby G, Wilson R, Panagiotopoulos F. 2005. A reconstructed Siberian High index since A.D. 1599 from Eurasian and North American tree rings. *Geophysical Research Letters* **32**(5): n/a–n/a. DOI: 10.1029/2004GL022271.

DeGaetano AT. 1998. Identification and Implications of Biases in U.S. Surface Wind Observation, Archival, and Summarization Methods. *Theoretical and Applied Climatology* **60**(1-4): 151–162. DOI: 10.1007/s007040050040.

Ding Y, Krishnamurti TN. 1987. Heat Budget of the Siberian High and the Winter Monsoon. *Monthly Weather Review* **115**(10): 2428–2449. DOI: 10.1175/1520-0493(1987)115<2428:HBOTSH>2.0.CO;2.

Domonkos P, Kyselý J, Piotrowicz K, Petrovic P, Likso T. 2003. Variability of extreme temperature events in south–central Europe during the 20th century and its relationship with large-scale circulation. *International Journal of Climatology* **23**(9): 987–1010. DOI: 10.1002/joc.929.

Doswell III CA, Schultz DM. 2006. On the Use of Indices and Parameters in Forecasting Severe Storms. *E-Journal of Severe Storms Meteorology* **1**(3): 1–22.

Draper NR, Smith H. 1998. *Applied Regression Analysis*. Wiley-Interscience.

Drechsel S, Mayr GJ. 2008. Objective Forecasting of Foehn Winds for a Subgrid-Scale Alpine Valley. *Weather and Forecasting* **23**(2): 205–218. DOI: 10.1175/2007WAF2006021.1.

Drobinski P, Dubos T. 2009. Linear breeze scaling: from large-scale land/sea breezes to mesoscale inland breezes. *Quarterly Journal of the Royal Meteorological Society* **135**(644): 1766–1775. DOI: 10.1002/qj.496.

Đurišić Ž, Bubnjević M, Mikičić D, Rajaković N. 2007. Wind atlas of Vojvodina. *Proceeding of European Wind Energy Conference & Exhibition (EWEC 2007)*. Milano, Italy.

Durran DR. 2003. DOWNSLOPE WINDS. In: Holton JR (ed) *Encyclopedia of Atmospheric Sciences*. Academic Press: Oxford, 644–650.

Efroymson M. 1960. *Multiple regression analysis*. John Wiley: New York.

Ek MB, Mitchell KE, Lin Y, Rogers E, Grunmann P, Koren V, Gayno G, Tarpley JD. 2003. Implementation of Noah land surface model advances in the National Centers for Environmental Prediction operational mesoscale Eta model. *Journal of Geophysical Research: Atmospheres* **108**(D22): 8851. DOI: 10.1029/2002JD003296.

Ferrier BS, Springs C, Jin Y, Lin Y, Black T, Rogers E, DiMego G. 2002. Implementation of a new grid-scale cloud and precipitation scheme in the NCEP Eta model. *15th Conference on Numerical Weather Prediction*. American Meteorological Society: San Antonio, TX, 280–283.

Flamant C, Drobinski P, Nance L, Banta R, Darby L, Dusek J, Hardesty M, Pelon J, Richard E. 2002. Gap flow in an Alpine valley during a shallow south föhn event: Observations, numerical simulations and hydraulic analogue. *Quarterly Journal of the Royal Meteorological Society* **128**(582): 1173–1210. DOI: 10.1256/003590002320373256.

Flocas HA, Simmonds I, Kouroutzoglou J, Keay K, Hatzaki M, Bricolas V, Asimakopoulos D. 2010. On Cyclonic Tracks over the Eastern Mediterranean. *Journal of Climate* **23**(19): 5243–5257. DOI: 10.1175/2010JCLI3426.1.

Gaberšek S, Durran DR. 2004. Gap Flows through Idealized Topography. Part I: Forcing by Large-Scale Winds in the Nonrotating Limit. *Journal of the Atmospheric Sciences* **61**(23): 2846–2862. DOI: 10.1175/JAS-3340.1.

Gaffin DM. 2007. Foehn Winds That Produced Large Temperature Differences near the Southern Appalachian Mountains. *Weather and Forecasting* **22**(1): 145–159. DOI: 10.1175/WAF970.1.

Gburčik P, Gburčik V, Gavrilović M, Srdanović V, Mastilović S. 2006. Complementary regimes of solar and wind energy in Serbia. *Geographica Pannonica* **10**: 22–25.

Giaiotti DB, Steinacker R, Stel F. 2007. *Atmospheric Convection: Research and Operational Forecasting Aspects*. Springer Science & Business Media.

Grey DM, Male DH (eds). 2004. *Handbook of Snow: Principles, Processes, Management and Use*. Blackburn Pr: Caldwell, N.J.

Grisogono B, Belušić D. 2009. A review of recent advances in understanding the meso- and microscale properties of the severe Bora wind. *Tellus A* **61**(1): 1–16. DOI: 10.1111/j.1600-0870.2008.00369.x.

Guo H, Xu M, Hu Q. 2011. Changes in near-surface wind speed in China: 1969–2005. *International Journal of Climatology* **31**(3): 349–358. DOI: 10.1002/joc.2091.

Haeger-Eugensson M, Holmer B. 1999. Advection caused by the urban heat island circulation as a regulating factor on the nocturnal urban heat island. *International Journal of Climatology* **19**(9): 975–988. DOI: 10.1002/(SICI)1097-0088(199907)19:9<975::AID-JOC399>3.0.CO;2-J.

Hara T, Ohya Y, Uchida T, Ohba R. 2009. Wind-Tunnel and Numerical Simulations of the Coastal Thermal Internal Boundary Layer. *Boundary-Layer Meteorology* **130**(3): 365–381. DOI: 10.1007/s10546-008-9343-5.

Hasanean HM, Almazroui M, Jones PD, Alamoudi AA. 2013. Siberian high variability and its teleconnections with tropical circulations and surface air temperature over Saudi Arabia. *Climate Dynamics* **41**(7-8): 2003–2018. DOI: 10.1007/s00382-012-1657-9.

Heidorn K. 2007. *The Weather Doctor Almanac 2007 The Mediterranean: Birthplace of the Winds*. The Weather Doctor. Education. .

Hisdal H, Stahl K, Tallaksen LM, Demuth S. 2001. Have streamflow droughts in Europe become more severe or frequent? *International Journal of Climatology* **21**(3): 317–333. DOI: 10.1002/joc.619.

Holt E, Wang J. 2012. Trends in Wind Speed at Wind Turbine Height of 80 m over the Contiguous United States Using the North American Regional Reanalysis (NARR). *Journal of Applied Meteorology and Climatology* **51**(12): 2188–2202. DOI: 10.1175/JAMC-D-11-0205.1.

Horvat K, Ivančan-Picek B, Ivatek-Šahdan S, Grubišić V. 2007. Differences in the dynamics a nd structure of the northern and southern Adriatic severe bora. *29th international conference on Alpine meteorology – Extended abstracts*. paper presented at the 29th international conference on Alpine meteorology. Meteo-France: Toulouse, 609–612.

Iacono MJ, Delamere JS, Mlawer EJ, Shephard MW, Clough SA, Collins WD. 2008. Radiative forcing by long-lived greenhouse gases: Calculations with the AER radiative transfer models. *Journal of Geophysical Research: Atmospheres* **113**(D13): D13103. DOI: 10.1029/2008JD009944.

Ib T, Petersen EL. 1989. *European Wind Atlas*. RISØ National Laboratory: Roskilde, Denmark.

Jaagus J. 2006. Climatic changes in Estonia during the second half of the 20th century in relationship with changes in large-scale atmospheric circulation. *Theoretical and Applied Climatology* **83**(1-4): 77–88. DOI: 10.1007/s00704-005-0161-0.

Janjić ZI. 1994. The Step-Mountain Eta Coordinate Model: Further Developments of the Convection, Viscous Sublayer, and Turbulence Closure Schemes. *Monthly Weather Review* **122**(5): 927–945. DOI: 10.1175/1520-0493(1994)122<0927:TSMECM>2.0.CO;2.

Jeong J-H, Ou T, Linderholm HW, Kim B-M, Kim S-J, Kug J-S, Chen D. 2011. Recent recovery of the Siberian High intensity. *Journal of Geophysical Research: Atmospheres* **116**(D23): n/a–n/a. DOI: 10.1029/2011JD015904.

Jeromel M, Vlado Malačič V, Rakovec J. 2009. Weibull distribution of bora and sirocco winds in the northern Adriatic Sea. *Geofizika* **26**(1): 85–100.

Jones HG, Pomeroy JW, Walker DA, Hoham RW (eds). 2011. *Snow Ecology: An Interdisciplinary Examination of Snow-Covered Ecosystems*. Cambridge University Press: Cambridge, UK.

Kalabokas PD, Mihalopoulos N, Ellul R, Kleanthous S, Repapis CC. 2008. An investigation of the meteorological and photochemical factors influencing the background rural and marine surface ozone levels in the Central and Eastern Mediterranean. *Atmospheric Environment* **42**(34): 7894–7906. DOI: 10.1016/j.atmosenv.2008.07.009.

Kalnay E, Kanamitsu M, Kistler R, Collins W, Deaven D, Gandin L, Iredell M, Saha S, White G, Woollen J, Zhu Y, Leetmaa A, Reynolds R, Chelliah M, Ebisuzaki W, Higgins W, Janowiak J, Mo KC, Ropelewski C, Wang J, Jenne R, Joseph D. 1996. The NCEP/NCAR 40-Year Reanalysis Project. *Bulletin of the American Meteorological Society* **77**(3): 437–471. DOI: 10.1175/1520-0477(1996)077<0437:TNYRP>2.0.CO;2.

Kendall MG. 1970. *Rank correlation methods*. Griffin: London.

Kistler R, Collins W, Saha S, White G, Woollen J, Kalnay E, Chelliah M, Ebisuzaki W, Kanamitsu M, Kousky V, van den Dool H, Jenne R, Fiorino M. 2001. The NCEP–NCAR 50–Year Reanalysis: Monthly Means CD–ROM and Documentation. *Bulletin of the American Meteorological Society* **82**(2): 247–267. DOI: 10.1175/1520-0477(2001)082<0247:TNNYRM>2.3.CO;2.

Klink K. 1999. Climatological mean and interannual variance of United States surface wind speed, direction and velocity1. *International Journal of Climatology* **19**(5): 471–488. DOI: 10.1002/(SICI)1097-0088(199904)19:5<471::AID-JOC367>3.0.CO;2-X.

Klink K. 2002. Trends and Interannual Variability of Wind Speed Distributions in Minnesota. *Journal of Climate* **15**(22): 3311–3317. DOI: 10.1175/1520-0442(2002)015<3311:TAIVOW>2.0.CO;2.

Koletsis I, Lagouvardos K, Kotroni V, Bartzokas A. 2009. The interaction of northern wind flow with the complex topography of Crete Island – Part 1: Observational study. *Nat. Hazards Earth Syst. Sci.* **9**(6): 1845–1855. DOI: 10.5194/nhess-9-1845-2009.

Kouroutzoglou J, Flocas HA, Keay K, Simmonds I, Hatzaki M. 2011. Climatological aspects of explosive cyclones in the Mediterranean. *International Journal of Climatology* **31**(12): 1785–1802. DOI: 10.1002/joc.2203.

Kreyszig E. 2011. *Advanced Engineering Mathematics*. Wiley: Hoboken, NJ.

Küttner J. 1940. Der Kosava in Serbien. *Meteorologische Zeitschrift* **57**: 120–123.

Lacis AA, Hansen J. 1974. A Parameterization for the Absorption of Solar Radiation in the Earth's Atmosphere. *Journal of the Atmospheric Sciences* **31**(1): 118–133. DOI: 10.1175/1520-0469(1974)031<0118:APFTAO>2.0.CO;2.

Laing A, Jenni-Louise E. 2011. *Introduction to tropical meteorology*. The COMET® Program.

Lazić L, Tošić I. 2000. Sensitivity of forecast trajectories to wind data inputs during strong local wind conditions. *Idő Ujárás (Budapest. 1905)* **104**(2): 91–107.

Li L, Pomeroy JW. 1997. Estimates of Threshold Wind Speeds for Snow Transport Using Meteorological Data. *Journal of Applied Meteorology* **36**(3): 205–213. DOI: 10.1175/1520-0450(1997)036<0205:EOTWSF>2.0.CO;2.

Lim E-P, Simmonds I. 2007. Southern Hemisphere winter extratropical cyclone characteristics and vertical organization observed with the ERA-40 reanalysis data in 1979-2001. *Journal of Climate* **20**: 2675–2690.

Lingis P, Michaelides SC. 2009. Teleconnection patterns of the Siberian Anticyclone and precipitation over Cyprus. *Atmospheric Research* **94**(4): 663–674. DOI: 10.1016/j.atmosres.2009.05.013.

Maheras P, Flocas H a., Patrikas I, Anagnostopoulou C. 2001. A 40 year objective climatology of surface cyclones in the Mediterranean region: spatial and temporal distribution. *International Journal of Climatology* **21**(1): 109–130. DOI: 10.1002/joc.599.

Makjanić B. 1978. Bura, jugo, etezije. *Prilozi poznavanju klime i vremena SFRJ,* **5**: 1–56.

Makorgiannis DTJ, Giles MBD, Flocas DAA. 1981. The problem of the extension of the Siberian anticyclone towards Southeast Europe, and its relation to atmospheric circulation anomalies over the Northern Hemisphere. *Archives for meteorology, geophysics, and bioclimatology, Series A* **30**(3): 185–196. DOI: 10.1007/BF02257842.

Malačič V, Petelin B, Vodopivec M. 2012. Topographic control of wind-driven circulation in the northern Adriatic. *Journal of Geophysical Research: Oceans* **117**(C6): C06032. DOI: 10.1029/2012JC008063.

Mankin G. 2015. *The Unified Post Processor: Subprogram CALGUST*. en. Developmental Testbed Center: Boulder, US.

Mann HB. 1945. Nonparametric Tests Against Trend. *Econometrica* **13**(3): 245–259. DOI: 10.2307/1907187.

Mayr GJ, Armi L, Gohm A, Zängl G, Durran DR, Flamant C, Gaberšek S, Mobbs S, Ross A, Weissmann M. 2007. Gap flows: Results from the Mesoscale Alpine Programme. *Quarterly Journal of the Royal Meteorological Society* **133**(625): 881–896. DOI: 10.1002/qj.66.

McNider RT, Pielke RA. 1984. Numerical Simulation of Slope and Mountain Flows. *Journal of Climate and Applied Meteorology* **23**(10): 1441–1453. DOI: 10.1175/0733-3021-23.10.1441.

McVicar TR, Roderick ML, Donohue RJ, Li LT, Van Niel TG, Thomas A, Grieser J, Jhajharia D, Himri Y, Mahowald NM, Mescherskaya AV, Kruger AC, Rehman S, Dinpashoh Y. 2012. Global review and synthesis of trends in observed terrestrial near-surface wind speeds: Implications for evaporation. *Journal of Hydrology* **416–417**: 182–205. DOI: 10.1016/j.jhydrol.2011.10.024.

Mellor M. 1965. *Cold Regions Science and Engineering Part III, Section A3c: Blowing Snow*. Monograph. U.S. Army Material Command Cold Regions Research & Engineering Laboratory: Hanover, New Hampshire, USA, 85.

Milosavljević K. 1972. Contribution a la connaissance des caracteristiques de la structure du vent fort, rafale kochava dans la region de Danube. paper presented at the Comptes Rendus du Veme Conférence de Météorologie des Carpates. Bucurest, 510–521.

Milosavljević K. 1975. Carasteristique du vent fort au Nord-East de la Yugoslavie dans la région des Alpes de Transylvanie. paper presented at the Comptes Rendus du 13-eme Congres International de Météorologic Alpine. Rivista Italiana di Geofisica e Scienze Affini: Saint-Vincent, 81–89.

Milosavljević M. 1950. Fizičke karakteristike vetrova iznad Beograda. Monograph, Belgrade, University of Belgrade.

Milosavljević M. 1976. Der Wind Koshava im östlichen Tell Jugoslawiens. *In: Yoshino, M. M. (ed.) Local Wind Bora*. University of Tokyo Press: Tokyo, 203–2014.

Mokhov I, Khon V. 2005. Interannual variability and long-term tendencies of change in atmospheric centers of action in the Northern Hemisphere: Analyses of observational data. *Izvestiya Atmospheric and Oceanic Physics* **41**(6): 657–666.

Murray RJ, Simmonds I. 1991a. A numerical scheme for tracking cyclone centres from digital data. Part I: Development and operation of the scheme. *Australian Meteorological Magazine* **39**: 155–166.

Murray RJ, Simmonds I. 1991b. A numerical scheme for tracking cyclone centres from digital data. Part II: Application to January and July general circulation model simulations. *Australian Meteorological Magazine* **39**: 167–180.

Niino H, Mori A, Satomura T, Akiba S. 2006. Flow Regimes of Nonlinear Heat Island Circulation. *Journal of the Atmospheric Sciences* **63**(5): 1538–1547. DOI: 10.1175/JAS3700.1.

Nissen KM, Leckebusch GC, Pinto JG, Renggli D, Ulbrich S, Ulbrich U. 2010. Cyclones causing wind storms in the Mediterranean: characteristics, trends and links to large-scale patterns. *Nat. Hazards Earth Syst. Sci.* **10**(7): 1379–1391. DOI: 10.5194/nhess-10-1379-2010.

Nissen KM, Leckebusch GC, Pinto JG, Ulbrich U. 2013. Mediterranean cyclones and windstorms in a changing climate. *Regional Environmental Change*. DOI: 10.1007/s10113-012-0400-8.

Niu G-Y, Yang Z-L, Mitchell KE, Chen F, Ek MB, Barlage M, Kumar A, Manning K, Niyogi D, Rosero E, Tewari M, Xia Y. 2011. The community Noah land surface model with multiparameterization options (Noah-MP): 1. Model description and evaluation with local-scale measurements. *Journal of Geophysical Research: Atmospheres* **116**(D12): D12109. DOI: 10.1029/2010JD015139.

Oard MJ. 1993. A Method for Predicting Chinook Winds East of the Montana Rockies. *Weather and Forecasting* **8**(2): 166–180. DOI: 10.1175/1520-0434(1993)008<0166:AMFPCW>2.0.CO;2.

Overland JE. 1984. Scale Analysis of Marine Winds in Straits and along Mountainous Coasts. *Monthly Weather Review* **112**(12): 2530–2534. DOI: 10.1175/1520-0493(1984)112<2530:SAOMWI>2.0.CO;2.

Palutikof JP, Kelly PM, Davies TD, Halliday JA. 1987. Impacts of Spatial and Temporal Windspeed Variability on Wind Energy Output. *Journal of Climate and*

Applied Meteorology **26**(9): 1124–1133. DOI: 10.1175/1520-0450(1987)026<1124:IOSATW>2.0.CO;2.

Panagiotopoulos F, Shahgedanova M, Stephenson DB. 2002. A review of Northern Hemisphere winter-time teleconnection patterns. *Journal de Physique IV (Proceedings)* **12**(10): 27–47. DOI: 10.1051/jp4:20020450.

Pandžić K, Likso T. 2005. Eastern Adriatic typical wind field patterns and large-scale atmospheric conditions. *International Journal of Climatology* **25**(1): 81–98. DOI: 10.1002/joc.1085.

Peel MC, Finlayson BL, McMahon TA. 2007. Updated world map of the Köppen-Geiger climate classification. *Hydrol. Earth Syst. Sci.* **11**(5): 1633–1644. DOI: 10.5194/hess-11-1633-2007.

Peros B, Boko I, Divac V. 2009. Wind shear characteristics of local winds. *The Seventh Asia - Pacific Conference on Wind Engineering*. paper presented at the APCWE-VII. Taipei, Taiwan.

Petrović N. 1977. Mezoanaliza košavske situacije u periodu od 16. do 18. oktobra 1976. god. Diplomski rad, Belgrade, Serbia, Prirodno-matematički fakultet, University of Belgrade.

Petrović P. 2003. Detecting of inhomogeneities in time series using Real Precision Method. *Proceedings Of the Fourth Seminar For Homogenization And Quality Control In Climatological Databases*. paper presented at the Fourth Seminar For Homogenization And Quality Control In Climatological Databases. WMO, WCDMP-No. 56: Budapest, Hungary, 79–88.

Petrović P. 2006. Detection of Inhomogeneities in Wind Direction and Speed Data. *Proceedings Of The Fifth Seminar For Homogenization And Quality Control In Climatological Databases*. paper presented at the Fifth Seminar For Homogenization And Quality Control In Climatological Databases. WMO, WCDMP-No. 71: Budapest, Hungary, 83–90.

Petrović P. 2011. Application of the redistributoion method on custom data subsets. *Seventh Seminar For Homogenization And Quality Control In Climatological Databases*. WMO, WCDMP-No. 78: Budapest, Hungary, 56–61.

Petrović P, Curley M. 2008. Detected Inhomogeneities In Wind Direction And Speed Data From Ireland. *Proceedings of the Sixth Seminar for Homogenization and*

Quality Control in Climatological Databases. paper presented at the Sixth Seminar for Homogenization and Quality Control in Climatological Databases. WMO, WCDMP-No. 76: Budapest, Hungary, 41–52.

Petterssen S. 1956. *Weather Analysis and Forecasting Volume I Motion and Motion Systems*. McGraw-Hill: New York.

Pezza AB, Ambrizzi T. 2003. Variability of Southern Hemisphere Cyclone and Anticyclone Behavior: Further Analysis. *Journal of Climate* **16**(7): 1075–1083. DOI: 10.1175/1520-0442(2003)016<1075:VOSHCA>2.0.CO;2.

Pinto JG, Spangehl T, Ulbrich U, Speth P. 2005. Sensitivities of a cyclone detection and tracking algorithm: individual tracks and climatology. *Meteorologische Zeitschrift* **14**(6): 823–838. DOI: 10.1127/0941-2948/2005/0068.

Pirazzoli PA, Tomasin A. 2003. Recent near-surface wind changes in the central Mediterranean and Adriatic areas. *International Journal of Climatology* **23**(8): 963–973. DOI: 10.1002/joc.925.

Plavcan D, Mayr GJ, Zeileis A. 2013. Automatic and Probabilistic Foehn Diagnosis with a Statistical Mixture Model. *Journal of Applied Meteorology and Climatology* **53**(3): 652–659. DOI: 10.1175/JAMC-D-13-0267.1.

Prtenjak MT, Viher M, Jurković J. 2010. Sea-land breeze development during a summer bora event along the north-eastern Adriatic coast. *Quarterly Journal of the Royal Meteorological Society* **136**(651): 1554–1571. DOI: 10.1002/qj.649.

Pryor SC, Barthelmie RJ. 2003. Long-term trends in near-surface flow over the Baltic. *International Journal of Climatology* **23**(3): 271–289. DOI: 10.1002/joc.878.

Puygrenier V, Lohou F, Campistron B, Saïd F, Pigeon G, Bénech B, Serça D. 2005. Investigation on the fine structure of sea-breeze during ESCOMPTE experiment. *Atmospheric Research* **74**(1–4): 329–353. DOI: 10.1016/j.atmosres.2004.06.011.

Qian T, Epifanio CC, Zhang F. 2011. Topographic Effects on the Tropical Land and Sea Breeze. *Journal of the Atmospheric Sciences* **69**(1): 130–149. DOI: 10.1175/JAS-D-11-011.1.

Radinović D. 1987. *Mediterranean Cyclones and Their Influence on the Weather and Climate*. WMO: Geneva, Switzerland.

Radosavljević M, Vojnović-Kljaić R. 1985. Prediction of Koshava wind velocity. paper presented at the XIth International Conference on Carpathian Meteorology, 14-16 September, 1983. Hungarian Meteorological Service: Budapest, Hungary, 58–60.

Rex DF. 1950. Blocking Action in the Middle Troposphere and its Effect upon Regional Climate. *Tellus* **2**(3): 196–211. DOI: 10.1111/j.2153-3490.1950.tb00331.x.

Romanić D, Ćurić M, Jovičić I, Lompar M. 2015a. Long-term trends of the "Koshava" wind during the period 1949–2010. *International Journal of Climatology* **35**(2): 288–302. DOI: 10.1002/joc.3981.

Romanić D, Ćurić M, Lompar M, Jovičić I. 2015b. Contributing factors to Koshava wind characteristics. *International Journal of Climatology* n/a–n/a. DOI: 10.1002/joc.4397.

Romanić D, Ćurić M, Zarić M, Lompar M, Jovičić I. 2015c. Investigation of an extreme Koshava wind episode of 30 January–4 February 2014. *Atmospheric Science Letters* n/a–n/a. DOI: 10.1002/asl.643.

Royal Meteorological Society. 2015. *Local Winds - Metlink Teaching Weather and Climate*. *MetLink*. Education. .

Sahsamanoglou HS, Makrogiannis TJ, Kallimopoulos PP. 1991. Some aspects of the basic characteristics of the Siberian anticyclone. *International Journal of Climatology* **11**(8): 827–839. DOI: 10.1002/joc.3370110803.

Saji NH, Goswami BN. 1996. An improved linear model of tropical surface wind variability. *Quarterly Journal of the Royal Meteorological Society* **122**(529): 23–53. DOI: 10.1002/qj.49712252903.

Satoh M. 2004. *Atmospheric Circulation Dynamics and Circulation Models*. Springer Science & Business Media: New York.

Schmidt RA. 1981. Estimates of threshold windspeed from particle sizes in blowing snow. *Cold Regions Science and Technology* **4**(3): 187–193. DOI: 10.1016/0165-232X(81)90003-3.

Schwarz G. 1978. Estimating the Dimension of a Model. *The Annals of Statistics* **6**(2): 461–464. DOI: 10.1214/aos/1176344136.

Schwarzkopf MD, Fels SB. 1991. The simplified exchange method revisited: An accurate, rapid method for computation of infrared cooling rates and fluxes. *Journal of Geophysical Research: Atmospheres* **96**(D5): 9075–9096. DOI: 10.1029/89JD01598.

Scorer RS. 1952. Mountain-gap winds; a study of surface wind at Gibraltar. *Quarterly Journal of the Royal Meteorological Society* **78**(335): 53–61. DOI: 10.1002/qj.49707833507.

Seibert DP. 1990. South foehn studies since the ALPEX experiment. *Meteorology and Atmospheric Physics* **43**(1-4): 91–103. DOI: 10.1007/BF01028112.

Sen PK. 1968. Estimates of the Regression Coefficient Based on Kendall's Tau. *Journal of the American Statistical Association* **63**(324): 1379–1389. DOI: 10.2307/2285891.

Sergijevski P. 1940. Vetrovi u Beogradu. .

Shahgedanova M. 2002. *The Physical Geography of Northern Eurasia*. Oxford University Press: Oxford, UK.

Sheridan P. 2011. *Review of techniques and research for gust forecasting and parameterisation*. Forecasting Research Technical Report. Met Office: Exeter, UK, 21.

Shin HH, Hong S-Y. 2011. Intercomparison of Planetary Boundary-Layer Parametrizations in the WRF Model for a Single Day from CASES-99. *Boundary-Layer Meteorology* **139**(2): 261–281. DOI: 10.1007/s10546-010-9583-z.

Simmonds I, Keay K. 2000. Mean Southern Hemisphere Extratropical Cyclone Behavior in the 40-Year NCEP–NCAR Reanalysis. *Journal of Climate* **13**(5): 873–885. DOI: 10.1175/1520-0442(2000)013<0873:MSHECB>2.0.CO;2.

Simmonds I, Murray JR, Leighton RM. 1999. A refinement cyclone tracking methods with data from FROST. *Australian Meteorological Magazine* **(Special ed.)**: 35–49.

Sisterson DL, Hicks BB, Coulter RL, Wesely ML. 1983. Difficulties in using power laws for wind energy assessment. *Solar Energy* **31**(2): 201–204. DOI: 10.1016/0038-092X(83)90082-8.

Smits A, Klein Tank AMG, Können GP. 2005. Trends in storminess over the Netherlands, 1962–2002. *International Journal of Climatology* **25**(10): 1331–1344. DOI: 10.1002/joc.1195.

Stanojević S. 1959. *Koshava wind*. Zbornik radova Poljoprivrednog fakulteta.

Steyn DG, Oke TR, Hay JE, Knox JL. 1981. On scales in meteorology and climatology. *McGill Climatological Bulletin* **30**: 1–8.

Sturman AP. 1987. Thermal influences on airflow in mountainous terrain. *Progress in Physical Geography* **11**(2): 183–206. DOI: 10.1177/030913338701100202.

Sukoriansky S, Galperin B, Perov V. 2005. Application of a New Spectral Theory of Stably Stratified Turbulence to the Atmospheric Boundary Layer over Sea Ice. *Boundary-Layer Meteorology* **117**(2): 231–257. DOI: 10.1007/s10546-004-6848-4.

Tabler R., Benson CS, Santana BW, Ganguly P. 1990. Estimating snow transport from wind speed records: estimates versus measurements at Prudhoe Bay, Alaska. *Proceedings of the 58th Annual Western Snow Conference*. paper presented at the 58th Annual Western Snow Conference. Western Snow Conference: Sacramento, California, USA, 61–72.

Talbot C, Bou-Zeid E, Smith J. 2012. Nested Mesoscale Large-Eddy Simulations with WRF: Performance in Real Test Cases. *Journal of Hydrometeorology* **13**(5): 1421–1441. DOI: 10.1175/JHM-D-11-048.1.

The World Bank. 2013. The World Development Indicators. .

Thompson R, Green DN. 2004. Mediterranean precipitation and its relationship with sea level pressure patterns. *Annals of Geophysics* **47**(5). DOI: 10.4401/ag-3364.

Todorović N, Paskota M. 2002. Koshava wind speed in Belgrade and air pressure gradient relation between Belgrade and Negotin measure points. paper presented at the 18th International Conference on Carpathian Meteorology. Belgrade.

Tomasevic E, Jurin J, Gamulin L. 2014. *Sailing Nautical Skills*. More Moje Slano.

Trigo IF, Davies TD, Bigg GR. 1999. Objective Climatology of Cyclones in the Mediterranean Region. *Journal of Climate* **12**(6): 1685–1696. DOI: 10.1175/1520-0442(1999)012<1685:OCOCIT>2.0.CO;2.

Trigo IF, Davies TD, Bigg GR. 2000. Decline in Mediterranean rainfall caused by weakening of Mediterranean cyclones. *Geophysical Research Letters* **27**(18): 2913–2916. DOI: 10.1029/2000GL011526.

Tutiš V. 2002. Violent Adriatic windstorms. *Proceedings of the 4th EGS Plinius Conference*. Mallorca, Spain.

Tyrlis E, Lelieveld J. 2013. Climatology and Dynamics of the Summer Etesian Winds over the Eastern Mediterranean*. *Journal of the Atmospheric Sciences* **70**(11): 3374–3396. DOI: 10.1175/JAS-D-13-035.1.

Unated Nations. 2006. World urbanisation prospects: The 2011 Revision. .

Unkašević M. 1994. *Klima Beograda*. Naučna knjiga: Belgrade, Serbia.

Unkašević M, Mališić J, Tošić I. 1998. On some new statistical characteristics of the wind "Koshava." *Meteorology and Atmospheric Physics* **66**(1-2): 11–21. DOI: 10.1007/BF01030445.

Unkašević M, Mališic J, Tošić I. 1999. Some aspects of the wind "Koshava" in the lower troposphere over Belgrade. *Meteorological Applications* **6**(1): 69–79. DOI: 10.1017/S1350482799000997.

Unkašević M, Tošić I. 2006. *Koshava monografija*. Akademska misao: Belgrade.

Unkašević M, Tošić I, Obradović M. 2007. Spectral analysis of the "Koshava" wind. *Theoretical and Applied Climatology* **89**(3-4): 239–244. DOI: 10.1007/s00704-006-0261-5.

Vautard R, Cattiaux J, Yiou P, Thépaut J-N, Ciais P. 2010. Northern Hemisphere atmospheric stilling partly attributed to an increase in surface roughness. *Nature Geoscience* **3**(11): 756–761. DOI: 10.1038/ngeo979.

Vergeiner DI, Dreiseitl DE. 1987. Valley winds and slope winds — Observations and elementary thoughts. *Meteorology and Atmospheric Physics* **36**(1-4): 264–286. DOI: 10.1007/BF01045154.

Vincenty T. 1975. Direct and Inverse Solutions of Geodesics on the Ellipsoid with Application of Nested Equations. *Survey Review* **23**(176): 88–93.

Vojnović-Kljaić R, Popović Z. 1978. Sinoptičko-aerološki uslovi pri pojavi orkanskih udara košave na dan 17.10.1976. godine. paper presented at the 1st

Conference on protection against atmospheric storms. Republic Hydrometeorological Service of Serbia: Belgrade, 1–10.

Vujević P. 1933. Podneblje Beograda. *Beogradske opštinske novine* **2**.

Vujević P. 1948. *Meteorologija*. Prirodno-matematički fakultet: Beograd.

Vukmirović D. 1985a. The Koshava wind events during the Alpex special observing period. paper presented at the 18-th International Conference for Alpine meteorology 25-29 September, 1984. Zbornik meteorologkih i hidrologkih radova: Opatija, 75–77.

Vukmirović D. 1985b. The spatial structure of the koshava wind. paper presented at the 11-th International Conference for Alpine meteorology 14-16 September, 1983. Hungarian Meteorological Service: Budapest, 10–15.

Vukmirović D. 1997. Ventilation factor during Koshava. paper presented at the XXV Savetovanje "Zaštita vazduha "97'. Belgrade, 19–21.

Vukmirović D, Merkle M. 1991. Characteristics of wind in the lower troposphere over Belgrade. *Zbornik radova*. Savez drustava inženjera i tehnčara Beograda: Belgrade, 1–9.

Wan H, Wang XL, Swail VR. 2010. Homogenization and Trend Analysis of Canadian Near-Surface Wind Speeds. *Journal of Climate* **23**(5): 1209–1225. DOI: 10.1175/2009JCLI3200.1.

Weitzman MS. 1970. *Measures of overlap of income distributions of white and Negro families in the United States*. Technical Report. Department of Commerce, Bureau of the Census: Washington, USA, 36.

Wever N. 2012. Quantifying trends in surface roughness and the effect on surface wind speed observations. *Journal of Geophysical Research: Atmospheres* **117**(D11): D11104. DOI: 10.1029/2011JD017118.

Whiteman CD. 2003. *Mountain Meteorology: Fundamentals and Applications*. Oxford University Press: New York, USA.

Wind of the World: Vardar (Vardarac) - Weather UK - weatheronline.co.uk. 2015. .

Xu L, Raman S, Madala RV. 1995. A Review of Non-hydrostatic Numerical Models for the Atmosphere. *Proceedings of the First World Congress on World*

Congress of Nonlinear Analysts '92, Volume IV. Walter de Gruyter & Co.: Hawthorne, NJ, USA, 3595–3609.

Zängl G. 2002a. Stratified flow over a mountain with a gap: Linear theory and numerical simulations. *Quarterly Journal of the Royal Meteorological Society* **128**(581): 927–949. DOI: 10.1256/0035900021643755.

Zängl G. 2002b. Idealized numerical simulations of shallow föhn. *Quarterly Journal of the Royal Meteorological Society* **128**(580): 431–450. DOI: 10.1256/003590002321042045.

Zarić M. 2014. *Olujni i orkanski udari Košave – mećava i vejavice u severnim i severoistočnim delovima Srbije*. Analiza sinoptičke situacije i vremena u periodu od 26. januara do 04. februara 2014. godine. Republic Hydrometeorological Service of Serbia: Belgrade, Serbia, 28.

Ziv B, Saaroni H, Alpert P. 2004. The factors governing the summer regime of the eastern Mediterranean. *International Journal of Climatology* **24**(14): 1859–1871. DOI: 10.1002/joc.1113.

Appendices

Appendix A. ΔPs and Δθs based on reanalysis data

Here, the MSLP differences (ΔPs) and potential temperature differences (Δθs) are calculated based on the NCEP/NCAR reanalysis 1 data (Kalnay *et al.*, 1996). The methodology for calculation of ΔPs is somewhat different compared to the method presented in Section 2.2. Namely, the ΔPs here are calculated using the area-averaged MSLP values compared to the point differences described in Section 2.2 and presented in Section 5.4. The calculation procedure for ΔPs is as follows:

$$\Delta P_k = \overline{P_i} - \overline{P_j}. \tag{A.1}$$

In the above equation i and j are R1, R2, R3, R4, KR, and $i \neq j$. The corresponding regions over which the MSLP were averaged are portrayed in Figure A.1a. The following combinations are considered: k = R2 – R3, R1 – R4, R1 – KR, R2 – KR, R3 – KR. It can be seen that these differences still represent across-mountain MSLP differences. Advantage of considering spatial averages of MSLP instead of station (point) values is taking into account pressures over broader regions. That way, the dynamic properties of large air masses are included into ΔPs. An average can also moderate a possible noise in the reanalysis' MSLP data close to a complex mountain regions.

The Δθs are computed based on point differences as described as Section 2.4. The crest and gap virtual stations (points) used to compute Δθs are shown in Figure A.1b. Potential temperature values at the "Far Crest", "Close Crest" and "Gap" positions are obtained from the reanalysis 2.5°×2.5° grid using a bilinear interpolation from the four closes reanalysis points. Due to a large uncertainty of interpolated potential temperatures in mountainous regions around the Iron

Gates, the $\Delta\theta$ analysis is performed only for the VG station. The following three cases are considered: $\theta_{FarCrest} - \theta_{VG}$, $\theta_{CloseCrest} - \theta_{VG}$ and $\theta_{Gap} - \theta_{VG}$.
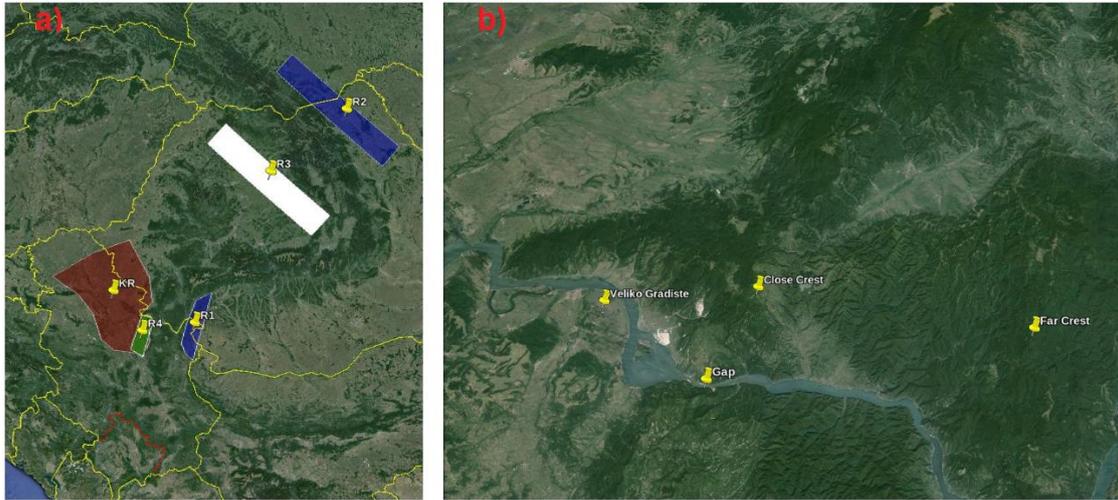

Figure A.1. a) Regions (R1, R2, R3, R4, and KR) over which MSLPs from reanalysis data were averaged for the calculation of ΔPs. b) Point locations used to calculate $\Delta\theta$s between Close/Far Crest – VG and Gap – VG based on reanalysis data.

The resulting ΔPs and $\Delta\theta$s are presented in the following Figure A.2 and Figure A.3. Comparing these figures with the results presented in Section 5.4 it can be seen that the same group of statistical distributions is used to describe ΔPs and $\Delta\theta$s regardless of the input data to compute these differences. The overlaps between Koshava and "no-Koshava" cases are larger when the differences are calculated from the reanalysis data. This finding is expected and is a consequence of the coarse spatial resolution of reanalysis data. The model orography in the global reanalysis model is a rough approximation of the real orography (Kistler *et al.*, 2001). Therefore, the results in this appendix should be used with caution, especially when it comes to the $\Delta\theta$s values.

The overlaps of Δθs are over 75 % in all three cases. They can not be used as a reliable deterministic parameter of Koshava's occurrence. It is noticeable that overlaps of ΔPs are considerably smaller than the overlaps of Δθs. The values, however, are still larger compared to the station ΔPs considered in Section 5.4.
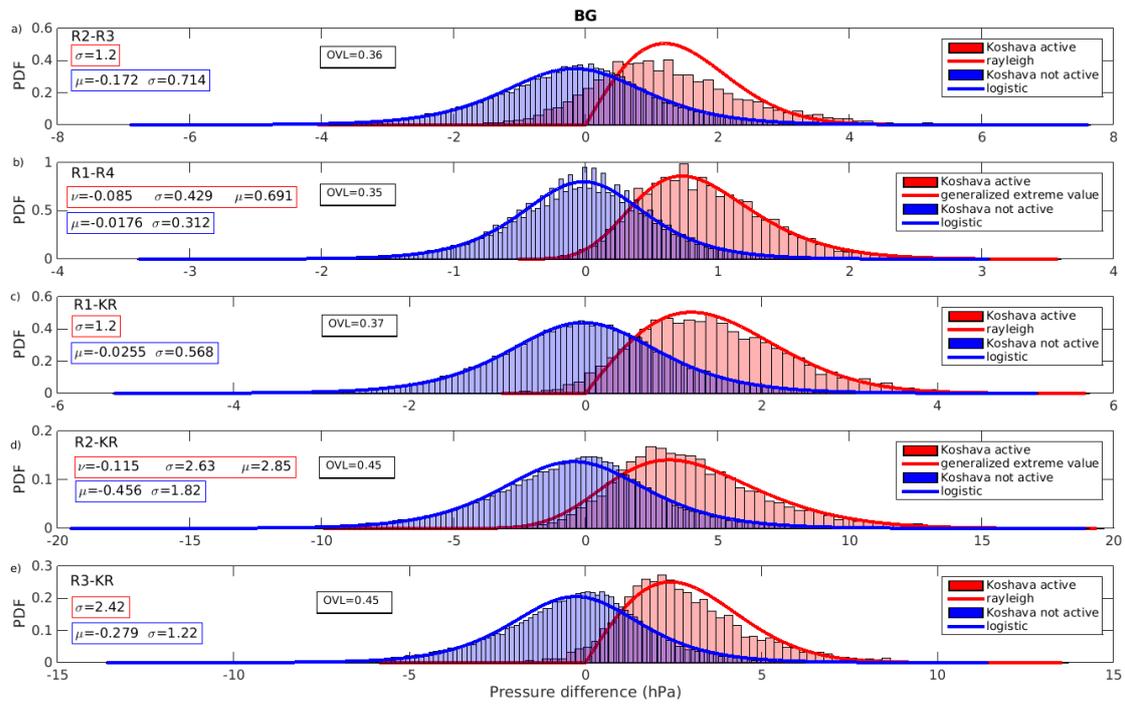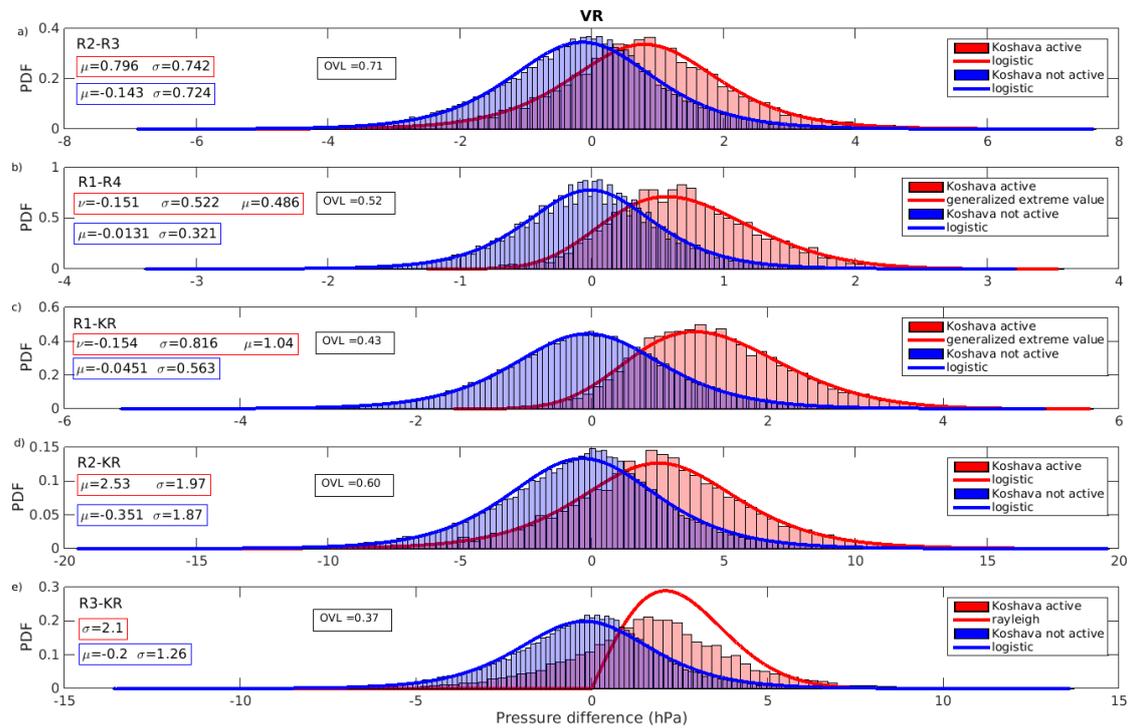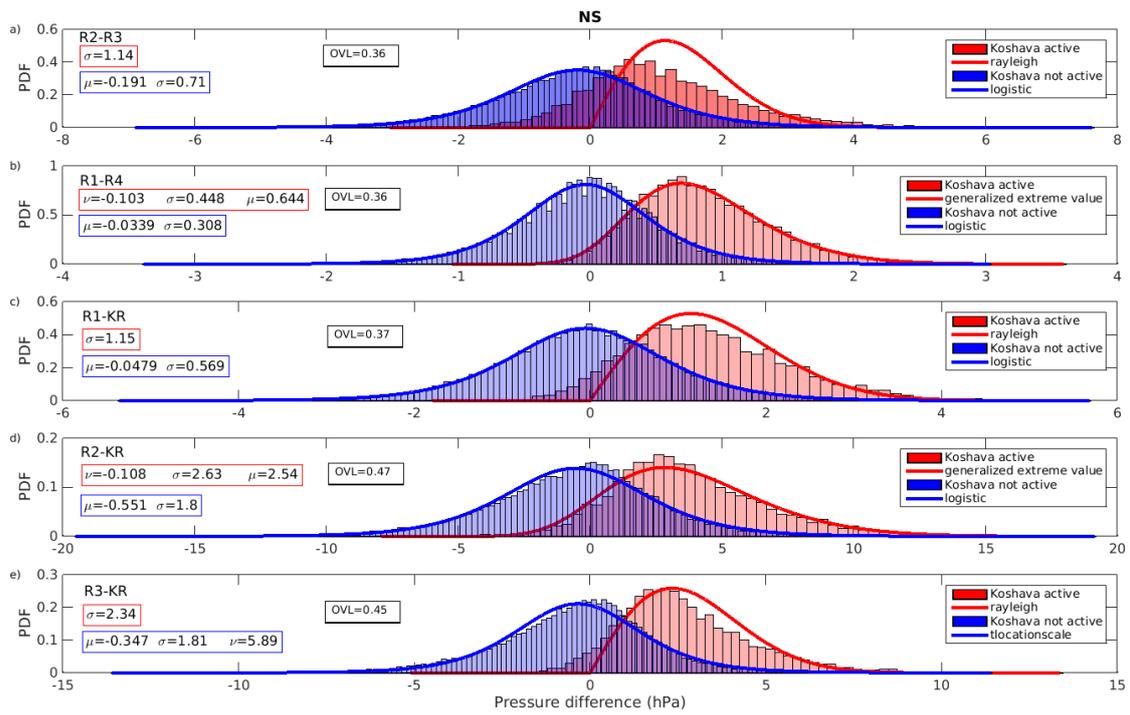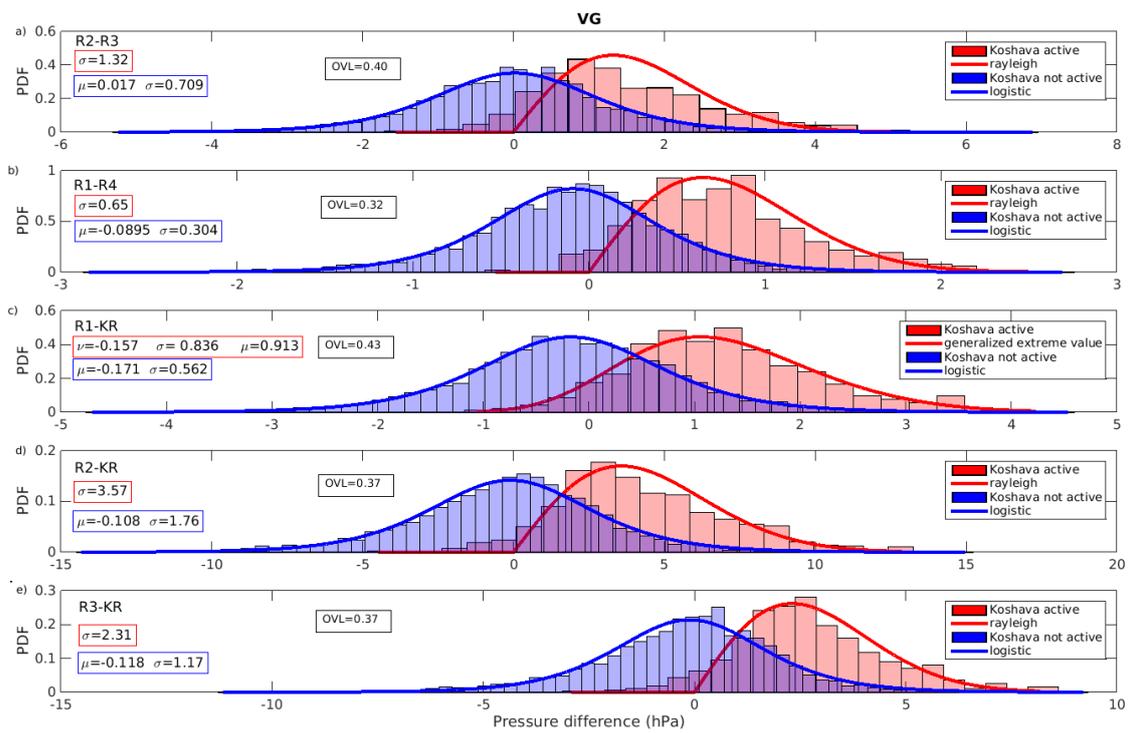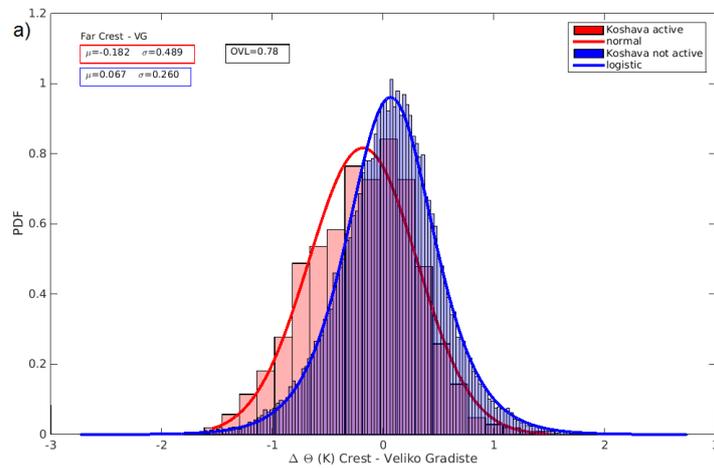
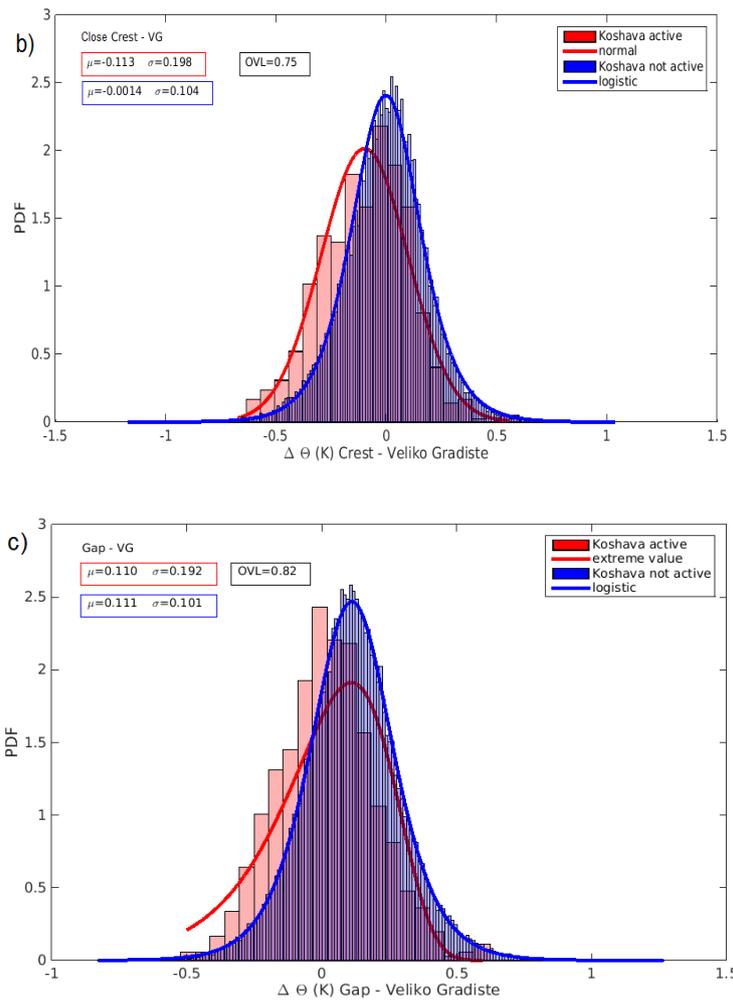Figure A.2. Across-mountain MSLP differences based on the reanalysis data for the BG, NS, VR and VG stations.

Figure A.3. Across-mountain potential temperature differences based on the reanalysis data for the VG station.

Biography

Đorđe Romanić was born in Pakrac, Croatia in 1984. In 1998, Đorđe enrolled in the Geology and Hydrometeorology High School "Milutin Milanković" in Belgrade, Serbia. He was one of the best meteorology students in his class. In 2002, he enrolled in the Faculty of Physics, University of Belgrade where he obtained his B.Sc. as well as his M.Sc. diplomas in meteorology in 2008. In 2007, Đorđe was selected in the group of 300 best undergraduate students in Serbia.

Đorđe started his professional career in 2009 in a consulting company "South East Europe Consultants Ltd.", from Belgrade, Serbia. He was responsible for preparation of wind resource assessment studies.

In 2009, Đorđe started his Ph.D. studies in the field of meteorology at the Institute for Meteorology, Faculty of Physics, University of Belgrade. His research topic was on the dynamics and climatology of the Koshava wind. Therefore, in parallel with his professional career in consulting, he was also working towards the PhD degree in meteorology. Then in 2012, Đorđe enrolled in one more PhD program, but this time at the Faculty of Civil & Environmental Engineering, Western University, London, Ontario, Canada. At Western, his research is related to the multiscale numerical modelling of synoptic and non-synoptic winds. He is schedule to graduate in 2016.

Đorđe is a teaching assistant for several undergraduate and graduate courses at the Western Engineering program. Combining published and under revision manuscripts, Đorđe has 7 journal articles, more than 15 conference papers and posters and more than 10 technical reports. In 2015, he was awarded the prestigious Alan G Davenport Memorial Scholarship and Dr. Robert Addie Scholarship in Wind Engineering.

Изјава о ауторству

Потписани-а _____ Ђорђе РОМАНИЋ _____
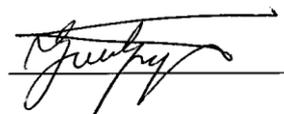
број уписа _____

Изјављујем

да је докторска дисертација под насловом

Dynamic characteristics of the Koshava wind

- резултат сопственог истраживачког рада,
- да предложена дисертација у целини ни у деловима није била предложена за добијање било које дипломе према студијским програмима других високошколских установа,
- да су резултати коректно наведени и
- да нисам кршио/ла ауторска права и користио интелектуалну својину других лица.

Потпис докторанда

У Београду, 07.12.2015.

186

Изјава о истоветности штампане и електронске верзије докторског рада

Име и презиме аутора ____ЂОРЂЕ РОМАНИЋ____

Број уписа _____

Студијски програм ____МЕТЕОРОЛОГИЈА____

Наслов рада DYNAMIC CHARACTERISTICS OF THE KOSHAVA WIND

Ментор ДР. МЛАЂЕН ЋУРИЋ, РЕДОВНИ ПРОФЕСОР

Потписани ____ЂОРЂЕ РОМАНИЋ____

изјављујем да је штампана верзија мог докторског рада истоветна електронској верзији коју сам предао/ла за објављивање на порталу **Дигиталног репозиторијума Универзитета у Београду.**

Дозвољавам да се објаве моји лични подаци везани за добијање академског звања доктора наука, као што су име и презиме, година и место рођења и датум одбране рада.

Ови лични подаци могу се објавити на мрежним страницама дигиталне библиотеке, у електронском каталогу и у публикацијама Универзитета у Београду.

Потпис докторанда

У Београду, 07. 12. 2015.

187

Прилог 3.

Изјава о коришћењу

Овлашћујем Универзитетску библиотеку „Светозар Марковић" да у Дигитални репозиторијум Универзитета у Београду унесе моју докторску дисертацију под насловом:

DYNAMIC CHARACTERISTICS OF THE KOSHAVA WIND

која је моје ауторско дело.

Дисертацију са свим прилозима предао/ла сам у електронском формату погодном за трајно архивирање.

Моју докторску дисертацију похрањену у Дигитални репозиторијум Универзитета у Београду могу да користе сви који поштују одредбе садржане у одабраном типу лиценце Креативне заједнице (Creative Commons) за коју сам се одлучио/ла.

1. Ауторство

2. Ауторство - некомерцијално

3. Ауторство – некомерцијално – без прераде

4. Ауторство – некомерцијално – делити под истим условима

5. Ауторство – без прераде

6. Ауторство – делити под истим условима

(Молимо да заокружите само једну од шест понуђених лиценци, кратак опис лиценци дат је на полеђини листа).

У Београду, 07.12.2015.

Потпис докторанда

188
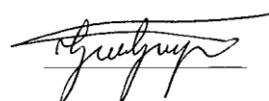
1. Ауторство - Дозвољавате умножавање, дистрибуцију и јавно саопштавање дела, и прераде, ако се наведе име аутора на начин одређен од стране аутора или даваоца лиценце, чак и у комерцијалне сврхе. Ово је најслободнија од свих лиценци.

2. Ауторство – некомерцијално. Дозвољавате умножавање, дистрибуцију и јавно саопштавање дела, и прераде, ако се наведе име аутора на начин одређен од стране аутора или даваоца лиценце. Ова лиценца не дозвољава комерцијалну употребу дела.

3. Ауторство - некомерцијално – без прераде. Дозвољавате умножавање, дистрибуцију и јавно саопштавање дела, без промена, преобликовања или употребе дела у свом делу, ако се наведе име аутора на начин одређен од стране аутора или даваоца лиценце. Ова лиценца не дозвољава комерцијалну употребу дела. У односу на све остале лиценце, овом лиценцом се ограничава највећи обим права коришћења дела.

4. Ауторство - некомерцијално – делити под истим условима. Дозвољавате умножавање, дистрибуцију и јавно саопштавање дела, и прераде, ако се наведе име аутора на начин одређен од стране аутора или даваоца лиценце и ако се прерада дистрибуира под истом или сличном лиценцом. Ова лиценца не дозвољава комерцијалну употребу дела и прерада.

5. Ауторство – без прераде. Дозвољавате умножавање, дистрибуцију и јавно саопштавање дела, без промена, преобликовања или употребе дела у свом делу, ако се наведе име аутора на начин одређен од стране аутора или даваоца лиценце. Ова лиценца дозвољава комерцијалну употребу дела.

6. Ауторство - делити под истим условима. Дозвољавате умножавање, дистрибуцију и јавно саопштавање дела, и прераде, ако се наведе име аутора на начин одређен од стране аутора или даваоца лиценце и ако се прерада дистрибуира под истом или сличном лиценцом. Ова лиценца дозвољава комерцијалну употребу дела и прерада. Слична је софтверским лиценцама, односно лиценцама отвореног кода.